

國立交通大學

電子工程學系 電子研究所碩士班

碩 士 論 文

IEEE 802.16m 空間多工模式閉迴路

多輸入傳輸之預編碼與等化研究

**A Study on Precoding and Equalization for the
Spatial Multiplexing Mode of IEEE 802.16m
Closed-Loop MIMO**

研 究 生：柯俊言

指導教授：林大衛 博士

中 華 民 國 一 〇 〇 年 七 月



IEEE 802.16m 空間多工模式閉迴路

多輸出入傳輸之預編碼與等化研究

A Study on Precoding and Equalization for the

Spatial Multiplexing Mode of IEEE 802.16m

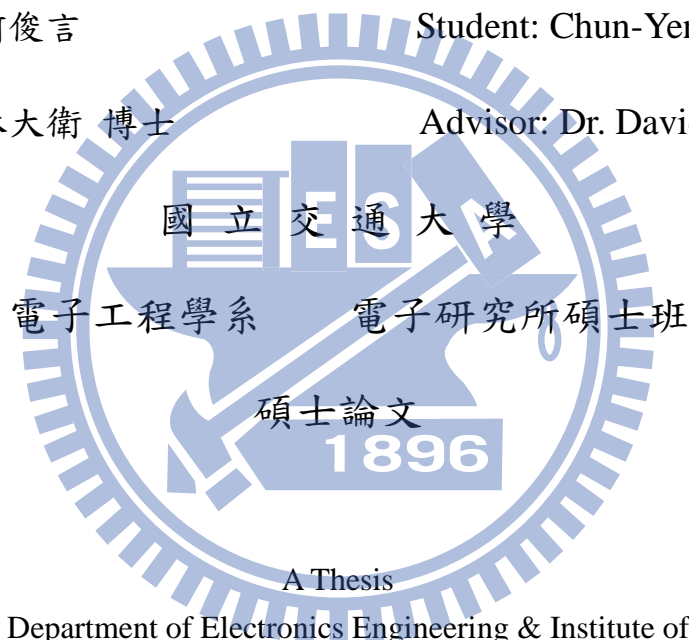
Closed-Loop MIMO

研 究 生：柯俊言

Student: Chun-Yen Ko

指導教授：林大衛 博士

Advisor: Dr. David W. Lin



Submitted to Department of Electronics Engineering & Institute of Electronics

College of Electrical and Computer Engineering

National Chiao Tung University

in Partial Fulfillment of the Requirements

for the Degree of

Master of Science

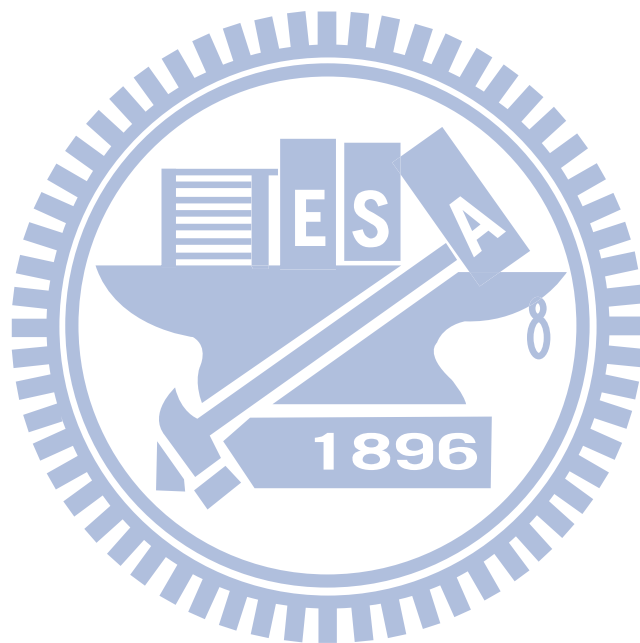
in

Electronics Engineering

July 2011

Hsinchu, Taiwan, Republic of China

中華民國一〇〇年七月



IEEE 802.16m 空間多工模式閉迴路 多輸出入傳輸之預編碼與等化研究

研究生:柯俊言

指導教授:林大衛博士

國立交通大學

電子工程學系 電子研究所碩士班

摘要

多輸出入傳輸技術近來在行動環境中廣受注目且已經應用在許多數位通訊系統中，因為跟單輸出入傳輸相比之下，容量和可靠度有顯著的提升。

我們聚焦在 IEEE 802.16m 空間多工模式閉迴路多輸出入傳輸之預編碼與等化研究。本篇論文採用兩種等化方法。第一種為迫零(ZF)等化器，他在頻域上為反向濾波器，這是一個最簡單的等化器，他可以消除符號干擾，但是他會造成雜訊放大。第二種為最小均方差(MMSE)等化器，最小均方差等化器是使設計估測通道信號及實際信號的均方誤差為最小，雖然沒辦法完全消除符號干擾，但是不會造成

雜訊放大。

我們依據這兩種等化器，再去設計選擇預編碼的方法。要計算預編碼的話，完整通道資訊必須要傳給傳輸端。這會產生一個問題，因為我們的回傳通道的頻寬是有限的。所以我們預先設計好預編碼，再回傳最合適的預編碼編號。我們提出兩種方法去找尋最適合的預編碼，第一種是基於最小均方差方法，我們把所有預編碼裡代入運算，找出最小均方差。第二種是找出使兩根天線最小的訊號雜訊比最大的預編碼，這個方法必須先計算出每個預編碼天線的訊號雜訊比，我們在找出最適合的回傳。我們會跟以下兩種方法做比較。第一種為基於奇異值的方法，首先把通道頻率響應做奇異值分解，其中通道頻率響應的正交輸入基向量是最佳的迫零等化器，我們把所有可能的預編碼跟他做旋距離計算，找出最小的預編碼回傳。第二種為最佳預編碼計算，我們會利用注水原理去求得最佳解。我們先在加成性白色高斯通道下驗證我們的模擬模型，然後在 IEEE802.16m 標準下於單路徑和多重路徑通道上模擬。

在本篇論文中，我們首先簡介 IEEE802.16m 的標準機制。接著，我們依照標準分別各傳輸下介紹兩種等化器搭配四種選擇預編碼方法並探討其效能。

A Study on Precoding and Equalization for the Spatial Multiplexing Mode of IEEE 802.16m Closed-Loop MIMO

Student: Chun-Yen Ko

Advisor: Dr. David W. Lin



Abstract

MIMO channels arising from the use of multiple antennas at both the transmitter and at the receiver have recently attracted significant interest because they provide a significant increase in capacity and reliability over single-input single-output (SISO) channels under some uncorrelation conditions.

We focus on Precoding and Equalization for the Spatial Multiplexing Mode of IEEE 802.16m Closed-Loop MIMO. We present two equalizer methods. One is Zero-forcing equalizer. It is an inverse filter in frequency

domain. This is the easiest equalizer. It can remove the ISI, but it will increase the noise. The other method is MMSE equalizer. This method is designed to minimize the mean square error of the receive signal and the transmit signal. It can not remove all of the ISI, but it will not increase the noise.

A problem associated with precoding is that the channel state information must be known at transmitter. This may be difficult since the bandwidth of the feedback channel is usually limited. Thus, a codebook-based limited feedback precoding scheme is generally used. The main idea is to quantize the precoding matrix and feedback the index of the optimum precoder. We based on these two equalizers to design the selection method to select the best precoder. We proposed MMSE-Based and MaxminSNR-Based method. MMSE-Based method finds the precoder has the minimum mean square error. MaxminSNR-Based method finds the precoder that maximizes the minimum SNR of the two antennas. This method has to calculate each precoder's antenna SNR. Then, we select the appropriate one to transmit back. We will compare with the following two methods. First is SVD-Based method. We take the singular value decomposition (SVD) of the channel matrix. The right singular vector of the channel matrix is the best ZF equalizer. We calculate all the chordal distance of the possible precoder and the best ZF equalizer. Then, we transmit the precoder. Second is the optimum precoder computation. We use water-filling method to get the solution. We verify our simulation model on AWGN channel and then do the simulation on singlepath and multipath channels for IEEE 802.16m.

In this thesis, we first introduce the standard of the IEEE 802.16m. Then we describe the precoding and equalization methods we use and discuss the performance in each transmission condition for IEEE 802.16m.

誌謝

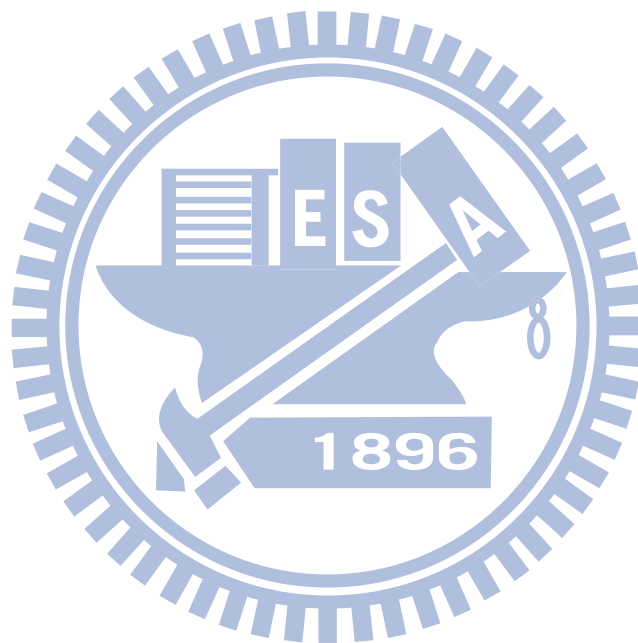
本篇論文的完成，首先要特別感謝我的指導教授林大衛博士，在我進入交大電子所開始，不論是課業或是研究上的困難，老師總能細心的給予適時方向去解決問題，使我學到了分析以及解決問題的能力。此外老師對於學生的認真以及親切樂觀的態度更是深遠影響了我，使我在研究所的這幾年得到了學術以外更重要的智慧。

此外，由衷的感謝通訊電子與訊號處理實驗室所有的成員，包含各位師長、同學、學長姐以及學弟妹們。特別感謝曲建全學長、林鴻志學長、蕭世璞學長、洪朝雄學長、蔡彰哲學長、邱頌恩學長、吳思賢學長和盧世榮學長對我在學術上的不吝指導與建議，謝謝你們幫我解決了許多通訊方面的疑問。感謝 98 級曉盈、威宇、卓翰、強丹、智凱、兆軒、郁婷、琬瑜、怡茹、頌文、書緯、偵源、凱翔、復凱及 99 級學弟們等實驗室成員，平日和我一起念書、討論、玩耍，讓我的研究生涯擁有美好的回憶。期待各位夥伴們畢業後都有不錯的發展。

最後，必須感謝我的家人，我父母親、姐姐及惠婷給予我的支持，使我在外地讀書時能無後顧之憂，感謝他們的支持，也謝謝所有幫助過我、陪我走過這段歲月的人。

柯俊言

民國一百年七月 於新竹



Contents

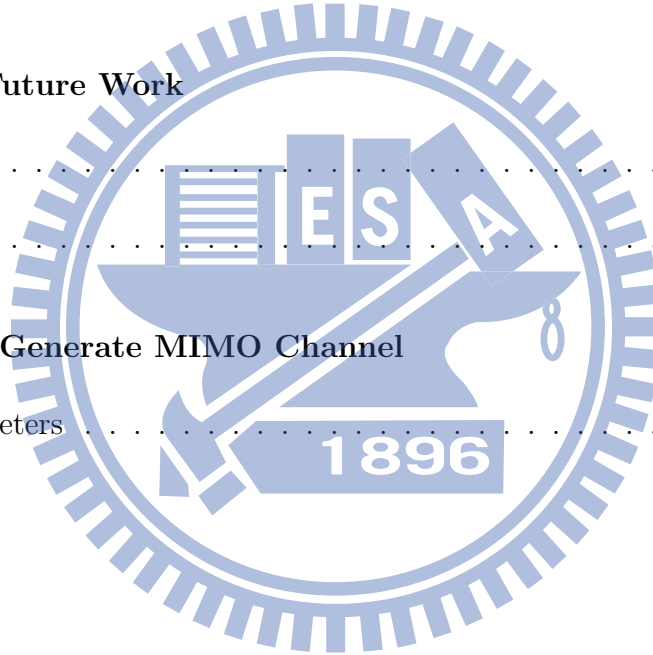
1	Introduction	1
1.1	Scope of the Work	1
1.2	Organization and Contribution of this Thesis	3
2	Introduction to IEEE 802.16m OFDMA	5
2.1	Basic OFDMA Symbol Structure and Frame Structure [10]	5
2.1.1	OFDMA Basic Terms	6
2.1.2	Frequency Domain Description	6
2.1.3	Primitive Parameters	7
2.1.4	Derived Parameters	7
2.1.5	Frame Structure	8
2.2	Downlink Transmission in IEEE 802.16m OFDMA[10]	11
2.2.1	Subband Partitioning	12
2.2.2	Miniband Permutation	15
2.2.3	Frequency Partitioning	16
2.3	Cell-Specific Resource Mapping [10]	20

2.3.1	CRU/DRU Allocation	21
2.3.2	Subcarrier Permutation	24
2.3.3	Random Sequence Generation	26
2.4	Test Case Generation	27
2.4.1	Subband Partitioning	28
2.4.2	Miniband Partitioning	30
2.4.3	Miniband Permutation	30
2.4.4	Frequency Partitioning	32
2.4.5	Random Sequence	34
2.4.6	CRU/DRU Allocation	35
2.5	MIMO Midamble [10]	35
2.6	Usage of Downlink Pilots [10]	38
2.7	Downlink control structure [10]	40
2.7.1	Advanced Preamble	40
2.7.2	Primary Advanced Preamble (PA-Preamble)	40
2.7.3	Secondary Advanced Preamble (SA-Preamble)	43
2.8	DL Control Channels [10]	44
2.8.1	Superframe Header	44
2.8.2	Primary Superframe Header	45
2.8.3	Secondary Superframe Header	45
2.8.4	Advanced MAP (A-MAP)	46

2.8.5	Non-user Specific A-MAP	48
2.8.6	HARQ Feedback A-MAP	48
2.8.7	Power Control A-MAP	49
2.8.8	Assignment A-MAP	49
2.9	Resource Mapping of DL Control Channels [10]	50
2.9.1	Superframe Header	51
2.9.2	Downlink Power Control	57
3	Introduction to IEEE 802.16m MIMO	59
3.1	Downlink MIMO Architecture and Data Processing [10]	59
3.2	MIMO Layer to MIMO Stream Mapping [10]	60
3.2.1	SFBC Encoding	61
3.2.2	Vertical Encoding (VE)	61
3.2.3	Multi-layer Encoding (ME)	61
3.2.4	CDR Encoding	62
3.3	MIMO Stream to Antenna Mapping [10]	62
3.3.1	Non-adaptive Precoding	62
3.3.2	Adaptive Precoding	65
3.4	Downlink MIMO Modes [10]	65
3.5	Transmission Schemes for Data Channels [10]	65
3.5.1	Encoding and Precoding of SU-MIMO	66
3.5.2	Encoding and Precoding of MU-MIMO	67

3.5.3	Mapping of Data and Pilot Subcarriers	69
3.5.4	Usage of MIMO Modes	70
3.6	Feedback Mechanisms and Operation [10]	70
3.6.1	Open-Loop Region	71
3.6.2	MIMO Feedback Mode Selection	72
3.6.3	MIMO Feedback Modes	72
3.6.4	Downlink Signaling Support of DL-MIMO Modes	74
3.6.5	Quantized MIMO Feedback for Closed-loop Transmit Precoding . . .	78
3.7	Uplink MIMO Transmission Schemes [10]	86
3.7.1	Uplink MIMO Architecture and Data Processing	86
3.7.2	MIMO Layer to MIMO Stream Mapping	87
3.7.3	MIMO Stream to Antenna Mapping	87
3.7.4	Uplink MIMO Transmission Modes	89
4	Equalization and Closed-Loop MIMO Technology	94
4.1	System Model	94
4.1.1	Linear Equalizer Matrix	95
4.2	Precoder Selection Methods	96
4.2.1	MaxminSNR-Based Search Method	96
4.2.2	MMSE-Based Exhaustive Search Method	97
4.2.3	SVD-Based Search Method [14]	98
4.2.4	Optimum Precoder Selection [17]	100

4.2.5	Matrix Computation Complexity	101
5	Downlink MIMO Simulation for IEEE 802.16m	103
5.1	System Parameters and Channel Model	103
5.2	Simulation Results for IEEE 802.16m	105
5.2.1	Simulation Flow	105
5.2.2	Validation with AWGN Channel	106
5.3	Simulation Results for Single-Path Channels	107
5.4	Simulation Results for Multipath Channels	125
6	Conclusion and Future Work	147
6.1	Conclusion	147
6.2	Future Work	147
7	Using Matlab to Generate MIMO Channel	149
7.1	System Parameters	149
	Bibliography	151



List of Figures

2.1	OFDMA parameters (from [10, Table 775]).	9
2.2	More OFDMA parameters (from [10, Table 775]).	10
2.3	Basic frame structure for 5, 10 and 20 MHz channel bandwidths (Fig.466 in [10]).	10
2.4	Example of downlink physical structure (Fig.485 in [10]).	12
2.5	Mapping between SAC and K_{SB} for FFT size 2048 (from [10, Table 783]). .	14
2.6	Mapping between SAC and K_{SB} for FFT size 1024 (from [10, Table 784]). .	14
2.7	Mapping between SAC and K_{SB} for FFT size 512 (from [10, Table 785]). . .	15
2.8	PRU to PRU_{SB} and PRU_{MB} mapping for BW = 10 MHz, and $K_{SB}=7$	15
2.9	Mapping from PRUs to PRU_{SB} and $PPRU_{MB}$ for BW = 10 MHz and $K_{SB} = 7$	17
2.10	Mapping between DFPC and frequency partitioning for FFT size 2048 (from [10, Table 786]).	18
2.11	Mapping between DFPC and frequency partitioning for FFT size 1024 (from [10, Table 787]).	18
2.12	Mapping between DFPC and frequency partitioning for FFT size 512 (from [10, Table 788]).	19

2.13	Frequency partitioning for $BW = 10$ MHz, $K_{SB} = 7$, $FPCT = 4$, $FPS = 12$, and $DFPSC = 2$	19
2.14	Mapping between $DCAS_{MB,0}$ and number of miniband based CRUs for FP_0 for FFT size 2048 (from [10, Table 789]).	22
2.15	Mapping between $DCAS_{MB,0}$ and number of miniband based CRUs for FP_0 for FFT size 1024 (from [10, Table 790]).	23
2.16	Mapping between $DCAS_{MB,0}$ and number of miniband based CRUs for FP_0 for FFT size 512 (from [10, Table 791]).	23
2.17	PRU to PRU_{SB} mapping for the test case.	29
2.18	PRU to PRU_{MB} mapping for the test case.	31
2.19	PRU_{MB} to $PPRU_{MB}$ mapping for the test case.	32
2.20	PRU_{SB} and $PPRU_{MB}$ to PRU_{FP1} mapping for the test case.	33
2.21	The mapping of PRU_{FP1} s to CRU/DRU for the test case.	35
2.22	OFDMA parameters (Table 793 in [10]).	37
2.23	OFDMA parameters (from [10, Table 794]).	37
2.24	Example of MIMO midamble structure for the case of 4 transmit antennas (Figure 502 in [10]).	37
2.25	Location of the A-Preamble symbols (Figure 506 in [10]).	41
2.26	Symbol structure of PA-Preamble in frequency domain (Figure 507 in [10]). .	41
2.27	Sequences of PA-Preamble in frequency domain (from [10, Table 796]). . . .	42
2.28	Boosting factors for PA-Preamble symbols (Table 797 in [10]).	43
2.29	Parameters and values for resource allocation of SFH (from [10, Table 806]).	45

2.30	Illustration of periodic transmission of S-SFH SPs with example transmission periodicity of 40 ms, 80 ms and 160 ms for SP1, SP2 and SP3, respectively (Figure 515 in [10]).	46
2.31	Transmission Periodicity of S-SFH SPs (from [10, Table 807]).	47
2.32	Example of locations of A-MAP regions in a TDD system (From [10, Fig 516]).	47
2.33	Structure of an A-MAP region (Figure 517 in [10]).	48
2.34	Physical processing block diagram for the P-SFH (Figure 518 in [10]).	50
2.35	Physical processing block diagram for the S-SFH (Figure 519 in [10]).	51
2.36	Chain of non-user specific A-MAP IE to non-user specific A-MAP symbols (Figure 520 in [10]).	52
2.37	Chain of HF-A-MAP IE to HF-A-MAP symbols (Figure 521 in [10]).	53
2.38	Chain of PC-A-MAP IE to PC-A-MAP symbols (Figure 522 in [10]).	55
2.39	Chain of A-A-MAP IE to A-A-MAP symbols (Figure 523 in [10]).	56
3.1	DL MIMO architecture (Fig. 537 in [10]).	59
3.2	Codebook subsets used for non-adaptive precoding in DL-DLRLU and NLRU (from [10, Table 842]).	63
3.3	Codebook subsets used for non-adaptive precoding in DL-SLRLU (from [10, Table 843]).	64
3.4	Downlink MIMO modes (from [10, Table 844]).	66
3.5	DL MIMO parameters (from [10, Table 845]).	67
3.6	DL MIMO parameters (from [10, Table 845]).	68

3.7	Supported Permutation for each DL MIMO mode outside the OL region (from [10, Table 846]).	70
3.8	Supported Permutation for each DL MIMO mode in the OL region (from [10, Table 847]).	70
3.9	Types of open-loop regions (from [10, Table 848]).	72
3.10	MIMO feedback modes (from [10, Table 849]).	75
3.11	DL MIMO control parameters (from [10, Table 850]).	76
3.12	DL MIMO control parameters (from [10, Table 850]).	77
3.13	Subset selection of the base codebook for four transmit antennas (from [10, Table 866]).	78
3.14	Base codebook $c(2,1,3)$ (from [10, Table 851]).	79
3.15	Base codebook $c(2,2,3)$ (from [10, Table 852]).	80
3.16	Quantization parameters for diagonal entries of R (from [10, Table 867]). . .	81
3.17	Quantization parameters for non-diagonal entries of R (from [10, Table 868]).	82
3.18	$D(2,1,4)$ codebook (from [10, Table 869]).	86
3.19	$D(2,2,4)$ codebook (from [10, Table 870]).	86
3.20	Codebook subsets used for non-adaptive precoding in UL DLRU and NLRU (from [10, Table 921]).	88
3.21	Codebook subsets used for non-adaptive precoding in UL SLRU (from [10, Table 922]).	88
3.22	Uplink MIMO modes (from [10, Table 923]).	89
3.23	UL MIMO parameters (from [10, Table 924]).	90

3.24	Supported permutation for each UL MIMO mode (from [10, Table 925]). . .	91
3.25	UL MIMO control parameters (from [10, Table 926]).	92
4.1	System model.	94
4.2	System model with feedback.	97
4.3	Number of flops of different matrix operations [16].	101
4.4	Number of flops per subcarrier of each method.	102
5.1	Suburban macrocell channel model [9].	104
5.2	IEEE 802.16m TDD frame structure for 10 MHz [9].	106
5.3	TDD structure for 10 MHz.	106
5.4	MSE and SER for QPSK resulting from simulation compared with theory in AWGN.	108
5.5	MSE and SER for QPSK using ZF equalizer with no feedback in Suburban channel.	109
5.6	MSE and SER for QPSK using ZF equalizer with SVD-Based search feedback in Suburban channel.	110
5.7	MSE and SER for QPSK using ZF equalizer with MMSE-Based exhaustive search feedback in Suburban channel.	111
5.8	MSE and SER for QPSK using ZF equalizer with MaxminSNR-Based search feedback in singlepath Suburban channel.	112
5.9	MSE and SER for QPSK using ZF equalizer with Optimum precoder feedback in Suburban channel.	113

5.10 MSE and SER for QPSK using ZF equalizer with different feedback methods at 30 km/h in Suburban channel.	114
5.11 MSE and SER for QPSK using ZF equalizer with different feedback methods at 120 km/h in Suburban channel.	115
5.12 MSE and SER for QPSK using MMSE equalizer with no feedback in Suburban channel.	116
5.13 MSE and SER for QPSK using MMSE equalizer with SVD-Based search feed- back in Suburban channel.	117
5.14 MSE and SER for QPSK using MMSE equalizer with MMSE-Based exhaus- tive search feedback in Suburban channel.	118
5.15 MSE and SER for QPSK using MMSE equalizer with MaxminSNR-Based search feedback in Suburban channel.	119
5.16 MSE and SER for QPSK using MMSE equalizer with Optimum precoder feedback in Suburban channel.	120
5.17 MSE and SER for QPSK using MMSE equalizer with different feedback meth- ods at 30 km/h in Suburban channel.	121
5.18 MSE and SER for QPSK using MMSE equalizer with different feedback meth- ods at 120 km/h in Suburban channel.	122
5.19 MSE and SER for QPSK using ZF and MMSE equalizer with different feed- back methods at 30 km/h in Suburban channel.	123
5.20 MSE and SER for QPSK using ZF and MMSE equalizer with different feed- back methods at 120 km/h in Suburban channel.	124

5.21 MSE and SER for QPSK using ZF equalizer with no feedback in multipath Suburban channel.	126
5.22 MSE and SER for QPSK using ZF equalizer with SVD-Based search feedback in multipath Suburban channel.	127
5.23 MSE and SER for QPSK using ZF equalizer with MMSE-Based exhaustive search feedback in multipath Suburban channel.	128
5.24 MSE and SER for QPSK using ZF equalizer with MaxminSNR-Based search feedback in multipath Suburban channel.	129
5.25 MSE and SER for QPSK using ZF equalizer with Optimum precoder feedback in multipath Suburban channel.	130
5.26 MSE and SER for QPSK using ZF equalizer with different feedback methods at 30 km/h in multipath Suburban channel.	131
5.27 MSE and SER for QPSK using ZF equalizer with different feedback methods at 120 km/h in multipath Suburban channel.	132
5.28 MSE and SER for QPSK using MMSE equalizer with no feedback in multipath Suburban channel.	133
5.29 MSE and SER for QPSK using MMSE equalizer with SVD-Based search feedback in multipath Suburban channel.	134
5.30 MSE and SER for QPSK using MMSE equalizer with MMSE-Based exhaustive search feedback in multipath Suburban channel.	135
5.31 MSE and SER for QPSK using MMSE equalizer with MaxminSNR-Based search feedback in multipath Suburban channel.	136

5.32 MSE and SER for QPSK using MMSE equalizer with Optimum precoder feedback in multipath Suburban channel.	137
5.33 MSE and SER for QPSK using MMSE equalizer with different feedback methods at 30 km/h in multipath Suburban channel.	138
5.34 MSE and SER for QPSK using MMSE equalizer with different feedback methods at 120 km/h in multipath Suburban channel.	139
5.35 MSE and SER for QPSK using ZF and MMSE equalizer with different feedback methods at 30 km/h in multipath Suburban channel.	140
5.36 MSE and SER for QPSK using ZF and MMSE equalizer with different feedback methods at 120 km/h in multipath Suburban channel.	141
5.37 MSE and SER for QPSK using ZF equalizer with SVD-Based search feedback in multipath Suburban channel with TX4 RX4 Rank2.	142
5.38 MSE and SER for QPSK using ZF equalizer with MMSE-Based exhaustive search feedback in multipath Suburban channel with TX4 RX4 Rank2. . . .	143
5.39 MSE and SER for QPSK using ZF equalizer with Optimum precoder feedback in multipath Suburban channel with TX4 RX4 Rank2.	144
5.40 MSE and SER for QPSK using ZF equalizer with different feedback methods at 30 km/h in multipath Suburban channel with TX4 RX4 Rank2.	145
5.41 MSE and SER for QPSK using ZF equalizer with different feedback methods at 120 km/h in multipath Suburban channel with TX4 RX4 Rank2.	146

List of Tables

2.1	PRU Structures for Different Types of Subframe	7
2.2	Mapping Between PRU Index and PRU_{SB} Index for the Test Case	28
2.3	Mapping Between PRU Index and $PPRU_{MB}$ Index for the Test Case	30
2.4	Mapping Between PRU_{MB} Index and $PPRU_{MB}$ Index for the Test Case	30
2.5	Mapping Between PRU_{SB} Index, $PPRU_{MB}$ Index, and PRU_{FP1} Index for the Test Case	32
2.6	Mapping Between PRU_{SB} Index, $PPRU_{MB}$ Index, and PRU_{FP2} Index for the Test Case	34
2.7	Mapping Between PRU_{SB} Index, $PPRU_{MB}$ Index, and PRU_{FP3} Index for the Test Case	34
2.8	Mapping Between PRU_{SB} Index, $PPRU_{MB}$ Index, and PRU_{FP4} Index for the Test Case	34
2.9	Random Sequence for the Test Case	34
2.10	Mapping Between PRU_{FP1} Index and CRU_{FP1}/DRU_{FP1} Index	35
5.1	OFDMA Downlink Parameters	105

Chapter 1

Introduction

1.1 Scope of the Work

Orthogonal frequency division multiple access (OFDMA) has emerged as one of the prime multiple access schemes for broadband wireless networks. Some major examples are IEEE 802.16 Mobile WiMAX, IEEE 802.20 and 3GPP LTE. As a special case of multicarrier multiple access schemes, OFDMA exclusively assigns each subchannel to only one user, eliminating intra-cell interference [12]. In frequency selective channels, an intrinsic advantage of OFDMA is its capability to exploit the so-called multiuser diversity provided by multipath channels. Other advantages of OFDMA include finer granularity and better link budget [12]. OFDMA can be easily generated using an inverse fast Fourier transform (IFFT) and received using a fast Fourier transform (FFT).

The IEEE 802.16 standard committee has developed a group of standards for wireless metropolitan area networks (MANs). OFDMA is used in the 2 to 11 GHz systems. The IEEE Standard 802.16-2004 was for broadband wireless access systems that provide a variety of wireless access services to fixed outdoor and indoor users. The 802.16e was designed to support terminal mobility with a speed up to 120 km/h [15]. The last two standards have now been combined in IEEE 802.16-2009.

In response to International Telecommunication Union Radiocommunication Section (ITU-R)'s plan for the fourth-generation mobile communication standard IMT-Advanced, the IEEE 802.16 standards group has set up the 802.16m (i.e., Advanced WiMAX) task group. The new frame structure developed by IEEE 802.16m can be compatible with IEEE 802.16e, reduce communication latency, support relay, and coexist with other radio access techniques (in particular, LTE). In the IEEE 802.16m working group, the high-level system description and evaluation methodology are captured in [9]. MIMO technologies again play an essential role in achieving the ambitious target set, which requires the 802.16m system to deliver twice the performance gain over a baseline 802.16e system in various measures, including sector throughput, average user throughput, and peak data rate, as well as cell-edge performance. Several new MIMO ingredients are proposed. Noticeable ones are transformed codebook for beamforming feedback, differential beamforming feedback, open-loop multiuser MIMO, and collaborative multicell MIMO [13]. We study the MIMO architecture and signal processing technology for 802.16m. In particular, we consider the zero-forcing (ZF) equalizer and minimum mean-square error (MMSE) equalizer approach wherein we employ the technique proposed in [2]. We follow [2] to introduce the ZF and MMSE equalizer with channel feedback selection problem.

This thesis focuses on the precoding and equalization for the spatial multiplexing mode of IEEE 802.16m closed-loop (CL) multi-input multi-output (MIMO) systems. A problem associated with precoding is that the channel state information must be known at the transmitter. This may be difficult since the bandwidth of the feedback channel is usually limited. Thus, a codebook-based limited feedback precoding scheme is generally used. The main idea is to quantize the precoding matrix and feedback the index of the optimum precoder. We propose two methods to select the best precoder from a finite set of precoding matrices and we will compare with two other methods. We simulate the IEEE 802.16m MIMO system

and study the performance of different channel feedback selection methods.

1.2 Organization and Contribution of this Thesis

This thesis is organized as follows.

- Chapter 2 introduces the IEEE 802.16m OFDMA.
- Chapter 3 introduces the IEEE 802.16m MIMO.
- Chapter 4 introduces equalization and closed-loop MIMO technology.
- Chapter 5 presents some simulation results.
- Chapter 6 gives the conclusion and indicates future work.

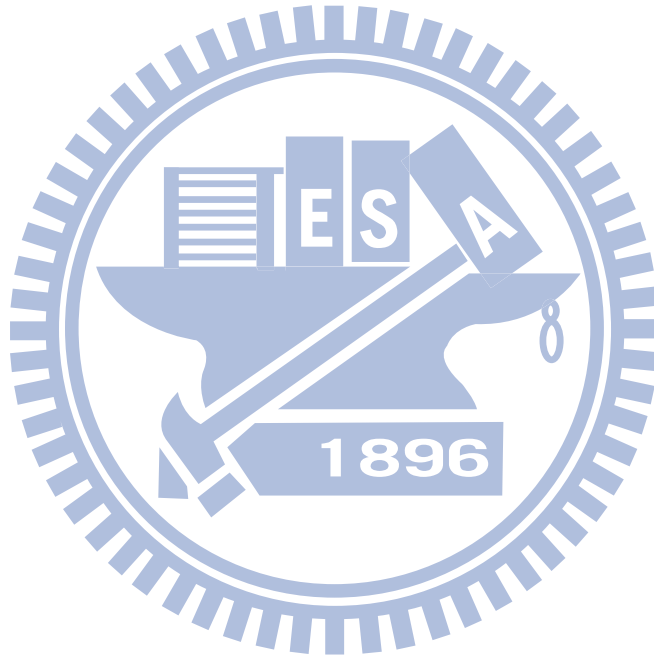
In this thesis, our work can be summarized as following:

- Study IEEE 802.16m OFDMA.
- Study IEEE 802.16m MIMO
- Study equalization and closed-loop MIMO
 - Study the equalization and feedback technology in the IEEE 802.16m MIMO systems.
 - Analyze the error performance.
 - Discuss on the feedback selection method.

Main contribution of this thesis are as follows:

1. Introduce feedback technology for the IEEE 802.16m MIMO systems.

2. Propose two feedback selection schemes for the IEEE 802.16m MIMO systems.
3. Develop an error analysis scheme for the IEEE 802.16m MIMO systems.
4. Compare performance of four different feedback selection methods for the IEEE 802.16m MIMO systems.



Chapter 2

Introduction to IEEE 802.16m OFDMA

We first introduce the basic concepts of the OFDMA in the specification of IEEE 802.16m and then MIMO techniques for multicarrier modulation in the specification of IEEE 802.16m. Much of the material in this chapter is taken from [10].

2.1 Basic OFDMA Symbol Structure and Frame Structure [10]

The Advanced Air Interface (AAI) defined by IEEE 802.16m is designed for nonline-of-sight (NLOS) operation in the licensed frequency bands below 6 GHz. The AAI supports both time-division duplexing (TDD) and frequency-division duplexing (FDD) operation, allowing also half-FDD (H-FDD) operation at mobile stations (MSs). Unless otherwise specified, the frame structure attributes and baseband processing are common for all duplex modes.

The AAI uses OFDMA as the multiple access scheme in the downlink and the uplink. The material of this section is taken from [10].

2.1.1 OFDMA Basic Terms

We introduce some basic terms in the OFDMA physical layer (PHY) of IEEE 802.16m. They help us understand the concepts of subcarrier allocation and transmission in IEEE 802.16m OFDMA.

- Physical and logical resource units: A physical resource unit (PRU) is the basic physical unit for resource allocation. It comprises $P_{sc}(= 18)$ consecutive subcarriers by N_{sym} consecutive OFDMA symbols, $N_{sym} = 6$ for type-1 subframes, $N_{sym} = 7$ for type-2 subframes, and $N_{sym} = 5$ for type-3 subframes. Table 1.1 summarizes the PRUs sizes for different subframe types. A logical resource unit (LRU) is the basic logical unit for distributed and localized resource allocations. An LRU contains $P_{sc} \cdot N_{sym}$ subcarriers for the three types of subframes. The LRU includes the pilots that are used in a PRU. The effective number of subcarriers in an LRU depends on the number of allocated pilots.
- Contiguous resource unit: The localized resource unit, also known as contiguous resource unit (CRU), contains a group of subcarriers which are contiguous across the localized resource allocations. The size of CRU equals the size of PRU, i.e., P_{sc} subcarriers by N_{sym} OFDMA symbols.
- Distributed resource unit: A distributed resource unit (DRU) contains a group of subcarriers which are spread across the distributed resource allocations within a frequency partition. The size of DRU also equals the size of PRU.

2.1.2 Frequency Domain Description

An OFDMA symbol is made up of subcarriers, the number of which determines the discrete Fourier transform (DFT) size used. There are several subcarrier types:

Table 2.1: PRU Structures for Different Types of Subframe

Subframe Type	Number of Subcarriers	Number of Symbols
Type-1	18	6
Type-2	18	7
Type-3	18	5

- Data subcarriers: used for data transmission.
- Pilot subcarriers: used for various estimation purposes.
- Null subcarriers: no transmission at all, used for guard bands and DC subcarrier.

The purpose of the guard bands is to help enable proper bandlimiting.

2.1.3 Primitive Parameters

Four primitive parameters characterize the OFDMA symbols:

- BW : the nominal channel bandwidth.
- N_{used} : number of used subcarriers (which includes the DC subcarrier).
- n : sampling factor. This parameter, in conjunction with BW and N_{used} , determines the subcarrier spacing and the useful symbol time. This value is given in Figs. 2.1 and 2.2 for each nominal bandwidth.
- G : This is the ratio of CP time to “useful” time, i.e., T_{cp}/T_s . The following values shall be supported: 1/16, 1/8, and 1/4.

2.1.4 Derived Parameters

The following parameters are defined in terms of the primitive parameters.

- N_{FFT} : smallest power of two greater than N_{used} .
- Sampling frequency: $F_s = \lfloor n \cdot BW/8000 \rfloor \times 8000$.
- Subcarrier spacing: $\Delta f = F_s/N_{FFT}$.
- Useful symbol time: $T_b = 1/\Delta f$.
- CP time: $T_g = G \times T_b$.
- OFDMA symbol time: $T_s = T_b + T_g$.
- Sampling time: T_b/N_{FFT} .

2.1.5 Frame Structure

The AAI basic frame structure is illustrated in Fig. 2.3. Each 20 ms superframe is divided into four 5-ms radio frames. When using the same OFDMA parameters as in Figs. 2.1 and 2.2 with channel bandwidth of 5, 10, or 20 MHz, each 5-ms radio frame further consists of eight subframes for $G = 1/8$ and $1/16$. With channel bandwidth of 8.75 or 7 MHz, each 5-ms radio frame further consists of seven and six subframes, respectively, for $G = 1/8$ and $1/16$. In the case of $G = 1/4$, the number of subframes per frame is one less than that of other CP lengths for each bandwidth case. A subframe shall be assigned for either downlink (DL) or uplink (UL) transmission. There are four types of subframes:

- Type-1 subframe consists of six OFDMA symbols.
- Type-2 subframe consists of seven OFDMA symbols.
- Type-3 subframe consists of five OFDMA symbols.

The nominal channel bandwidth, BW(MHz)			5	7	8.75	10	20
Sampling factor, n			28/25	8/7	8/7	28/25	28/25
Sampling frequency, F_s (MHz)			5.6	8	10	11.2	22.4
FFT size, N_{FFT}			512	1024	1024	1024	2048
Subcarrier spacing, Δf (kHz)			10.94	7.81	9.77	10.94	10.94
Useful symbol time, $T_b(\mu s)$			91.4	128	102.4	91.4	91.4
CP ratio, G=1/8	OFDMA symbol time, $T_s(\mu s)$		102.857	144	115.2	102.857	102.857
	FDD	Number of OFDMA symbols per 5ms frames	48	34	43	48	48
		Idle time(μs)	62.857	104	46.40	62.857	62.857
	TDD	Number of OFDMA symbols per 5ms frames	47	33	42	47	47
		TTG+RTG(μs)	165.714	248	161.6	165.714	165.714
CP ratio, G=1/16	OFDMA symbol time, $T_s(\mu s)$		97.143	136	108.8	97.143	97.143
	FDD	Number of OFDMA symbols per 5ms frames	51	36	45	51	51
		Idle time(μs)	45.71	104	104	45.71	45.71
	TDD	Number of OFDMA symbols per 5ms frames	50	35	44	50	50
		TTG+RTG(μs)	142.853	240	212.8	142.853	142.853

Figure 2.1: OFDMA parameters (from [10, Table 775]).

CP ratio, G=1/4	OFDMA symbol time, T _s (μs)		114.286	160	128	114.286	114.286
	FDD	Number of OFDMA symbols per 5ms frames	43	31	39	43	43
		Idle time(μs)	85.694	40	8	85.694	85.694
	TDD	Number of OFDMA symbols per 5ms frames	42	30	38	42	42
		TTG+RTG(μs)	199.98	200	136	199.98	199.98
Number of Guard Subcarriers	Left		40	80	80	80	160
	Right		39	79	79	79	159
Number of Used Subcarriers			433	865	865	865	1729
Number of Physical Resource Unit(18×6) in a type-1 subframe			24	48	48	48	96

Figure 2.2: More OFDMA parameters (from [10, Table 775]).

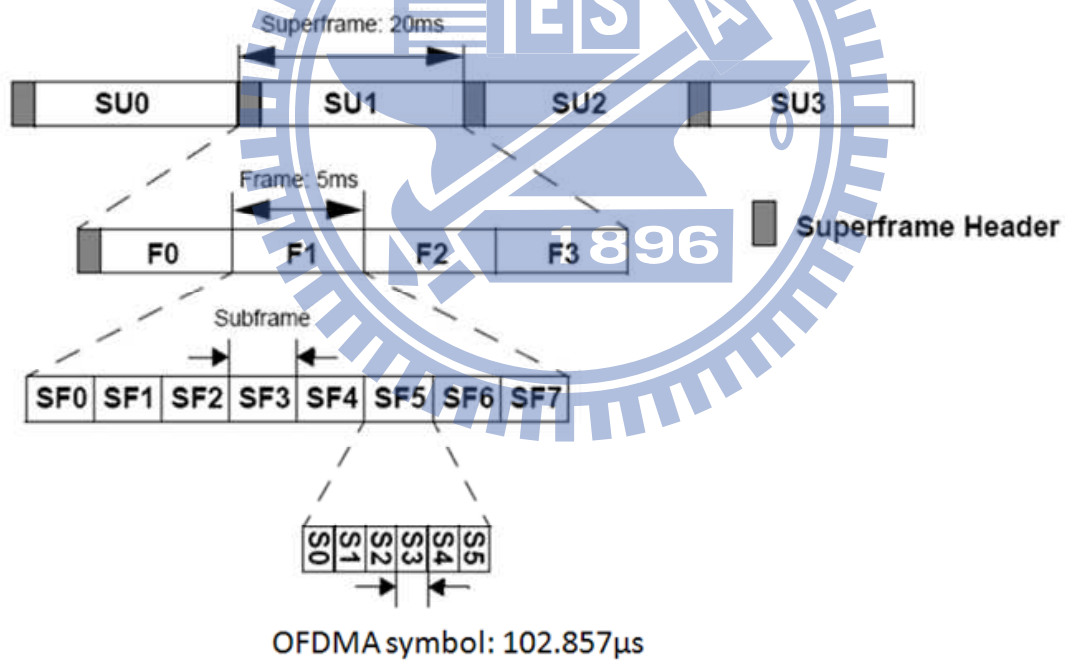


Figure 2.3: Basic frame structure for 5, 10 and 20 MHz channel bandwidths (Fig.466 in [10]).

- Type-4 subframe consists of nine OFDMA symbols. This type shall be applied only to UL subframe for the 8.75 MHz channel bandwidth when supporting the WirelessMAN-OFDMA frames.

The basic frame structure is applied to FDD and TDD duplexing schemes, including H-FDD MS operation. The number of switching points in each radio frame in TDD systems shall be two, where a switching point is defined as a change of directionality, i.e., from DL to UL or from UL to DL.

A data burst shall occupy either one subframe (i.e., the default transmission time interval [TTI] transmission) or contiguous multiple subframes (i.e., the long TTI transmission). The long TTI in FDD shall be 4 subframes for both DL and UL. The long TTI in TDD shall be the whole DL (UL) subframes for DL (UL) in a frame. Every superframe shall contain a superframe header (SFH). The SFH shall be located in the first DL subframe of the superframe and shall include broadcast channels.

2.2 Downlink Transmission in IEEE 802.16m OFDMA[10]

Again this section is mainly taken from [10]. Each DL subframe is divided into 4 or fewer frequency partitions; each partition consists of a set of PRUs across the total number of OFDMA symbols available in the subframe. Each frequency partition can include contiguous (localized) and/or non-contiguous (distributed) PRUs. Each frequency partition can be used for different purposes such as fractional frequency reuse (FFR) or multicast and broadcast services (MBS). Fig. 2.4 illustrates the downlink physical structure in an example of two frequency partitions with frequency partition 2 including both CRUs and DRUs.

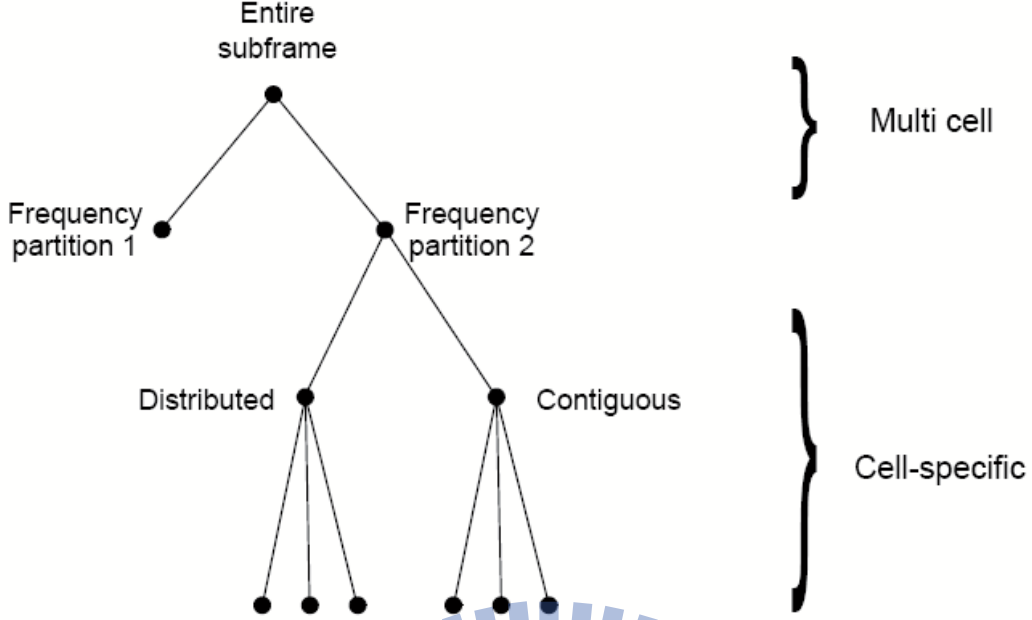


Figure 2.4: Example of downlink physical structure (Fig.485 in [10]).

2.2.1 Subband Partitioning

The PRUs are first subdivided into subbands and minibands where a subband comprises N_1 adjacent PRUs and a miniband comprises N_2 adjacent PRUs, where $N_1 = 4$ and $N_2 = 1$. Subbands are suitable for frequency selective allocations as they provide a contiguous allocation of PRUs in frequency. Minibands are suitable for frequency diverse allocation and are permuted in frequency.

The number of subbands reserved is denoted by K_{SB} . The number of PRUs allocated to subbands is denoted by L_{SB} , where $L_{SB} = N_1 \cdot K_{SB}$, depending on system bandwidth. A 5, 4 or 3 bit field called Downlink Subband Allocation Count ($DSAC$) determines the value of K_{SB} depending on FFT size. The $DSAC$ is transmitted in the SFH. The remaining PRUs are allocated to minibands. The number of minibands in an allocation is denoted by K_{MB} . The number of PRUs allocated to minibands is denoted by L_{MB} , where $L_{MB} = N_2 \cdot K_{MB}$.

The total number of PRUs is denoted as N_{PRU} where $N_{PRU} = L_{SB} + L_{MB}$. The maximum number of subbands that can be formed is denoted as N_{sub} where $N_{sub} = \lfloor N_{PRU}/N_1 \rfloor$.

Figs. 2.5 and 2.7 show the mapping between SAC and K_{SB} for FFT sizes 2048, 1024, and 512, respectively. For system bandwidths in the range of (10, 20]MHz, the mapping between $DSAC$ and K_{SB} is based on Fig 2.5, and the maximum valid value of K_{SB} is $N_{PRU}/4 - 3$. For system bandwidths in the range of [5, 10]MHz, the mapping between $DSAC$ and K_{SB} is based on Fig 2.6, and the maximum valid value of K_{SB} is $N_{PRU}/4 - 2$.

The subband PRUs and miniband PRUs are denoted PRU_{SB} and PRU_{MB} , respectively. The set of PRU_{SB} is numbered from 0 to $L_{SB} - 1$, and the set of PRU_{MB} is numbered from 0 to $L_{MB} - 1$. The mapping of PRUs to PRU_{SB} is

$$PRU_{SB}[j] = PRU[i], \quad j = 0, 1, \dots, L_{SB} - 1, \quad (2.1)$$

where

$$i = N_1 \cdot \left\{ \left\lceil \frac{N_{sub}}{K_{SB}} \right\rceil \cdot \left\lfloor \frac{j}{N_1} \right\rfloor + \left\lfloor \frac{j}{N_1} \right\rfloor \cdot \frac{GCD(N_{sub}, \lceil \frac{N_{sub}}{K_{SB}} \rceil)}{N_{sub}} \right\} \bmod N_{sub} + j \cdot N_1 \quad (2.2)$$

with $GCD(x, y)$ being the greatest common divisor of x and y . And the mapping of PRUs to PRU_{MB} is defined as

$$PRU_{MB}[k] = PRU[i], \quad k = 0, 1, \dots, L_{MB} - 1, \quad (2.3)$$

where

$$i = \begin{cases} N_1 \cdot \left\{ \left\lceil \frac{N_{sub}}{K_{SB}} \right\rceil \cdot \left\lfloor \frac{k}{N_1} \right\rfloor + \left\lfloor \frac{k}{N_1} \right\rfloor \cdot \frac{GCD(N_{sub}, \lceil \frac{N_{sub}}{K_{SB}} \rceil)}{N_{sub}} \right\} \bmod N_{sub} & K_{SB} > 0, \\ + (k) \bmod N_1, & \\ k, & K_{SB} = 0. \end{cases} \quad (2.4)$$

Fig 2.8 illustrates the PRU to PRU_{SB} and PRU_{MB} mapping for a 10MHz bandwidth system with $K_{SB} = 7$.

SAC	# of subbands allocated(K_{SB})	SAC	# of subbands allocated(K_{SB})
0	0	16	16
1	1	17	17
2	2	18	18
3	3	19	19
4	4	20	20
5	5	21	21
6	6	22	NA.
7	7	23	NA.
8	8	24	NA.
9	9	25	NA.
10	10	26	NA.
11	11	27	NA.
12	12	28	NA.
13	13	29	NA.
14	14	30	NA.
15	15	30	NA.

Figure 2.5: Mapping between SAC and K_{SB} for FFT size 2048 (from [10, Table 783]).

SAC	# of subbands allocated(K_{SB})	SAC	# of subbands allocated(K_{SB})
0	0	8	8
1	1	9	9
2	2	10	10
3	3	11	NA.
4	4	12	NA.
5	5	13	NA.
6	6	14	NA.
7	7	15	NA.

Figure 2.6: Mapping between SAC and K_{SB} for FFT size 1024 (from [10, Table 784]).

SAC	# of subbands allocated (K_{SB})	SAC	# of subbands allocated (K_{SB})
0	0	4	4
1	1	5	NA.
2	2	6	NA.
3	3	7	NA.

Figure 2.7: Mapping between SAC and K_{SB} for FFT size 512 (from [10, Table 785]).

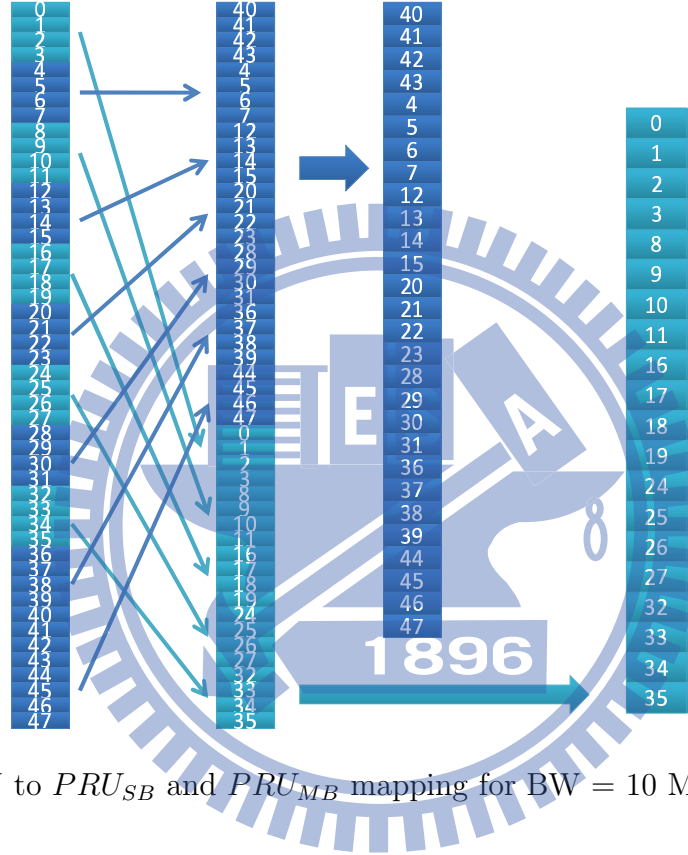


Figure 2.8: PRU to PRU_{SB} and PRU_{MB} mapping for BW = 10 MHz, and $K_{SB}=7$.

2.2.2 Miniband Permutation

The miniband permutation maps the PRU_{MBs} to Permuted PRU_{MBs} ($PPRU_{MBs}$) to ensure that frequency diverse PRUs are allocated to each frequency partition. Fig. 2.8 together with Fig 2.19 shows an example. The following equation provides a mapping from PRU_{MB} to

$PPRU_{MB}$:

$$PPRU_{MB}[j] = PRU_{MB}[i], \quad j = 0, 1, \dots, L_{MB} - 1, \quad (2.5)$$

where

$$i = (q(j) \bmod D) \cdot P + \lfloor \frac{q(j)}{D} \rfloor, \quad (2.6)$$

$$P = \min(K_{MB}, N_1/N_2), \quad (2.7)$$

$$r(j) = \max(j - ((K_{MB} \bmod P) \cdot D), 0), \quad (2.8)$$

$$q(j) = j + \lfloor \frac{r(j)}{D - 1} \rfloor, \quad (2.9)$$

$$D = \lfloor \frac{K_{MB}}{P} + 1 \rfloor. \quad (2.10)$$

2.2.3 Frequency Partitioning

The PRU_{SB} and $PPRU_{MB}$ are allocated to one or more frequency partitions. By default, only one partition is present. The maximum number of frequency partitions is 4. The frequency partition configuration is transmitted in the SFH in a 4 or 3 bit called the Downlink Frequency Partition Configuration (DFPC) depending on FFT size. Frequency Partition Count (FPCT) defines the number of frequency partitions. Frequency Partition Size (FPS_i) defines the number of PRUs allocated to FP_i . FPCT and FPS_i are determined from FPC as shown in Figs.2.10 to 2.12. A 3, 2, or 1-bit parameter called the Downlink Frequency Partition Subband Count (DFPSC) defines the number of subbands allocated to FP_i , $i > 0$. Fig. 2.13 continues the examples in Fig. 2.8 and 2.9 and shows how PRU_{SB} and $PPRU_{MB}$ can be mapped to frequency partitions.

The number of subbands in i th frequency partition is denoted by K_{SB,FP_i} . The number of minibands is denoted by K_{MB,FP_i} , which is determined by FPS_i and $DFPSC$ fields. When $DFPC = 0$, $DFPSC$ must be equal to 0. The number of subband PRUs in each frequency partition is denoted by L_{SB,FP_i} , which is given by $L_{SB,FP_i} = N_1 \cdot K_{SB,FP_i}$. The

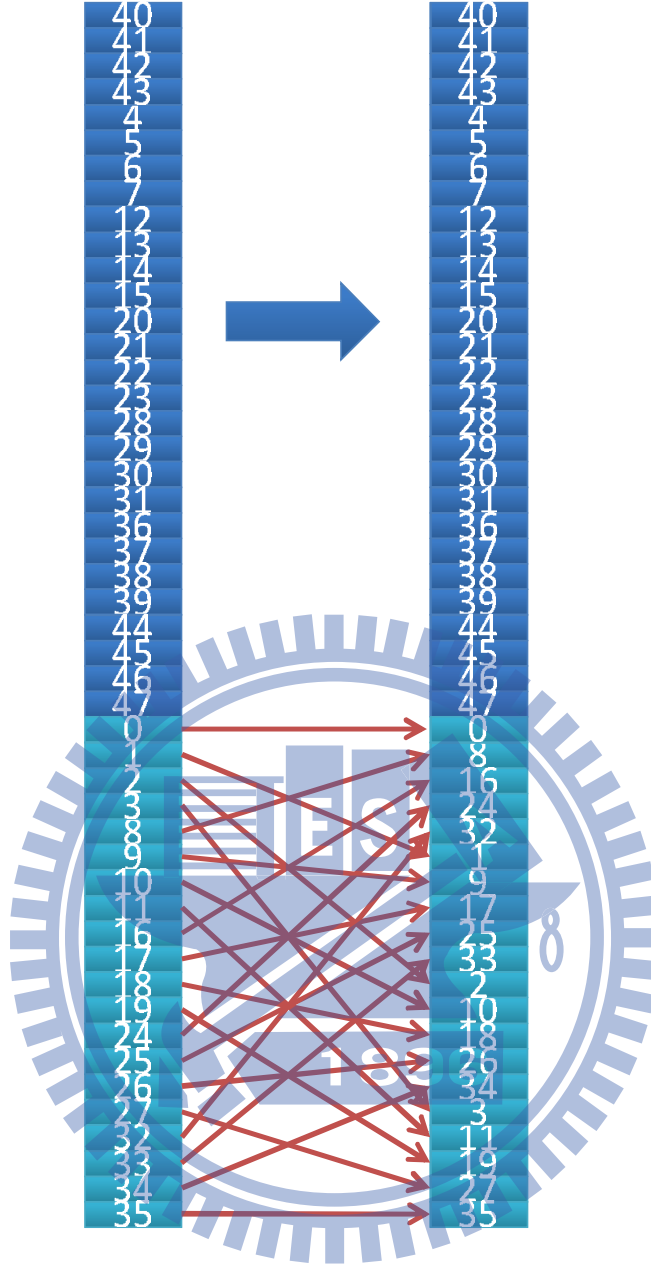


Figure 2.9: Mapping from PRUs to PRU_{SB} and $PPRU_{MB}$ for $BW = 10$ MHz and $K_{SB} = 7$.

number of miniband PRUs in each frequency partition is denoted by $L_{MB,FPi}$, which is given by $L_{MB,FPi} = N_2 \cdot K_{MB,FPi}$. The number of subbands for each frequency partition is given

DFPC	Freq. Partitionong($FP_0:FP_1:FP_2:FP_3$)	FPCT	FPS_0	$FPS_i(i>0)$
0	1 : 0 : 0 : 0	1	N_{PRU}	0
1	0 : 1 : 1 : 1	3	0	$FPS_1 = N_{PRU} - 2 * \text{floor}(N_{PRU}/3)$ $FPS_2 = \text{floor}(N_{PRU}/3)$ $FPS_3 = \text{floor}(N_{PRU}/3)$
2	1 : 1 : 1 : 1	4	$N_{PRU} - 3 * \text{floor}(N_{PRU}/4)$	$\text{floor}(N_{PRU}/4)$
3	3 : 1 : 1 : 1	4	$N_{PRU} - 3 * \text{floor}(N_{PRU}/6)$	$\text{floor}(N_{PRU}/6)$
4	5 : 1 : 1 : 1	4	$N_{PRU} - 3 * \text{floor}(N_{PRU}/8)$	$\text{floor}(N_{PRU}/8)$
5	9 : 1 : 1 : 1	4	$N_{PRU} - 3 * \text{floor}(N_{PRU}/12)$	$\text{floor}(N_{PRU}/12)$
6	9 : 5 : 5 : 5	4	$N_{PRU} - 3 * \text{floor}(N_{PRU} * 5/24)$	$\text{floor}(N_{PRU} * 5/24)$
7	0 : 1 : 1 : 0	2	0	$N_{PRU}/2$ for $i=1, 2$ 0 for $i=3$
8	1 : 1 : 1 : 0	3	$N_{PRU} - 2 * \text{floor}(N_{PRU}/3)$	$\text{floor}(N_{PRU}/3)$ for $i=1, 2$ 0 for $i=3$
9-15	Reserved			

Figure 2.10: Mapping between DFPC and frequency partitioning for FFT size 2048 (from [10, Table 786]).

FPC	Freq. Partitionong($FP_0:FP_1:FP_2:FP_3$)	FPCT	FPS_0	$FPS_i(i>0)$
0	1 : 0 : 0 : 0	1	N_{PRU}	0
1	0 : 1 : 1 : 1	3	0	$FPS_1 = N_{PRU} - 2 * \text{floor}(N_{PRU}/3)$ $FPS_2 = \text{floor}(N_{PRU}/3)$ $FPS_3 = \text{floor}(N_{PRU}/3)$
2	1 : 1 : 1 : 1	4	$N_{PRU} - 3 * \text{floor}(N_{PRU}/4)$	$\text{floor}(N_{PRU}/4)$
3	3 : 1 : 1 : 1	4	$N_{PRU} - 3 * \text{floor}(N_{PRU}/6)$	$\text{floor}(N_{PRU}/6)$
4	5 : 1 : 1 : 1	4	$N_{PRU} - 3 * \text{floor}(N_{PRU}/8)$	$\text{floor}(N_{PRU}/8)$
5	9 : 5 : 5 : 5	4	$N_{PRU} - 3 * \text{floor}(N_{PRU} * 5/24)$	$\text{floor}(N_{PRU} * 5/24)$
6	0 : 1 : 1 : 0	2	0	$N_{PRU}/2$ for $i=1, 2$ 0 for $i=3$
7	1 : 1 : 1 : 0	3	$N_{PRU} - 2 * \text{floor}(N_{PRU}/3)$	$\text{floor}(N_{PRU}/3)$ for $i=1, 2$ 0 for $i=3$

Figure 2.11: Mapping between DFPC and frequency partitioning for FFT size 1024 (from [10, Table 787]).

FPC	Freq. Partitionong($FP_0:FP_1:FP_2:FP_3$)	FPCT	FPS_0	$FPS_i(i>0)$
0	1:0:0:0	1	N_{PRU}	0
1	0:1:1:1	3	0	$N_{PRU}/3$
2	1:1:1:1	4	$N_{PRU}/4$	$N_{PRU}/4$
3	3:1:1:1	4	$N_{PRU}/6$	$N_{PRU}/6$
4	9:5:5:5	4	$N_{PRU} * 3/8$	$N_{PRU} * 5/24$
5	0:1:1:0	2	0	$N_{PRU}/2$ for $i=1, 2$ 0 for $i=3$
6	1:1:1:0	3	$N_{PRU}/3$	$N_{PRU}/3$ for $i=1, 2$ 0 for $i=3$
7	Reserved			

Figure 2.12: Mapping between DFPC and frequency partitioning for FFT size 512 (from [10, Table 788]).

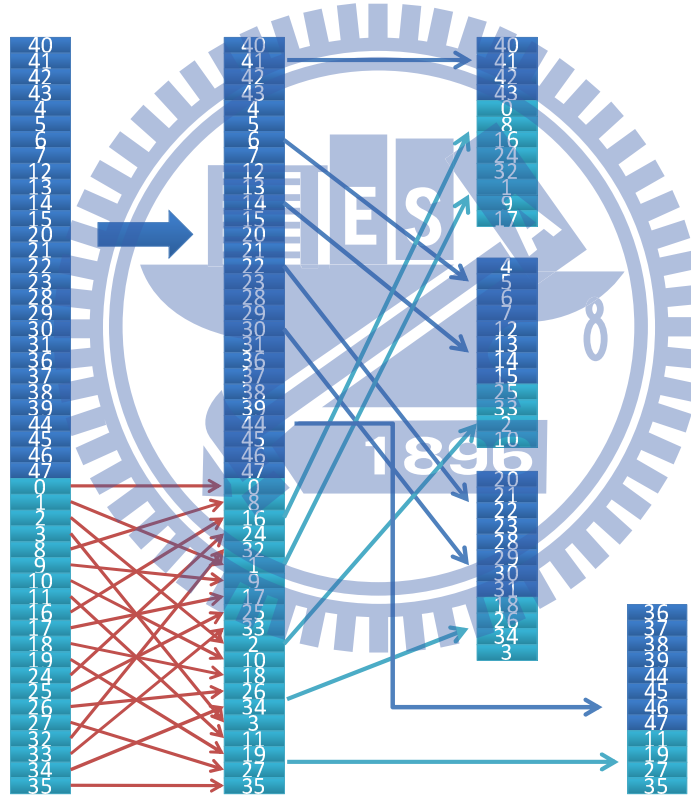


Figure 2.13: Frequency partitioning for $BW = 10$ MHz, $K_{SB} = 7$, $FPCT = 4$, $FPS = 12$, and $DFPSC = 2$.

by

$$K_{SB,FPi} = \begin{cases} K_{SB} - (FPCT - 1) \cdot DFPSC, & i = 0, FPCT = 4, \\ DFPSC, & i > 0, FPCT = 4, \\ DFPSC, & i > 0, FPSC = 3, DFPC = 1, \\ K_{SB} - (FPCT - 1) \cdot DFPSC, & i = 0, FPCT = 3, DFPC \neq 1, \\ DFPSC, & i = 1, 2, FPCT = 3, DFPC \neq 1, \\ DFPSC, & i = 1, 2, FPCT = 2, \\ K_{SB}, & i = 0, FPCT = 1, \end{cases} \quad (2.11)$$

where $FPCT = 2$ and $DFPSC = K_{SB}/2$. The number of minibands for each frequency partition is given by

$$K_{MB,FPi} = (FPS_i - K_{SB,FPi} \cdot N_1)/N_2, \quad 0 \leq i < FPCT. \quad (2.12)$$

The mapping of subband PRUs and miniband PRUs to the frequency partition is given by

$$PRU_{FPi}(j) = \begin{cases} PRU_{SB}(k_1), & 0 \leq j < L_{SB,FPi}, \\ PPRU_{MB}(k_2), & L_{SB,FPi} \leq j < (L_{SB,FPi} + L_{MB,FPi}), \end{cases} \quad (2.13)$$

where

$$k_1 = \sum_{m=0}^{i-1} L_{SB,FPm} + j \quad (2.14)$$

and

$$k_2 = \sum_{m=0}^{i-1} L_{SB,FPm} + j - L_{SB,FPi}. \quad (2.15)$$

Fig. 2.13 depicts the frequency partitioning for $BW = 10MHz$, $K_{SB} = 7$, $FPCT = 4$, $FPS_0 = FPS_i = 12$, and $DFPSC = 2$.

2.3 Cell-Specific Resource Mapping [10]

PRU_{FPi} s are mapped to LRUs. All further PRU and subcarrier permutations are constrained to the PRUs of a frequency partition.

2.3.1 CRU/DRU Allocation

The partition between CRUs and DRUs is done on a sector-specific basis. Let L_{SB-CRU,FP_i} and L_{MB-CRU,FP_i} denote the number of allocated subband CRUs and miniband CRUs for FP_i ($i \geq 0$). The number of total allocated subband and miniband CRUs, in units of a subband (i.e., N_1 PRUs), for FP_i ($i \geq 0$) is given by the downlink CRU allocation size, $DCAS_i$. The numbers of subband-based and miniband-based CRUs in FP_0 are given by $DCAS_{SB,0}$ and $DCAS_{MB,0}$, in units of a subband and a miniband, respectively. When $DFPC = 0$, $DCAS_i$ must be equal to 0.

For FP_0 , the value of $DCAS_{SB,0}$ is explicitly signaled in the SFH as a 5, 4 or 3 bit field to indicate the number of subbands in unsigned binary format, where $DCAS_{SB,0} \leq K_{SB,FP}$. A 5, 4 or 3 bit downlink miniband based CRU allocation size ($DCAS_{MB,0}$) is sent in the SFH only for partition FP_0 , depending on FFT size. The number of subband based CRUs for FP_0 is given by

$$L_{SBCRU,FP_0} = N_1 \cdot DCAS_{SB,0}. \quad (2.16)$$

The mapping between $DCAS_{MB,0}$ and the number of miniband based CRUs for FP_0 is shown in the Figs. 2.14 to 2.16 for FFT sizes of 2048, 1024 and 512, respectively. For those system bandwidths in range of (10, 20], the mapping between $DCAS_{MB,0}$ and number of miniband-based CRUs for FP_0 is based on Fig. 2.14, and the maximum valid value of L_{MB-CRU,FP_0} is less than $\lfloor 88 \cdot N_{PRU} \rfloor / 96$. For system bandwidths in the range of [5, 10], the mapping between $DCAS_{MB,0}$ and number of miniband-based CRUs for FP_0 is based on Fig. 2.15, and the maximum valid value of L_{MB-CRU,FP_0} is less than $\lfloor 42 \cdot N_{PRU} \rfloor / 48$.

For FP_i ($i > 0$, $FPCT \geq 2$) only one value for $DCAS_i$ is explicitly signaled for all $i > 0$, in the SFH as a 3, 2 or 1 bit field to signal the same numbers of allocated CRUs for FP_i ($i > 0$, $FPCT \geq 2$).

$DCAS_{MB,0}$	Number of miniband based CRU for FP_0	$DCAS_{MB,0}$	Number of miniband based CRU for FP_0
0	0	16	28
1	2	17	32
2	4	18	36
3	6	19	40
4	8	20	44
5	10	21	48
6	12	22	52
7	14	23	56
8	16	24	60
9	18	25	64
10	19	26	68
11	20	27	72
12	21	28	76
13	22	29	80
14	23	30	84
15	24	31	88

Figure 2.14: Mapping between $DCAS_{MB,0}$ and number of miniband based CRUs for FP_0 for FFT size 2048 (from [10, Table 789]).

For FP_i ($i > 0$, $FPCT \geq 2$), the number of subband CRUs (L_{SB-CRU,FP_i}) and miniband CRUs (L_{MB-CRU,FP_i}) are derived using the two equations.

$$L_{SB-CRU,FP_i} = N_1 \cdot \min\{DCAS_i, K_{SB,FP_i}\}, \quad (2.17)$$

$$L_{MB-CRU,FP_i} = \begin{cases} 0, & DCAS_i \leq K_{SB,FP_i}, \\ (DCAS_i - K_{SB,FP_i}) \cdot N_1, & DCAS_i > K_{SB,FP_i}, \end{cases} \quad (2.18)$$

When $FPCT = 2$, $DCAS_{SB,i}$ and $DCAS_{MB,i}$ for $i = 1$ and 2 are signaled using the $DCAS_{SB,0}$ and $DCAS_{MB,0}$ fields in the SFH. Since FP_0 and FP_3 are empty, $L_{SB-CRU,FP_0} = L_{MB-CRU,FP_0} = L_{DRU,FP_0} = 0$ and $L_{SB-CRU,FP_3} = L_{MB-CRU,FP_3} = L_{DRU,FP_3} = 0$. For $i = 1$ and 2, $L_{SB-CRU,FP_i} = N_1 \cdot DCAS_{SB,0}$ and L_{MB-CRU,FP_i} is obtained from $DCAS_{MB,0}$ using

$DCAS_{MB,0}$	Number of miniband based CRU for FP_0	$DCAS_{MB,0}$	Number of miniband based CRU for FP_0
0	0	8	16
1	2	9	18
2	4	10	20
3	6	11	22
4	8	12	24
5	10	13	38
6	12	14	40
7	14	15	42

Figure 2.15: Mapping between $DCAS_{MB,0}$ and number of miniband based CRUs for FP_0 for FFT size 1024 (from [10, Table 790]).

$DCAS_{MB,0}$	Number of miniband based CRU for FP_0	$DCAS_{MB,0}$	Number of miniband based CRU for FP_0
0	0	4	8
1	2	5	10
2	4	6	18
3	6	7	20

Figure 2.16: Mapping between $DCAS_{MB,0}$ and number of miniband based CRUs for FP_0 for FFT size 512 (from [10, Table 791]).

the mappings in Figs. 2.14 through 2.16 for FFT sizes of 2048, 1024 and 512, respectively.

The number of CRUs in each frequency partition is denoted L_{CRU,FP_i} , where

$$L_{CRU,FP_i} = L_{SB-CRU,FP_i} + L_{MB-CRU,FP_i}. \quad (2.19)$$

The number of DRUs in each frequency partition is denoted by L_{DRU,FP_i} , where

$$L_{DRU,FP_i} = FPS_i - L_{CRU,FP_i}. \quad (2.20)$$

and FPS_i is the number of PRUs allocated to FP_i .

The mapping from PRU_{FP_i} to CRU_{FP_i} is given by

$$CRU_{FP_i}[j] = \begin{cases} PRU_{FP_i}[j], & 0 \leq j < L_{SB-CRU,FP_i} \cdot N_1, & 0 \leq i < FPCT, \\ PRU_{FP_i}[k + L_{SB-CRU,FP_i} \cdot N_1], & L_{SB-CRU,FP_i} \leq j < L_{CRU,FP_i}, & 0 \leq i < FPCT. \end{cases} \quad (2.21)$$

where $k = s[j - L_{SB-CRU,FP_i}]$, with $s[\cdot]$ being the CRU/DRU allocation sequence defined as

$$s[j] = \{PermSeq(j) + DL_PermBase\} \bmod \{FPS_i - L_{SB-CRU,FP_i} \cdot N_1\} \quad (2.22)$$

where $PermSeq()$ is the permutation sequence of length $(FPS_i - L_{SB-CRU,FP_i})$ and is determined by $SEED = ID_{cell} \cdot 343 \bmod 2^{10}$, $DL_PermBase$ is an interger ranging from 0 to 31, which is set to preamble ID_{cell} . The mapping of PRU_{FP_i} to DRU_{FP_i} is given by

$$DRU_{FP_i}[j] = PRU_{FP_i}[k + L_{SB-CRU,FP_i}], \quad 0 \leq j < L_{DRU,FP_i} \quad (2.23)$$

where $k = s[j + L_{CRU,FP_i} - L_{SB-CRU,FP_i}]$.

2.3.2 Subcarrier Permutation

The DL DRUs are used to form two stream distributed logical resource unit (DLRU)s by subcarrier permutation. The subcarrier permutation defined for the DL distributed resource allocations within a frequency partition spreads the subcarriers of the DRU across the whole

distributed resource allocations. The granularity of the subcarrier permutation is equal to a pair of subcarriers.

After mapping all pilots, the remainder of the used subcarriers are used to define the distributed LRUs. To allocate the LRUs, the remaining subcarriers are paired into contiguous tone-pairs. Each LRU consists of a group of tone-pairs.

Let $L_{SC,l}$ denote the number of data subcarriers in l th OFDMA symbol within a PRU, i.e., $L_{SC,l} = P_{SC} - n_l$, where n_l denotes the number of pilot subcarriers in the l th OFDMA symbol within a PRU. Let $L_{SP,l}$ denote the number of data subcarrier-pairs in the l th OFDMA symbol within a PRU and is equal to $L_{SC,l}/2$. A permutation sequence $\text{PermSeq}()$ is defined in section 2.3.3, performs the DL subcarrier permutation as follows. For each l th OFDMA symbol in the subframe:

1. Allocate the n_l pilots within each DRU as described in Section 2.3.3. Denote the data subcarriers of $DRU_{FPi}[j]$ in the l th OFDMA symbol as

$$SC_{DRU,j,l}^{FPi}[k], \quad 0 \leq j < L_{DRU,FPi}, \quad 0 \leq k < L_{SC,l}. \quad (2.24)$$

2. Renumber the $L_{DRU,FPi} \cdot L_{SC,l}$ data subcarriers of the DRUs in order, from 0 to $L_{DRU,FPi} \cdot L_{SC,l} - 1$. Group these contiguous and logically renumbered subcarriers into $L_{DRU,FPi} \cdot L_{SP,l}$ pairs and renumber them from 0 to $L_{DRU,FPi} \cdot L_{SP,l} - 1$. The renumbered subcarrier pairs in the l th OFDMA symbol are denoted as

$$RSP_{FPi,l}[u] = \{SC_{DRU,j,l}^{FPi}[2v], SC_{DRU,j,l}^{FPi}[2v+1]\}, \quad 0 \leq u < L_{DRU,FPi}L_{SP,l}, \quad (2.25)$$

where $j = \lfloor u/L_{SP,l} \rfloor$, $v = \{u\} \bmod (L_{SP,l})$.

3. Apply the subcarrier permutation formula to map $RSP_{FPi,l}$ into the s th distributed LRU, $s = 0, 1, \dots, L_{DRU,FPi} - 1$, where the subcarrier permutation formula is given by

$$SC_{LRUs,l}^{FPi}[m] = RSP_{FPi,l}[k], \quad 0 \leq m < L_{SP,l}, \quad (2.26)$$

where

$$k = L_{DRU,FPi} \cdot f(m, s, l) + g(PermSeq(), s, m, l). \quad (2.27)$$

In the above,

1. $SC_{LRU, s, l}^{FPi}[m]$ is the m th subcarrier pair in the l th OFDMA symbol in the s th distributed LRU of the t th AAI subframe;
2. m is the subcarrier pair index, 0 to $L_{SP, l} - 1$;
3. l is the OFDMA symbol index, 0 to $N_{sym} - 1$;
4. s is the distributed LRU index, 0 to $L_{DRU, FPi} - 1$;
5. $PermSeq()$ is the permutation sequence of length $L_{DRU, FPi}$ and is determined by $SEED = \{ID_{cell} \cdot 1367\} \bmod 2^{10}$; and
6. $g(PermSeq(), s, m, l)$ is a function with value from the set $[0, L_{DRU, FPi} - 1]$, which is defined according to

$$g(PermSeq(), s, m, l) = \{PermSeq[\{f(m, s) + s + l\} \bmod \{L_{DRU, FPi}\}] + DL_PermBase\} \bmod L_{DRU, FPi} \quad (2.28)$$

where $DL_PermBase$ is an integer ranging from 0 to 31 (Section 2.3.3), which is set to preamble ID_{cell} , and $f(m, s, l) = (m + 13 \cdot (s + l)) \bmod L_{SP, l}$.

2.3.3 Random Sequence Generation

The permutation sequence generation algorithm with 10-bit SEED $(S_{n-10}, S_{n-9}, \dots, S_{n-1})$ shall generate a permutation sequence of size M according to the following process:

- Initialization

1. Initialize the variables of the first order polynomial equation with the 10-bit seed, SEED. Set $d_1 = \lfloor SEED/2^5 \rfloor + 619$ and $d_2 = SEED \bmod 2^5$.
 2. Initialize the maximum iteration number, $N = 4$.
 3. Initialize an array A with size M to contents $0, 1, \dots, M - 1$ (i.e., $A[i] = i$, for $0 \leq i < M$).
 4. Initialize the counter i to $M - 1$.
 5. Initialize x to -1 .
- Repeat the following steps if $i > 0$
 1. Increment x by i .
 2. Calculate the output variable of $y = \{(d_1 \cdot x + d_2) \bmod 1031\} \bmod M$.
 3. If $y \leq i$, set $y = y \bmod (i + 1)$.
 4. Swap $A[i]$ and $A[y]$.
 5. Decrement i by 1.
 - $PermSeq[i] = A[i]$, where $0 \leq i < M$.

2.4 Test Case Generation

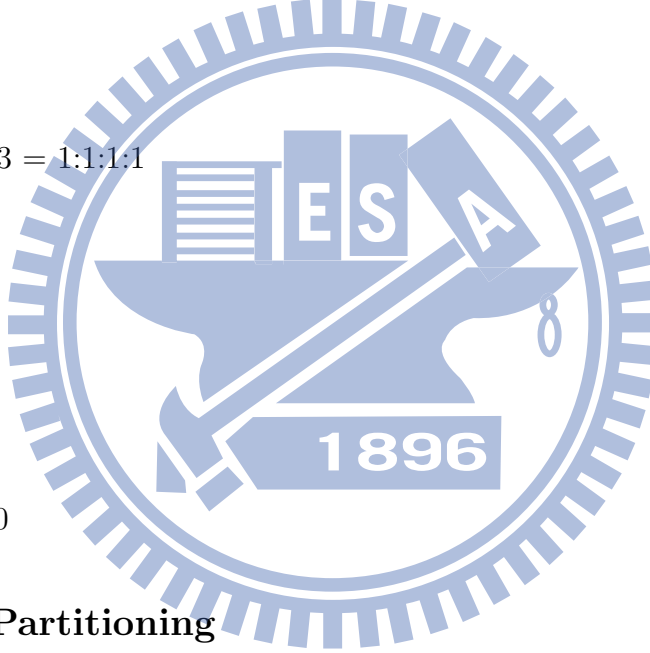
We set some system parameters to build a frame as a test case. The parameters are as given below. We will walk through some of the derived mappings in subsequent subsections.

- $NPRU = 48$
- $SAC = 6$
- $K_{SB} = 7$

Table 2.2: Mapping Between PRU Index and PRU_{SB} Index for the Test Case

PRU_{SB} Index	0	1	2	3	4	5	6	7	8	9	10	11	12	13
PRU Index	40	41	42	43	4	5	6	7	12	13	14	15	20	21
PRU_{SB} Index	14	15	16	17	18	19	20	21	22	23	24	25	26	27
PRU Index	22	23	28	29	30	31	36	37	38	39	44	45	46	47

- $K_{MB} = 20$
- $L_{SB} = N_1 \cdot K_{SB} = 28$
- $N_{sub} = 12$
- $FPC = 1$
- $FPCT = 4$
- $FP0:FP1:FP2:FP3 = 1:1:1:1$
- $FPSC = 2$
- $ID_Cell = 2$
- $SEED = 343$
- $DL_PermBase = 0$



2.4.1 Subband Partitioning

The 48 PRUs map to the subbands according the formulas described in Section 2.3.1. Fig. 2.17 illustrates the PRU to PRU_{SB} mapping for a 10 MHz bandwidth with $K_{SB} = 6$. Table 2.2 shows the resulting mapping between the PRU index and the PRU_{SB} index.

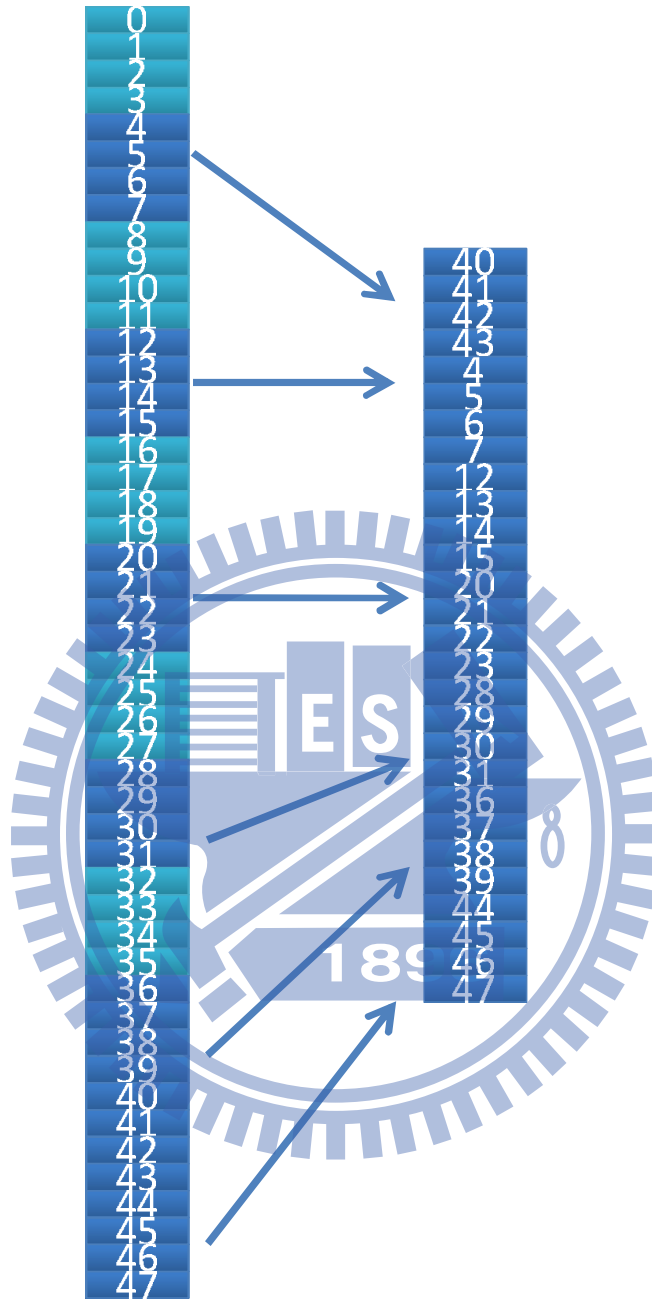


Figure 2.17: PRU to PRU_{SB} mapping for the test case.

Table 2.3: Mapping Between PRU Index and $PPRU_{MB}$ Index for the Test Case

PRU_{MB} Index	0	1	2	3	4	5	6	7	8	9
PRU Index	0	1	2	3	8	9	10	11	16	17
PRU_{MB} Index	10	11	12	13	14	15	16	17	18	19
PRU Index	18	19	24	25	26	27	32	33	34	35

Table 2.4: Mapping Between PRU_{MB} Index and $PPRU_{MB}$ Index for the Test Case

$PPRU_{MB}$ Index	0	1	2	3	4	5	6	7	8	9
PRU_{MB} Index	0	8	16	24	32	1	9	17	25	33
$PPRU_{MB}$ Index	10	11	12	13	14	15	16	17	18	19
PRU_{MB} Index	2	10	18	26	34	3	11	19	27	35

2.4.2 Miniband Partitioning

The remainder of the PRUs are allocated to minibands according the formulas given previously. Fig. 2.18 illustrates the PRU to PRU_{MB} mapping for a 10 MHz bandwidth with $K_{MB} = 20$. Table 2.3 shows the resulting mapping between the PRU index and the PRU_{MB} index.

2.4.3 Miniband Permutation

The miniband permutation maps the PRU_{MB} s to Permuted PRU_{MB} s ($PPRU_{MB}$ s) to ensure that frequency diverse PRUs are allocated to each frequency partition. The mapping rule is as described previously. Fig. 2.19 illustrates the PRU_{MB} to $PPRU_{MB}$ mapping for a 10 MHz bandwidth with $K_{MB} = 20$. Table 2.4 shows the resulting mapping between the PRU_{MB} index and the $PPRU_{MB}$ index.

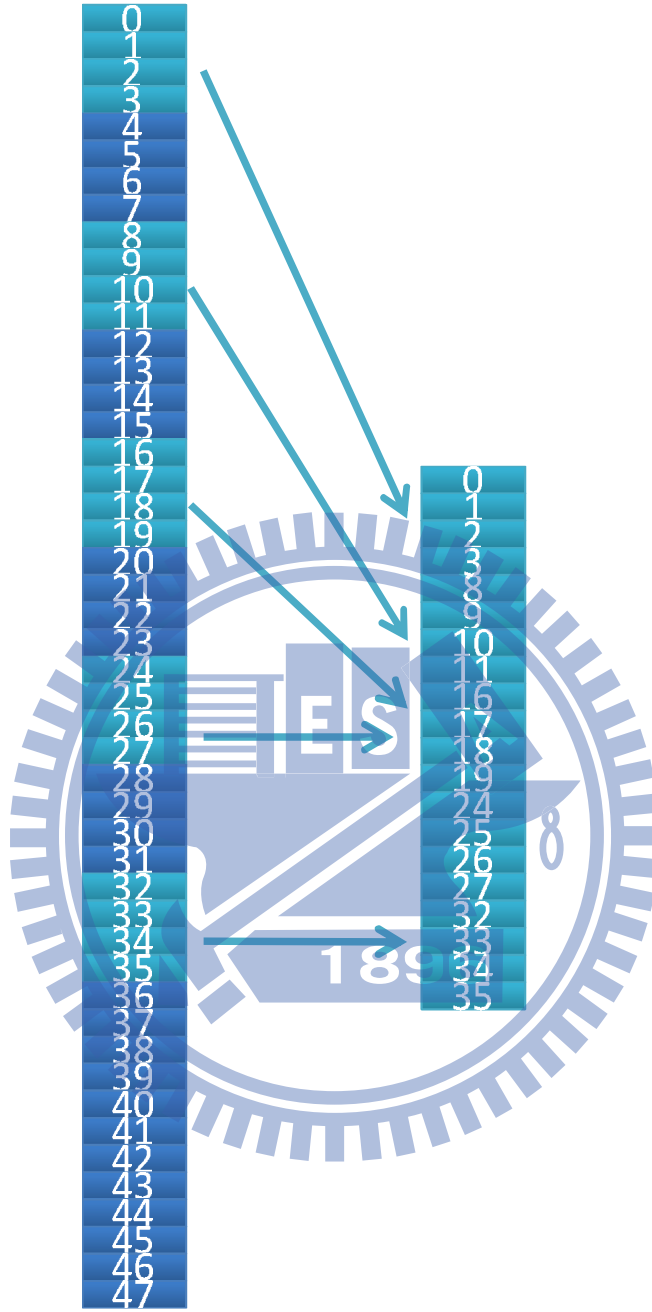


Figure 2.18: PRU to PRU_{MB} mapping for the test case.

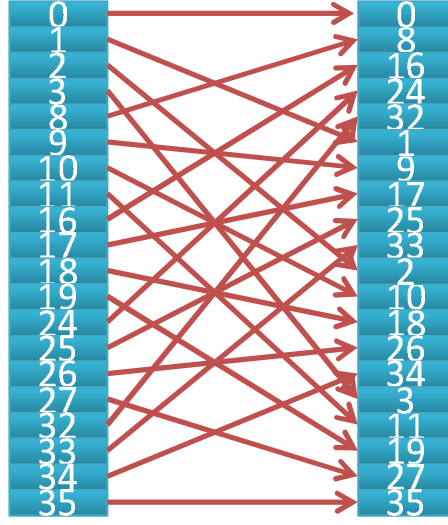


Figure 2.19: PRU_{MB} to $PPRU_{MB}$ mapping for the test case.

Table 2.5: Mapping Between PRU_{SB} Index, $PPRU_{MB}$ Index, and PRU_{FP1} Index for the Test Case

PRU_{FP1} index	0	1	2	3	4	5	6	7	8	9	10	11
PRU_{SB} index	0	1	2	3	x	x	x	x	x	x	x	x
$PPRU_{MB}$ index	x	x	x	x	0	1	2	3	4	5	6	7

2.4.4 Frequency Partitioning

The PRU_{SB} and $PPRU_{MB}$ are allocated to the frequency partitions. There are 4 frequency partitions used because $FPCT = 4$. The PRU_{SB} and $PPRU_{MB}$ map to frequency partitions 1, 2, 3, and 4 according the formulas given previously. Fig. 2.20 illustrates the PRU_{SB} and $PPRU_{MB}$ to frequency partitions mapping for a 10 MHz bandwidth. Tables 2.5 through 2.8 show the resulting mapping between the PRU_{SB} index, $PPRU_{MB}$ index, and PRU_{FPi} index for $1 \leq i \leq 4$.

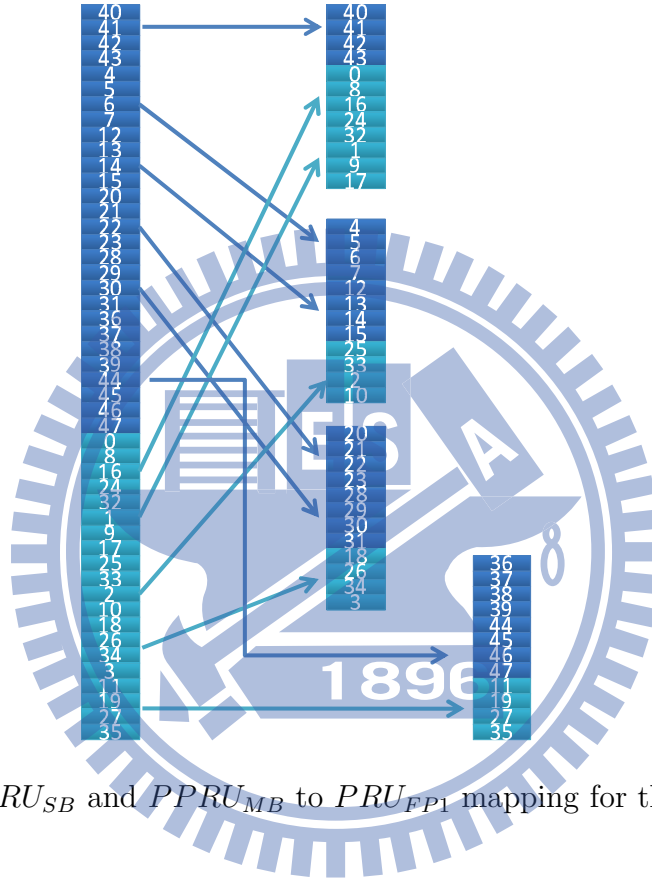


Figure 2.20: PRU_{SB} and $PPRU_{MB}$ to PRU_{FPI} mapping for the test case.

Table 2.6: Mapping Between PRU_{SB} Index, $PPRU_{MB}$ Index, and PRU_{FP2} Index for the Test Case

PRU_{FP2} index	0	1	2	3	4	5	6	7	8	9	10	11
PRU_{SB} index	4	5	6	7	8	9	10	11	x	x	x	x
$PPRU_{MB}$ index	x	x	x	x	x	x	x	x	8	9	10	11

Table 2.7: Mapping Between PRU_{SB} Index, $PPRU_{MB}$ Index, and PRU_{FP3} Index for the Test Case

PRU_{FP3} index	0	1	2	3	4	5	6	7	8	9	10	11
PRU_{SB} index	12	13	14	15	16	17	18	19	x	x	x	x
$PPRU_{MB}$ index	x	x	x	x	x	x	x	x	12	13	14	15

Table 2.8: Mapping Between PRU_{SB} Index, $PPRU_{MB}$ Index, and PRU_{FP4} Index for the Test Case

PRU_{FP4} index	0	1	2	3	4	5	6	7	8	9	10	11
PRU_{SB} index	20	21	22	23	24	25	26	27	x	x	x	x
$PPRU_{MB}$ index	x	x	x	x	x	x	x	x	16	17	18	19

Table 2.9: Random Sequence for the Test Case

k	0	1	2	3	4	5	6	7
PermSeq[k]	2	1	0	3	4	5	6	7

2.4.5 Random Sequence

We generate a random sequence with $ID_Cell = 2$, $DL_PermBase = 0$. Then $SEED = \{ID_Cell \times 1367\} \bmod 2^{10} = 343$. The random sequence is generated according to the formulas given previously. Table 2.9 shows the random sequence.

Table 2.10: Mapping Between PRU_{FP1} Index and CRU_{FP1}/DRU_{FP1} Index

PRU_{FP1} index	0	1	2	3	4	5	6	7	8	9	10	11
CRU_{FP1} index	0	1	2	3	4	5	6	7	x	x	x	x
DRU_{FP1} index	x	x	x	x	x	x	x	x	0	4	3	2

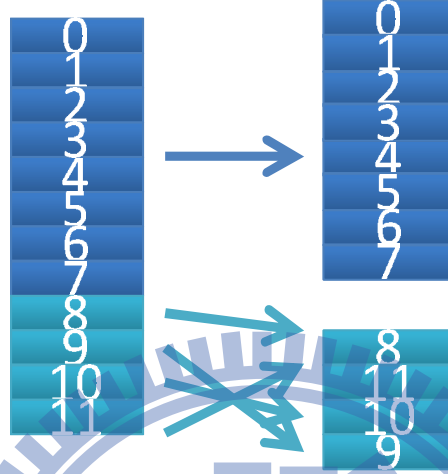


Figure 2.21: The mapping of PRU_{FP1} s to CRU/DRU for the test case.

2.4.6 CRU/DRU Allocation

The PRU_{FP1} s map to the CRUs and DRUs according to the formulas given previously. Fig. 2.21 illustrates the PRU_{FP1} to CRU/DRU mapping for a 10 MHz bandwidth. Table 2.10 show the resulting mapping between the PRU_{FP1} index and the CRU/DRU index.

2.5 MIMO Midamble [10]

Again this section is mainly taken from [10]. MIMO midamble is used for preferred matrix index (PMI) selection in CL MIMO. For open loop (OL) MIMO, midamble can be used to calculate channel quality index (CQI). MIMO midamble shall be transmitted every frame on the second DL AAI subframe. The midamble signal occupies the first OFDMA symbol in a

DL type-1 or type-2 AAI subframe. For type-1 AAI subframe, the remaining 5 consecutive symbols form a type-3 AAI subframe. For type-2 AAI subframe, the remaining 6 consecutive symbols form a type-1 AAI subframe. The MIMO midamble signal transmitted by the ABS antenna is defined

$$s(t) = \text{Re} \left\{ e^{j2\pi f_c t} \sum_{\substack{k=0 \\ k \neq \frac{N_{used}-1}{2}}}^{k=N_{used}-1} b_k e^{j2\pi(k - \frac{N_{used}-1}{2})\Delta f(t-T_g)} \right\} \quad (2.29)$$

where b_k is a coefficient modulating a subcarrier in the midamble symbol

$$b_k = \begin{cases} 2.18 \cdot \{1 - (2G([k + u + \text{offset}(fft)] \bmod fft))\}, k \neq \frac{N_{used}-1}{2} \text{ and} \\ (k-s) \bmod (3 \times N_t) = 3g + (\lfloor \frac{ID_{cell}}{256} \rfloor + \lfloor \frac{k-s}{N_1 - N_{SC}} \rfloor) \bmod 3, \\ 0, \text{ otherwise.} \end{cases} \quad (2.30)$$

where k is the subcarrier index ($0 \leq k \leq N_{used}-1$), N_{used} is the number of used subcarriers, $G(x)$ is the Golay sequence defined in Fig. 2.22 ($0 \leq x \leq 2047$), fft is the FFT size used, u is a shift value given by $u = \text{mod}(ID_{cell}, 256)$, $\text{offset}(fft)$ is an FFT size specific offset as defined in Fig. 2.23, g is an advanced base station (ABS) transmit antenna index ($0 \leq g \leq N_t - 1$), N_t is the number of ABS transmit antennas, parameter $s = 0$ for $k \leq \frac{N_{used}-1}{2}$ and $s = 1$, for $k > \frac{(N_{used}-1)}{2}$. An example of the physical structure of the MIMO midamble is shown in Fig. 2.24 for the case with 4 transmit (TX) antennas and $ID_{cell} = 0$. In Fig. 2.22, the hexadecimal series should be read as a sequence of bits where each 16-bit word starts at the most significant bit (MSB) and ends at the least significant bit (LSB) where the second word's MSB follows. The first bit of the sequence is referenced as having offset 0.

0xEDE2	0xED1D	0xEDE2	0x12E2	0xEDE2	0xED1D	0x121D	0xED1D	0xEDE2	0xED1D	0xEDE2	0x12E2
0x121D	0x12E2	0xEDE2	0x12E2	0xEDE2	0xED1D	0xEDE2	0x12E2	0xEDE2	0xED1D	0x121D	0xED1D
0x121D	0x12E2	0x121D	0xED1D	0xEDE2	0xED1D	0x121D	0xED1D	0xEDE2	0xED1D	0xEDE2	0x12E2
0xEDE2	0xED1D	0x121D	0xED1D	0xEDE2	0xED1D	0xEDE2	0x12E2	0x121D	0x12E2	0xEDE2	0x12E2
0x121D	0x12E2	0x121D	0xED1D	0x121D	0x12E2	0xEDE2	0x12E2	0xEDE2	0xED1D	0xEDE2	0x12E2
0x121D	0x12E2	0xEDE2	0x12E2	0xEDE2	0xED1D	0xEDE2	0x12E2	0xEDE2	0xED1D	0x121D	0xED1D
0xEDE2	0xED1D	0xEDE2	0x12E2	0x121D	0x12E2	0xEDE2	0x12E2	0xEDE2	0xED1D	0xEDE2	0x12E2
0xEDE2	0xED1D	0x121D	0xED1D	0x121D	0x12E2	0x121D	0xED1D	0xEDE2	0xED1D	0x121D	0xED1D
0x121D	0x12E2	0x121D	0xED1D	0x121D	0x12E2	0xEDE2	0x12E2	0x121D	0x12E2	0x121D	0xED1D
0xEDE2	0xED1D	0x121D	0xED1D	0xEDE2	0xED1D	0xEDE2	0x12E2	0xEDE2	0xED1D	0x121D	0xED1D
0x121D	0x12E2	0x121D	0xED1D	0xEDE2	0xED1D	0x121D	0xED1D				

Figure 2.22: OFDMA parameters (Table 793 in [10]).

FFT Size	Offset
2048	30
1024	60
512	40

Figure 2.23: OFDMA parameters (from [10, Table 794]).

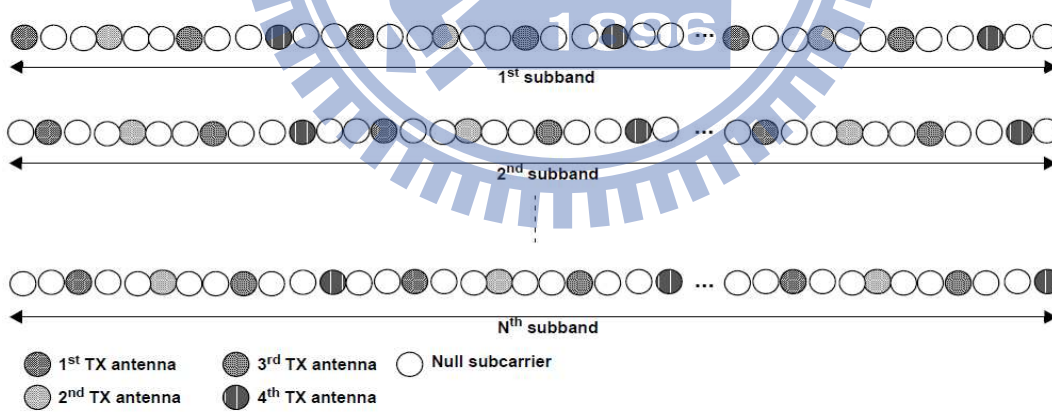


Figure 2.24: Example of MIMO midamble structure for the case of 4 transmit antennas (Figure 502 in [10]).

2.6 Usage of Downlink Pilots [10]

Again this section is mainly taken from [10]. The demodulation pilots in a given PRU on a given pilot stream shall be precoded the same way as the data transmitted on the same stream in that PRU. In DLRU the data transmitted in a given PRU on a given stream may be sent to several advanced mobile station (AMS)s but in different tones using the same precoder.

Two pilot streams shall always be transmitted in the DLRUs, whether inside or outside the OL region type 0, and whether or not data is being transmitted by the ABS in all DLRUs. If no data are transmitted by the ABS on all or some contiguous logical resource unit (CLRU)s in the OL region type 1 or type 2, then $\max M_t$ pilots shall still be transmitted across all CLRUs in that OL region. If no data are transmitted by the ABS on all or some CLRUs outside any OL region, then pilots shall not be transmitted on the CLRUs where no data are sent.

The precoder may be adaptive (user-specific) or non-adaptive (non user-specific) depending on the DL MIMO mode. Non-adaptive precoders are determined according to the DL MIMO mode, the number of streams, the type of LRU, operation inside or outside the OL region, and the physical index of the subband or miniband where the precoder is applied.

In MU-MIMO transmissions in CLRU each pilot stream is dedicated to one AMS. The AMS shall use its dedicated pilot stream for channel estimation within the allocation. Other pilot streams may be used for inter-stream interference estimation. The total number of streams in the transmission and the index of the dedicated pilot stream are indicated in the DL Basic Assignment A-MAP IE, DL Persistent Allocation A-MAP IE or DL Subband Assignment A-MAP IE.

Channel estimation for demodulation of data burst at AMS should be performed as

follows:

- In DLRU: the 2-streams non-adaptively precoded common pilots across the DLRU should be used for channel estimation by all AMSs allocated a burst in the DLRU. Within each frequency partition, all pilots are shared by all AMSs for demodulation in DLRU. Only the pilots located within a physical subband should be used for channel estimation within that subband.
- In CLRU: The AMS should use its dedicated pilot streams for channel estimation in the allocation. Pilots are not shared by AMSs for demodulation in CLRU, whether they are non-adaptively or adaptively precoded.

MIMO feedback measurements at the AMS should be performed as follows:

- For MIMO feedback reports requested with a MIMO feedback mode for operation in an OL region, measurements should be taken on the max M_t streams non-adaptively precoded pilots in that OL region. All pilots are shared by all AMSs for MIMO feedback measurements in each OL region.

Wideband CQI reports inside OL region should be averaged over OL region pilots of the PRUs in the frequency partition 0.

- For MIMO feedback reports requested with a MIMO feedback mode for operation outside the OL region, measurements should be taken on the downlink MIMO midamble.

Wideband CQI reports outside OL region (measured on MIMO midamble) should be averaged over the frequency partition indicated by Frequency Partition Indicator (PFI) in Feedback Allocation A-MAP IE or according to FPCT for feedback allocated by Feedback Polling A-MAP IE.

For reports requested with a MIMO feedback mode for OL MIMO operation, the AMS should adjust the non-precoded MIMO channel estimated from the midamble by applying it with the non-adaptive precoder according to the MIMO feedback modes (MFM), the subband index and assumption on space time code(STC) rate.

For reports requested with a MIMO feedback mode for CL MIMO operation, the AMS should adjust the non-precoded MIMO channel estimated from the midamble with an estimated adaptive precoder.

Subband CQI reports (inside and outside OL region) should be reported for subbands in subband logical resource unit (SLRU)s indicated by superframe header(SFH).

2.7 Downlink control structure [10]

Again this section is mainly taken from [10].

2.7.1 Advanced Preamble

There are two types of Advanced Preamble (A-Preamble): primary advanced preamble (PA-Preamble) and secondary advanced preamble (SA-Preamble). One PA-Preamble symbol and three SA-Preamble symbols exist in a superframe. An A-Preamble symbol is located at the first symbol of a frame. The PA-Preamble is located at the first symbol of the second frame in a superframe while a SA-Preamble is located at the first symbol of each of the remaining three frames. Fig. 2.25 depicts the location of A-Preamble symbols.

2.7.2 Primary Advanced Preamble (PA-Preamble)

The length of sequence for PA-Preamble is 216 regardless of the FFT size. PA-Preamble carries the information of system bandwidth and carrier configuration. With the subcarrier

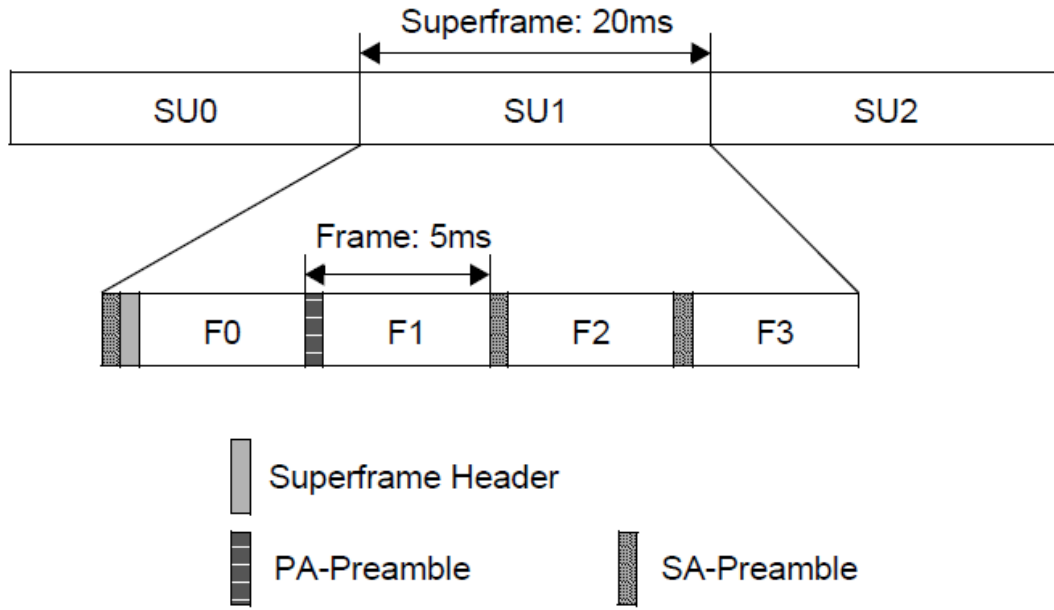


Figure 2.25: Location of the A-Preamble symbols (Figure 506 in [10]).

index 256 reserved for DC, the allocation of subcarriers is given by

$$PAPreambleCarrierSet = 2 \cdot k + 41 \quad (2.31)$$

where $PAPreambleCarrierSet$ specifies all subcarriers allocated to the PA-Preamble and k is a running index from 0 to 215. Fig. 2.26 depicts the symbol structure of the PA-Preamble in the frequency domain.

Fig. 2.27 lists the sequences of the PA-Preamble in hexadecimal format. A series is

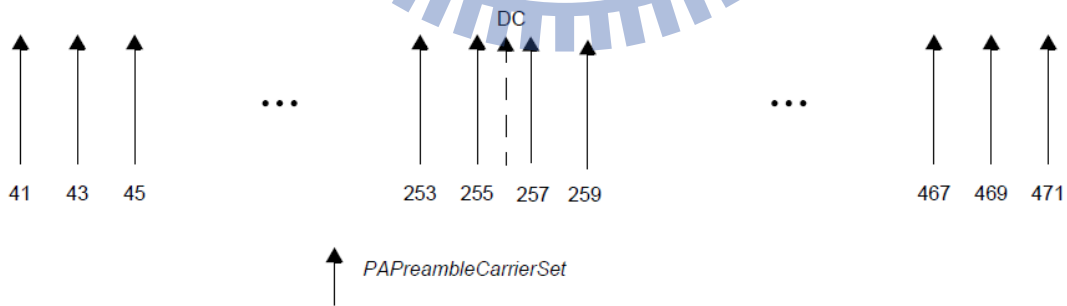


Figure 2.26: Symbol structure of PA-Preamble in frequency domain (Figure 507 in [10]).

Index	Carrier	BW	Series to modulate
0	Fully configured	5MHz	6DB4F3B16BCE59166C9CEF7C3C8CA5EDF C16A9D1DC01F2AE6AA08F
1		7,8.75 and 10 MHz	1799628F3B9F8F3B22C1BA19EAF94FEC4D 37DEE97E027750D298AC
2		20MHz	92161C7C19BB2FC0ADE5CEF3543AC1B6C E6BE1C8DCABDDD319EAF7
3		Reserved	6DE116E665C395ADC70A8971690862086 8A60340BF35ED547F8281
4		Reserved	BCFDF60DFAD6B027E4C39DB20D783C9F4 67155179CBA31115E2D04
5		Reserved	7EF1379553F9641EE6ECDBF5F144287E32 9606C616292A3C77F928
6		Reserved	8A9CA262B8B3D37E3158A3B17BFA4C9FC FF4D396D2A93DE65A0E7C
7		Reserved	DA8CE648727E4282780384AB53CEEBD1C BF79E0C5DA7BA85DD3749
8		Reserved	3A65D1E6042E8B8AADC701E210B5B4B65 0B6AB31F7A918893FB04A
9		Reserved	D46CF86FE51B56B2CAA84F26F6F204428C 1BD23F3D888737A0851C
10	Partially configured	N/A	640267A0C0DF11E475066F1610954B5AE5 5E189EA7E72EFD57240F

Figure 2.27: Sequences of PA-Preamble in frequency domain (from [10, Table 796]).

mapped onto subcarriers in ascending order, MSB first, with 0 mapped to +1 and 1 mapped to -1.

The sequences of indexes from 3 to 9 in the figure are reserved for the irregular nominal channel bandwidth to support tone dropping. The magnitude boosting levels in single carrier mode for different FFT sizes are shown in Fig. 2.28.

512	1k	2k
2.3999	3.4143	5.1320

Figure 2.28: Boosting factors for PA-Preamble symbols (Table 797 in [10]).

2.7.3 Secondary Advanced Preamble (SA-Preamble)

The number of subcarriers allocated for SA-Preamble N_{SAP} are 144, 288, and 576 for 512-FFT, 1024-FFT, and 2048-FFT, respectively. The allocation of subcarriers is according to

$$SAPreambleCarrierSet_n = n + 3 \cdot k + 40 \cdot \frac{N_{SAP}}{144} + \lfloor \frac{2 \cdot k}{N_{SAP}} \rfloor \quad (2.32)$$

where $SAPreambleCarrierSet_n$ specifies all subcarriers allocated to the specific SA-Preamble, n is the index of the SA-Preamble carrier-set 0, 1 and 2 representing segment ID, k is a running index 0 to $N_{SAP} - 1$ for each FFT size and the subcarrier indexes 256, 512, and 1024 are reserved for DC for 512-FFT, 1024-FFT, and 2048-FFT, respectively. No circular shift is assumed in the above equation. Each segment uses an SA-Preamble composed of a carrier-set out of the three available carrier-sets in that segment i uses SA-Preamble carrier-set i where $i = 0, 1, 2$. Each cell has an integer value ID_{cell} from 0 to 767. The ID_{cell} is defined by segment index and an index per segment as

$$ID_{cell} = 256n + Idx \quad (2.33)$$

where n is the index of the SA-Preamble carrier-set 0, 1 and 2 representing segment ID and

$$Idx = 2 \bmod (128, n) + \lfloor q/128 \rfloor \quad (2.34)$$

with q being a the running index from 0 to 255. SA-Preamble sequences are partitioned and each partition is dedicated to a specific BS type like macrocell ABS, macro hotzone ABS, femto ABS. The BS types are categorized into macro ABS and non-macro ABS cells by hard partition with 258 sequences (86 sequences per segment, 3 segments) dedicated for macro

ABS. The non-macro ABS information is broadcasted in a hierarchical structure, which is composed of S-SFH SP3 and AAI SCD messages. In S-SFH SP3, non-macro ABS cell type is partitioned into public and closed subscriber group (CSG) femto BSs. A total of 16 cases of IDcell partition for public and CSG-femto ABSs constitute IDcell partitions based on a 30 sequence (10 sequences per segmentation) granularity.

2.8 DL Control Channels [10]

Again this section is mainly taken from [10]. DL control channels convey information essential for system operation. Information on DL control channels is transmitted hierarchically over different time scales from the superframe level to the AAI subframe level. In mixed mode operation (WirelessMAN-OFDMA/Advanced Air Interface), an AMS can access the system without decoding WirelessMAN-OFDMA FCH and MAP messages.

2.8.1 Superframe Header

The Superframe Header (SFH) carries essential system parameters and system configuration information. The SFH is located in the first AAI subframe within a superframe. The SFH uses the last 5 OFDM symbols within the first AAI subframe.

All PRUs in the first AAI subframe of a superframe have 5 OFDM symbols with the 2 stream pilot pattern. The resource mapping process in the SFH AAI subframe is as follows. The AAI subframe where SFH is located always has one frequency partition FP_0 . All N_{PRU} PRUs in the AAI subframe where SFH is located are permuted to generate the distributed LRUs. The permutation and frequency partition of the SFH AAI subframe can be described by $DSAC = 0$ (all minibands, without subband), $DFPC = 0$ (reuse 1 only), $DCAS_{SB0} = 0$ (no subband CRU allocated), and $DCAS_{MB0} = 0$ (no miniband CRU allocated).

Parameters	Description	Value
N_{SFH}	The number of distributed LRUs which are occupied by SFH. Note that $N_{SFH} = N_{P-SFH} + N_{S-SFH}$	$N_{P-SFH} + N_{S-SFH}$
N_{P-SFH}	The number of distributed LRUs which are occupied by P-SFH.	Fixed (value is TBD)
N_{S-SFH}	The number of distributed LRUs which are occupied by S-SFH.	Variable according to the type of S-SFH SP

Figure 2.29: Parameters and values for resource allocation of SFH (from [10, Table 806]).

The SFH occupies the first N_{SFH} distributed LRUs in the first AAI subframe of a superframe where $N_{SFH} \leq 24$. The remaining distributed LRUs in the first AAI subframe of a superframe are used for other control and data transmission. The SFH is divided into two parts: Primary Superframe Header (P-SFH) and Secondary Superframe Header (S-SFH). Figure 2.29 describes the parameters and values for resource allocation of the SFH.

2.8.2 Primary Superframe Header

The Primary Superframe Header (P-SFH) shall be transmitted in every superframe. The first N_{P-SFH} distributed LRUs of the first AAI subframe are allocated for P-SFH transmission, where N_{P-SFH} is a fixed value.

2.8.3 Secondary Superframe Header

The Secondary Superframe Header (S-SFH) may be transmitted in every superframe. If the S-SFH is present, the S-SFH shall be mapped to the N_{S-SFH} distributed LRUs following the N_{P-SFH} distributed LRUs. The value of N_{S-SFH} is indicated in P-SFH IE. The S-SFH can be repeated over two consecutive superframes. The information transmitted in S-SFH is divided into three sub-packets. The sub-packets of S-SFH are transmitted periodically where each sub-packet has a different transmission periodicity as illustrated in Fig. 2.30. The “SP

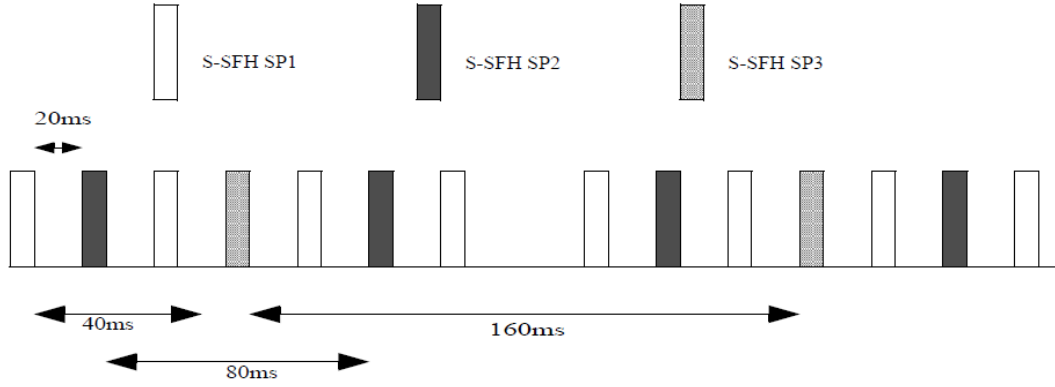


Figure 2.30: Illustration of periodic transmission of S-SFH SPs with example transmission periodicity of 40 ms, 80 ms and 160 ms for SP1, SP2 and SP3, respectively (Figure 515 in [10]).

scheduling periodicity information” field of S-SFH SP3 is used to indicate the transmission periodicity of the S-SFH SPs (1, 2, 3). Fig. 2.31 shows the transmission periodicity of different S-SFH SPs for different values of “SP scheduling periodicity information” field.

When there is no S-SFH SP in the SFH, the SFH resources are used for transmitting other control information or A-MAP.

2.8.4 Advanced MAP (A-MAP)

The Advanced MAP (A-MAP) carries unicast service control information. Unicast service control information consists of user-specific control information and non-user-specific control information. User-specific control information is further divided into assignment information, HARQ feedback information, and power control information, and they are transmitted in the assignment A-MAP, HARQ feedback A-MAP, and power control A-MAP, respectively. All the A-MAPs share a region of physical resources called A-MAP region. A-MAP regions shall be present in all DL unicast AAI subframes. When default TTI is used, DL data allocations corresponding to an A-MAP region occupy resources in the AAI subframe where the A-MAP region is located Figure 2.32 illustrates the location of A-MAP region in the

SP scheduling periodicity information	Transmission periodicity of S-SFH SP1	Transmission periodicity of S-SFH SP2	Transmission periodicity of S-SFH SP3
0000	40ms	80ms	160ms
0001	40ms	80ms	320ms
0010-1111:reserved			

Figure 2.31: Transmission Periodicity of S-SFH SPs (from [10, Table 807]).

A-MAP	A-MAP	A-MAP	A-MAP	UL SF4	UL SF5	UL SF6	UL SF7
DL SF0	DL SF1	DL SF2	DL SF3				

Figure 2.32: Example of locations of A-MAP regions in a TDD system (From [10, Fig 516]).

TDD mode.

If FFR is used in a DL AAI subframe, both the reuse 1 partition and the power-booster reuse 3 partition may contain an A-MAP region. In a DL AAI subframe, non-user specific, HARQ feedback, and power control A-MAPs are located in a frequency partition called the primary frequency partition. The primary frequency partition can be either the reuse 1 partition or the power-booster reuse 3 partition, which is indicated by ABS through S-SFH SP1 IE. Assignment A-MAP can be in the reuse 1 partition or the power-booster reuse 3 partition or both. The number of assignment A-MAPs in each frequency partition is signaled through non-user specific A-MAP.

The structure of an A-MAP region is illustrated in the example in Figure 2.33. The resource occupied by each A-MAP may vary depending on the system configuration and scheduler operation.

In DL AAI subframes other than the first AAI subframe of a superframe, an A-MAP region consists of the first N_{A-MAP} distributed LRUs in a frequency partition and the LRUs

2.8.7 Power Control A-MAP

Power Control A-MAP carries fast power control command to AMS.

2.8.8 Assignment A-MAP

Assignment A-MAP contains resource assignment information which is categorized into multiple types of assignment A-MAP IEs. Each assignment A-MAP IE is coded separately and carries information for one or a group of AMSs. The minimum logical resource unit in the assignment A-MAP is called MLRU, consisting of $N_{MLRU} = 56$ data tones.

The assignment A-MAP IE shall be transmitted with one MLRU or multiple concatenated MLRUs in the A-MAP region. The number of logically contiguous MLRUs is determined based on the assignment A-MAP IE size and channel coding rate, where channel coding rate is selected based on AMS link condition.

Assignment A-MAP IEs are grouped together based on channel coding rate. Assignment A-MAP IEs in the same group are transmitted in the same frequency partition with the same channel coding rate. Each assignment A-MAP group contains several logically contiguous MLRUs. The number of assignment A-MAP IEs in each assignment A-MAP group is signaled through non-user specific A-MAP in the same AAI subframe.

If two assignment A-MAP groups using two channel coding rates are present in an A-MAP region, assignment A-MAP group using lower channel coding rate is allocated first, followed by assignment A-MAP group using higher channel coding rate.

If a broadcast assignment A-MAP IE, i.e., the assignment A-MAP IE intended for all the AMSs, exists in a DL AAI subframe, it shall be present at the beginning of either assignment A-MAP group 1 or assignment A-MAP group 3.

All the multicast assignment A-MAP IEs, i.e., all the assignment A-MAP IEs intended for

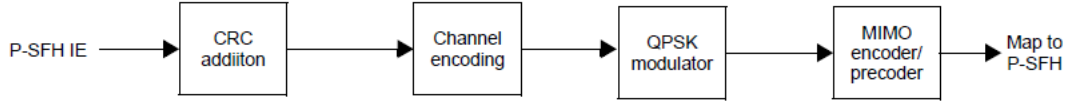


Figure 2.34: Physical processing block diagram for the P-SFH (Figure 518 in [10]).

a specific group of AMSs, present in any assignment A-MAP group, shall occupy a contiguous set of MLRUs starting from the beginning of the assignment A-MAP group. If the broadcast assignment A-MAP IE is present in the assignment A-MAP group, the multicast assignment A-MAP IEs are located right after the broadcast assignment A-MAP IE. The Group Resource Allocation A-MAP IE is an example of multicast assignment A-MAP IEs.

All the unicast assignment A-MAP IEs intended for a particular AMS shall be transmitted in the same assignment A-MAP group. The DL/UL Basic Assignment A-MAP IEs are an example of unicast assignment A-MAP IEs.

The maximum number of assignment A-MAP IEs in one AAI subframe that the ABS may allocate to an AMS is 8. This number includes all of the assignment A-MAP IEs that are required to be considered by the AMS (its STID, group ID of GRA, Broadcast ID). For a segmentable assignment A-MAP IE (assignment A-MAP IE that occupies more than 1 MLRU in QPSK 1/2, each segment is counted as 1 assignment A-MAP IE.

2.9 Resource Mapping of DL Control Channels [10]

Again this section is mainly taken from [10].

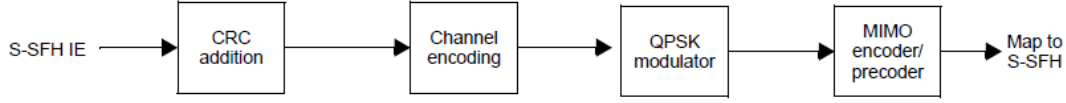


Figure 2.35: Physical processing block diagram for the S-SFH (Figure 519 in [10]).

2.9.1 Superframe Header

Primary Superframe Header

The P-SFH IE shall be appended with 5 bits CRC. The generating polynomial is $G(x) = x^5 + x^4 + x^2 + 1$. The resulting sequence of bits shall be encoded by the TBCC with parameter $M = N_{Rep,P-SFH}$ and $K_{bufsize} = 4L$, where L is the number of information bits and $N_{Rep,P-SFH}$ is the number of repetition for effective code rate of 1/16 or 1/24.

The modulated symbols shall be mapped to two transmission streams using SFBC. The two streams using SFBC shall be precoded and mapped to the transmit antennas.

Antenna specific symbols at the output of the MIMO encoder/precoder shall be mapped to the resource elements.

Secondary Superframe Header

Figure 519 shows the physical processing block diagram for the S-SFH.

The S-SFH IE shall be appended with a 16-bit CRC.

The resulting sequence of bits shall be encoded by the TBCC with parameter $M = N_{Rep,S-SFH}K_{bufsize}$ and $K_{bufsize} = 4L$, where L is the number of information bits.

The value of $N_{Rep,S-SFH}$ is indicated in P-SFH.

The encoded bit sequences shall be modulated using QPSK.

The modulated symbols shall be mapped to two transmission streams using SFBC. The

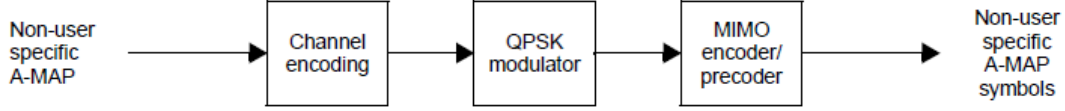


Figure 2.36: Chain of non-user specific A-MAP IE to non-user specific A-MAP symbols (Figure 520 in [10]).

two streams using SFBC shall be precoded and mapped to the transmit antennas.

Antenna specific symbols at the output of the MIMO encoder/precoder shall be mapped to the resource elements.

Advanced MAP (A-MAP)

SFBC with precoding shall be used for the A-MAP region.

Non-user Specific A-MAP

The coding chain for non-user-specific A-MAP IE to non-user-specific A-MAP symbols is shown in Figure 2.36. The non-user specific A-MAP IE is encoded by TBCC with parameter $M = 3K_{bufsize}$ and $K_{bufsize} = 4L$ for 1/12 code, where L is the number of information bits. In FFR configurations, the non-user specific A-MAP is also encoded with a code rate of 1/12 when it is in the frequency reuse 1 partition. When the non-user specific A-MAP is in the power-booster frequency reuse 3 partition, it should be encoded with parameter $M = K_{bufsize} = 4L$ for 1/4 code rate. The encoded sequence is modulated using QPSK.

For each Tx antenna, symbols at the output of MIMO encoder, denoted by $S_{NUS}[0]$ to $S_{NUS}[L_{NUS} - 1]$, are mapped to tone-pairs from $RMP[(L_{HF} + L_{PC})/2]$ to $RMP[(L_{HF} + L_{PC} + L_{NUS})/2 - 1]$, where RMP refers to the renumbered A-MAP tone-pairs and L_{HF} is the number of tones required to transmit the entire HARQ feedback A-MAP; L_{PC} is the number of tones required to transmit the entire power control A-MAP; L_{NUS} is the number

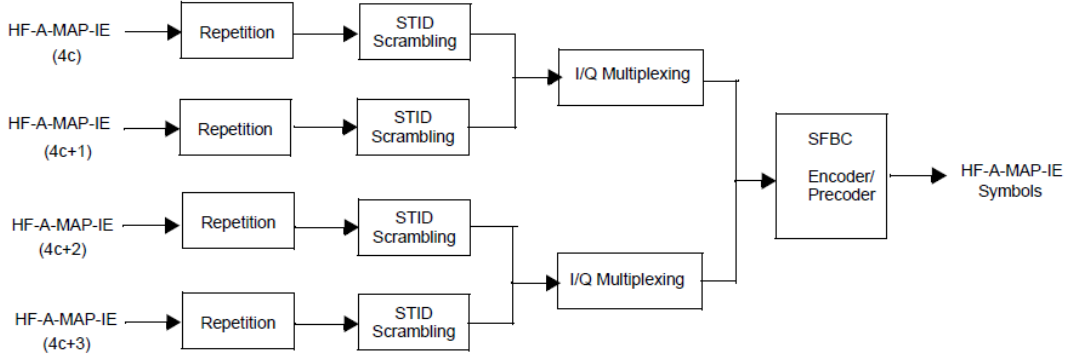


Figure 2.37: Chain of HF-A-MAP IE to HF-A-MAP symbols (Figure 521 in [10]).

of tones required to transmit the non-user specific-A-MAP.

HARQ Feedback A-MAP

HARQ feedback A-MAP (HF-A-MAP) contains HARQ-feedback-IEs for ACK/NACK feedback information to uplink data transmission.

Figure 2.37 shows the construction procedure of HF-A-MAP symbols from HF-A-MAP-IE. Each HF-A-MAP IE carries 1 bit information. Firstly, it is repeated $N_{Rep, HF-A-MAP}$ times, where $N_{Rep, HF-A-MAP}$ is 8. Then, Repeated HF-A-MAP IE bits are scrambled by the $N_{Rep, HF-A-MAP}LSBs$ of the STID of the associated AMS. Depending on the channel conditions, power scaling can be applied to each scrambled sequence. Before MIMO encoding, each scrambled sequence is mapped to either real part or imaginary part in the signal constellation and multiplexed with other scrambled sequence, if exist.

Figure 2.37 shows a cluster of HF-A-MAP channels, which consists of 4 HF-A-MAP channels numbered as $4c, 4c + 1, 4c + 2, 4c + 3$ where c is the HF-A-MAP cluster index in a HF-A-MAP region. Channel $4c$ in the cluster occupies the real part of the first symbol in each tone pair before the SFBC encoder. Channel $4c + 1$ in the cluster occupies the imaginary part of the first symbol in each tone pair before the SFBC encoder. Channel

$4c + 2$ in the cluster occupies the real part of the second symbol in each tone pair before the SFBC encoder. Channel $4c + 3$ in the cluster occupies the imaginary part of the second symbol in each tone pair before the SFBC encoder.

For each Tx antenna, symbols at the output of MIMO encoder, denoted by $S_{HF}[0]$ to $S_{HF}[L_{HF}-1]$, are mapped to tone-pairs from $RMP[0]$ to $RMP[L_{HF}/2-1]$, where RMP refers to the renumbered A-MAP tone-pairs and L_{HF} is the number of tones required to transmit the entire HARQ feedback A-MAP. Clusters of the HF-A-MAP are indexed sequentially from index 0 within an HF-A-MAP region in the mapping process.

There is one HF-A-MAP region in each DL AAI subframe. Within each HF-A-MAP region, the index for HF-A-MAP channel is calculated as follows.

For the deallocation of a persistent allocation, the HF-A-MAP resource index is specified in the HFA the of UL Persistent Allocation A-MAP IE.

For group resource allocation, the HF-A-MAP resource index for the l^{th} AMS in the GRA allocation is $(i_{start} + \lfloor l \cdot N_{HF-A-MAP}/N_{GRA} \rfloor) \bmod N_{HF-A-MAP}$, where i_{start} is the ACK Channel Offset in the UL group resource allocation A-MAP IE, $N_{HF-A-MAP}$ is the total number of HF-A-MAP configured per HF-A-MAP region, and N_{GRA} is the User Bit Map Size in the UL group resource allocation A-MAP IE.

For the BR-ACK A-MAP IE, the HF-A-MAP resource index for the l^{th} AMS grant in the BR-ACK bitmap is $(i_{start} + \lfloor l \cdot N_{HF-A-MAP}/N_{BR-ACK} \rfloor) \bmod N_{HF-A-MAP}$, where i_{start} is the HFA start offset in the BR-ACK A-MAP IE, $N_{HF-A-MAP}$ is the total number of HF-A-MAP channels configured per HF-A-MAP region, and N_{BR-ACK} is the number of AMSs with grants in the BR-ACK A-MAP IE.

For resource allocation using the UL Basic Assignment A-MAP IE, UL Subband Assignment A-MAP IE, CDMA Allocation A-MAP IE and the UL Persistent Allocation A-MAP

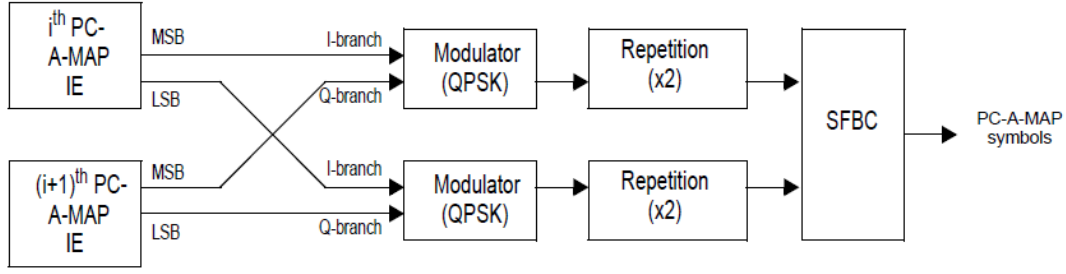


Figure 2.38: Chain of PC-A-MAP IE to PC-A-MAP symbols (Figure 522 in [10]).

IE, the HF-A-MAP resource index is $(M(j) + n) \bmod N_{HF-A-MAP}$, where j is HF-A-MAP Index Parameter in the Non-user specific A-MAP IE, n is a 3 bit HFA value in each assignment A-MAP IE, $N_{HF-A-MAP}$ is the total number of HF-A-MAP channels configured per HF-A-MAP region. $M(j)$ is STID for the UL Basic Assignment A-MAP IE and UL Subband Assignment A-MAP IE and RA-ID for CDMA Allocation A-MAP IE when $j = 0$ and $M(j)$ is the lowest LRU index of the corresponding UL transmission when $j = 1$. For the UL persistent allocation A-MAP IE, $M(j)$ is always STID regardless of value j .

Power Control A-MAP

Power Control A-MAP (PC-A-MAP) contains PC-A-MAP-IEs for closed-loop power control of the uplink transmission. The ABS shall transmit PC-A-MAP-IE to every AMS which operates in closed-loop power control mode.

Figure 2.38 shows the construction procedure of PC-A-MAP symbols from PC-A-MAP-IE. The i^{th} PC-A-MAP-IE shall have the size of 2 bits according to power correction value.

The i^{th} and $(i + 1)^{th}$ PC-A-MAP IEs shall be mapped to two QPSK symbols as depicted in Figure 2.38. Only the i^{th} PC-A-MAP may also be mapped to two QPSK symbols for transmitting to the corresponding MS with poor channel quality.

Power scaling by $\sqrt{P_i}$ ($0 \leq i \leq N_{PC-A-MAP-IE}$) shall be applied to the i^{th} PC-A-

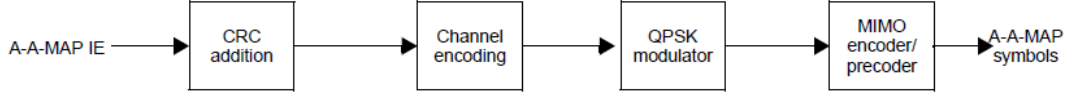


Figure 2.39: Chain of A-A-MAP IE to A-A-MAP symbols (Figure 523 in [10]).

MAP-IE where $N_{PC-A-MAP-IE}$ is the number of PC-A-MAP-IEs and $\text{sqrt}(\text{Pi})$ is the value determined by the management entity to satisfy the link performance.

The QPSK symbols are repeated $N_{rep,PC-A-MAP-IE}$ times, where $N_{rep,PC-A-MAP-IE}$ equals two.

Figure 2.38 shows a cluster of PC-A-MAP channels, which consists of 2 PC-A-MAP channels numbered as $2c$ and $2c + 1$ where c is the PC-A-MAP cluster index in the A-MAP region. Channel $2c$ in the cluster occupies the real part of both symbols in each tone pair before the SFBC encoder. Channel $2c + 1$ occupies the imaginary part of both symbols in each tone pair before the SFBC encoder.

For each Tx antenna, symbols at the output of MIMO encoder, denoted by $S_{PC}[0]$ to $S_{PC}[L_{PC} - 1]$, are mapped to tone-pairs from $RMP[(L_{HF}/2)]$ to $RMP[(L_{HF} + L_{PC})/2 - 1]$, where RMP refers to the renumbered A-MAP tone-pairs and L_{HF} is the number of tones required to transmit the entire HARQ feedback A-MAP; L_{PC} is the number of tones required to transmit the entire power control A-MAP. Clusters of the PC-A-MAP are indexed sequentially in the mapping process.

Assignment A-MAP

The Assignment A-MAP (A-A-MAP) shall include one or multiple A-A-MAP IEs and each A-A-MAP IE is encoded separately. Figure 2.39 describes the procedure for constructing A-A-MAP symbols.

A 16-bit CRC is generated based on the contents of the assignment A-MAP IE. Denote the

assignment A-MAP IE by $m(x) = b_{N-1}x^{N-1} + b_{N-2}x^{N-2} + \dots + b_1x + b_0$, where b_{N-1} is the MSB of the assignment A-MAP IE and b_0 is the LSB of the assignment A-MAP IE. The 16-bit CRC is calculated as the remainder of dividing $m(x)x^{16}$ by the 16-bit CRC generator polynomial $g(x) = x^{16} + x^{12} + x^5 + 1$. The resulted CRC is denoted by $p(x) = p_{15}x^{15} + p_{14}x^{14} + \dots + p_1x + p_0$ where p_{15} is the MSB of the CRC and p_0 is the LSB of the CRC.

The 16-bit CRC mask is then applied to the 16-bit CRC by bitwise XOR operation.

The masked CRC is then appended to the assignment A-MAP IE, resulting in a bit sequence of $m(x) * x^{16} + p(x) \oplus q(x)$. The resulting sequence of bits shall be encoded by the TBCC.

Coded bits can be repeated to improve the robustness of an A-A-MAP channel based on the link condition of a particular AMS.

For a given system configuration, assignment A-MAP IEs can be encoded with two different effective code rates. The set of code rates is $(1/2, 1/4)$ or $(1/2, 1/8)$ and is explicitly signaled in the S-SFH.

In case of FFR, two code rates, either $(1/2, 1/4)$ or $(1/2, 1/8)$, can be used in the reuse 1 partition. $1/2$ or $1/4$ code rate is used in the power-booster reuse 3 partition and signaled in the S-SFH.

The parameters for TBCC are $M = K_{bufsize} = 2L$ for $1/2$ code rate, $M = K_{bufsize} = 4L$ for $1/4$ code rate, and $M = 2K_{bufsize}$ and $K_{bufsize} = 4L$ for $1/8$ code rate where L is the number of information bits. The encoded bit sequences shall be modulated using QPSK.

2.9.2 Downlink Power Control

The ABS should be capable of controlling the transmit power per AAI subframe and per user. An ABS can exchange necessary information with neighbor ABS through backbone

network to support downlink power control.

Power Control for A-MAP

Downlink transmit power density of A-MAP transmission for an AMS may be set in order to satisfy target error rate for the given MCS level which is used for the A-MAP transmission. Detail algorithm is left to vendor-specific implementations.



Chapter 3

Introduction to IEEE 802.16m MIMO

We introduce the MIMO transmission mechanism in IEEE 802.16m. Much of the material is taken from [10].

3.1 Downlink MIMO Architecture and Data Processing [10]

This section is mainly taken from [10]. The architecture of downlink MIMO at the transmitter side is shown in Fig. 3.1. The MIMO encoder block maps L MIMO layers ($L \geq 1$) onto M_t MIMO streams ($M_t \geq L$), which are fed to the precoder block. For the spatial multiplexing modes in SU-MIMO, “rank” is defined as the number of MIMO streams to be used for the user allocated to the Resource Unit (RU). For SU-MIMO, only one user is

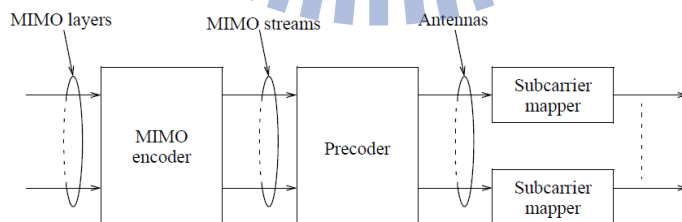


Figure 3.1: DL MIMO architecture (Fig.537 in [10]).

scheduled in one RU, and only one forward error correction (FEC) block exists at the input of the MIMO encoder (vertical MIMO encoding at transmit side). For MU-MIMO, multiple users can be scheduled in one RU, and multiple FEC blocks exist at the input of the MIMO encoder (horizontal MIMO encoding or combination of vertical and horizontal MIMO encoding at transmit side, which is called multi-layer encoding). The precoder block maps MIMO stream(s) to antennas by generating the antenna-specific data symbols according to the selected MIMO mode. The subcarrier mapper blocks map antenna-specific data to the OFDM symbol.

3.2 MIMO Layer to MIMO Stream Mapping [10]

Again this section is mainly taken from [10]. MIMO layer to MIMO stream mapping is performed by the MIMO encoder. The MIMO encoder is a batch processor that operates on M input symbols at a time. The input to the MIMO encoder is represented by an $M \times 1$ vector as

$$\mathbf{s} = \begin{bmatrix} s_1 \\ s_2 \\ \vdots \\ s_M \end{bmatrix} \quad (3.1)$$

where s_i is the i th input symbol within a batch. In MU-MIMO transmissions, the M symbols belong to different AMSs. Two consecutive symbols may belong to a single MIMO layer. One AMS shall have at most one MIMO layer. MIMO layer to MIMO stream mapping of the input symbols is done in the space dimension first. The output of the MIMO encoder is an $M_t \times N_F$ MIMO STC matrix as,

$$\mathbf{x} = S(\mathbf{s}), \quad (3.2)$$

which serves as the input to the precoder, where M_t is the number of MIMO streams, N_F is the number of subcarriers occupied, \mathbf{x} is the output of the MIMO encoder, \mathbf{s} is the input MIMO layer vector, and $S()$ is a function that maps an input MIMO layer vector to an

STC matrix which will be further defined specifically for various cases below. There are four MIMO encoder formats (MEF): SFBC, vertical encoding (VE), multi-layer encoding (ME), and conjugate data repetition (CDR). For SU-MIMO transmissions, the STC rate is defined as $R = \frac{M}{N_F}$

For MU-MIMO transmissions, the STC rate per user (R) is equal to 1 or 2.

3.2.1 SFBC Encoding

The input to the MIMO encoder is a 2×1 vector

$$\mathbf{s} = \begin{bmatrix} s_1 \\ s_2 \end{bmatrix}, \quad (3.3)$$

and the MIMO encoder generates the 2×2 SFBC matrix

$$\mathbf{x} = \begin{bmatrix} s_1 & -s_2^* \\ s_2 & s_1^* \end{bmatrix}. \quad (3.4)$$

Where \mathbf{x} is a 2×2 matrix. The matrix \mathbf{x} occupies two consecutive subcarriers.

3.2.2 Vertical Encoding (VE)

The input and the output of MIMO encoder are both the same $M \times 1$ vector as

$$\mathbf{x} = \mathbf{s} = \begin{bmatrix} s_1 \\ s_2 \\ \vdots \\ s_M \end{bmatrix} \quad (3.5)$$

where s_i , $1 \leq i \leq M$, belong to the same MIMO layer. The encoder is an identity operation.

3.2.3 Multi-layer Encoding (ME)

The input and the output of MIMO encoder are again the same $M \times 1$ vector

$$\mathbf{x} = \mathbf{s} = \begin{bmatrix} s_1 \\ s_2 \\ \vdots \\ s_M \end{bmatrix}, \quad (3.6)$$

but now s_i , $1 \leq i \leq M$ belong to different MIMO layers, where two consecutive symbols may belong to a single MIMO layer. Multi-layer encoding is only used for MU-MIMO mode. The encoder is an identity operation.

3.2.4 CDR Encoding

The input to the MIMO encoder is a 1×1 vector

$$s = s_1, \quad (3.7)$$

yielding

$$\mathbf{x} = [s_1 \quad s_1^*], \quad (3.8)$$

The CDR matrix \mathbf{x} occupies two consecutive subcarriers.

3.3 MIMO Stream to Antenna Mapping [10]

Again this section is mainly taken from [10]. MIMO stream to antenna mapping is performed by the precoder. The output of the MIMO encoder is multiplied by an $N_t \times M_t$ precoder \mathbf{W} to yield an $N_t \times N_F$ matrix \mathbf{z} as

$$\mathbf{z} = \mathbf{W}\mathbf{x} = \begin{bmatrix} z_{1,1} & z_{1,2} & \cdots & z_{1,N_F} \\ z_{2,1} & z_{2,2} & \cdots & z_{2,N_F} \\ \vdots & \vdots & \ddots & \vdots \\ z_{N_t,1} & z_{N_t,2} & \cdots & z_{N_t,N_F} \end{bmatrix} \quad (3.9)$$

where N_t is the number of transmit antennas and $z_{j,k}$ is the output symbol to be transmitted via the j th physical antenna on the k th subcarrier. Pilots within PRU are precoded in the same way as the data subcarriers.

3.3.1 Non-adaptive Precoding

With non-adaptive precoding, the precoding matrix is an $N_t \times M_t$ matrix $\mathbf{W}(k)$, where N_t is the number of transmit antennas, M_t is the number of MIMO streams, and k is the physical

MEF	RU with M_t pilot MIMO streams outside OL region	RU in OL region with $\text{Max}M_t$ MIMO streams
SFBC	$N_t=2: C_{DL,OL,SU}(2, M_t, 1), M_t=2$ $N_t=4: C_{DL,OL,SU}(4, M_t, 4), M_t=2$ $N_t=8: C_{DL,OL,SU}(8, M_t, 4), M_t=2$	$N_t=2: C_{DL,OL,SU}(2, M_t, 1), \text{Max}M_t=2$ $N_t=4: C_{DL,OL,SU}(4, M_t, 4), \text{Max}M_t=2$ $N_t=8: C_{DL,OL,SU}(8, M_t, 4), \text{Max}M_t=2$
VE	$N_t=2: C_{DL,OL,SU}(2, M_t, 1), M_t=1,2$ $N_t=4: C_{DL,OL,SU}(4, M_t, 4), M_t=1,2,3,4$ $N_t=8: C_{DL,OL,SU}(8, M_t, 4), M_t=1,2,3,4$ N_w depends on M_t	$N_t=2: C_{DL,OL,SU}(2, M_t, 1), \text{Max}M_t=2$ $N_t=4: C_{DL,OL,SU}(4, M_t, 4), \text{Max}M_t=2$ $N_t=8: C_{DL,OL,SU}(8, M_t, 4), \text{Max}M_t=2$
ME	n.a	n.a
CDR	n.a	$N_t=2: C_{DL,OL,SU}(2, M_t, 2), \text{Max}M_t=1$ $N_t=4: C_{DL,OL,SU}(4, M_t, 4), \text{Max}M_t=1$ $N_t=8: C_{DL,OL,SU}(8, M_t, 8), \text{Max}M_t=1$

Figure 3.2: Codebook subsets used for non-adaptive precoding in DL-DLRU and NLRU (from [10, Table 842]).

index of the subcarrier where $\mathbf{W}(k)$ is applied. The precoding matrix is selected from the base codebook or from a subset of the base codebook of size N_w for a given rank, as specified in Figs. 3.2 and 3.3, where $C_{DL,OL,SU}(N_t, M_t, N_w)$ denotes a DL OL SU-MIMO codebook subset which consists of N_w complex matrices of dimension N_t by M_t . The base codebook and the codebook subsets are defined in Quantized MIMO feedback for CL transmit precoding.

- Non-adaptive precoding outside the OL region: In an RU allocated outside the OL region, with MEF using SFBC or VE and non-adaptive precoding, the precoding matrix changes every $N_1 P_S C$ contiguous physical subcarriers, and it does not depend on the AAI subframe number. The $N_t \times M_t$ precoding matrix $\mathbf{W}(k)$ applied on subcarrier k in physical subband s is selected as the codeword of index i in the codebook of rank M_t specified in Figs. 3.2 or 3.3, with i given by

$$i = s \mod N_w, \quad s = 0, \dots, N_{sub} - 1, \quad (3.10)$$

where N_{sub} denotes the number of physical subbands across the entire system bandwidth. In an RU allocated outside the OL region, with MEF using ME and non-

MEF	RU with M_t pilot MIMO streams outside OL region	RU in OL region with $\text{Max}M_t$ MIMO streams
SFBC	n.a	n.a
VE	$N_t=2$: $C(2, M_v, 3)$, $M_t=1, \dots, \text{Max}M_t$ $N_t=4$: $C(4, M_v, 4)$, $M_t=1, \dots, \text{Max}M_t$ $N_t=8$: $C(8, M_v, 4)$, $M_t=1, \dots, \text{Max}M_t$	$N_t=2$: $C(2, M_v, 3)$, $\text{Max}M_t=2$ $N_t=4$: $C(4, M_v, 4)$, $\text{Max}M_t=2$ $N_t=8$: $C(8, M_v, 4)$, $\text{Max}M_t=2$
ME	$N_t=2$: $C(2, M_v, 3)$, $M_t=2, \dots, \text{Max}M_t$ $N_t=4$: $C(4, M_v, 4)$, $M_t=2, \dots, \text{Max}M_t$ $N_t=8$: $C(8, M_v, 4)$, $M_t=2, \dots, \text{Max}M_t$	$N_t=2$: $C(2, M_v, 3)$, $\text{Max}M_t=2$ $N_t=4$: $C(4, M_v, 4)$, $\text{Max}M_t=2$ $N_t=8$: $C(8, M_v, 4)$, $\text{Max}M_t=2$
CDR	n.a	$N_t=2$: $C(2, M_v, 3)$, $\text{Max}M_t=1$ $N_t=4$: $C(4, M_v, 4)$, $\text{Max}M_t=1$ $N_t=8$: $C(8, M_v, 4)$, $\text{Max}M_t=1$

Figure 3.3: Codebook subsets used for non-adaptive precoding in DL-SLRU (from [10, Table 843]).

adaptive precoding, the precoding matrix changes every N_1 PRUs, and it does not depend on the AAI subframe number. The $N_t \times M_t$ precoding matrix $\mathbf{W}(k)$ applied on subcarrier k in subband s is selected as any M_t unordered columns of the codeword of index i in the codebook of rank $\text{max} M_t$ specified in Fig. 3.3, where i is given by (3.10), and $\text{max} M_t$ is specified in Feedback Allocation A-MAP IE or Feedback Polling A-MAP IE. The AMS shall assume $M_t = \text{max} M_t$ in the codebook of Fig. 3.2 for its feedback of stream index.

- Non-adaptive precoding inside the OL region: In an RU allocated in the $\text{max} M_t$ MIMO streams OL region, the precoding matrix changes every N PRUs, where $N = N_1$ in all OL regions except in the OL region of type 1 with NLRU. The $N_t \times \text{max} M_t$ precoding matrix $\mathbf{W}(k)$ applied on subcarrier k in physical subband s is selected as the codeword of index i in the codebook of rank $\text{max} M_t$ specified in Fig. 3.2 or 3.3, with i given by

$$i = s \mod N_w, \quad s = 0, \dots, N_{sub} - 1, \quad (3.11)$$

where N_{sub} denotes the number of physical subbands across the entire system band-

width. In the OL region of type 1 with NLRU, $N = N_2$, and the $N_t \times 1$ precoding matrix $\mathbf{W}(k)$ applied on subcarrier k in PRU m in AAI subframe number t is selected as the codeword of index i in the codebook of rank $\max M_t = 1$ specified in Fig. 3.2, with i given by

$$i = (m + (t \bmod 2)) \bmod N_w, \quad m = 0, \dots, N_{PRU} - 1, \quad (3.12)$$

where N_{PRU} denotes the number of physical PRUs across the entire system bandwidth.

3.3.2 Adaptive Precoding

With adaptive precoding, the precoder \mathbf{W} is derived from the feedback of the AMS. For codebook-based adaptive precoding (codebook feedback), there are three feedback modes: base mode, transformation mode and differential mode. For TDD sounding-based adaptive precoding, the value of \mathbf{W} is derived from the AMS sounding feedback.

3.4 Downlink MIMO Modes [10]

Again this section is mainly taken from [10]. There are six MIMO transmission modes for unicast DL MIMO transmission as listed in Fig. 3.4 and 3.6. The allowed values of the parameters for each DL MIMO mode are shown in Figure 3.6. * 2 streams to one AMS and 1 stream to another AMS, with 1 layer each. ** 2 streams to one AMS and 1 stream each to the other two AMSs, with 1 layer each. M_t refers to the number of MIMO streams transmitted to one AMS with MIMO modes 0, 1, 2 and 5. M_t refers to the total number of MIMO streams transmitted to multiple AMS on the same RU with MIMO modes 3 and 4.

3.5 Transmission Schemes for Data Channels [10]

Again this section is mainly taken from [10].

Mode index	Description	MIMO encoding format (MEF)	MIMO precoding
Mode 0	OL SU-MIMO (Tx diversity)	SFBC	Non-adaptive
Mode 1	OL SU-MIMO (SM)	VE	Non-adaptive
Mode 2	CL SU-MIMO (SM)	VE	Adaptive
Mode 3	OL MU-MIMO (SM)	ME	Non-adaptive
Mode 4	CL MU-MIMO (SM)	ME	Adaptive
Mode 5	OL SU-MIMO (Tx diversity)	CDR	Non-adaptive

Figure 3.4: Downlink MIMO modes (from [10, Table 844]).

3.5.1 Encoding and Precoding of SU-MIMO

Encoding of SU-MIMO Modes

- MIMO mode 0: Uses SFBC encoding.
- MIMO mode 1: Uses VE. The number of MIMO streams is $M_t \leq \min(N_t, N_r)$ where N_r is the number of receive antennas and M_t is no more than 8.
- MIMO mode 2: Uses VE. The number of MIMO streams is $M_t \leq \min(N_t, N_r)$ where M_t is no more than 8.
- MIMO mode 5: Uses CDR encoding.
- MIMO mode 0: Uses non-adaptive precoding with $M_t = 2$ MIMO streams.
- MIMO mode 1: Uses non-adaptive precoding with M_t MIMO streams.
- MIMO mode 2: Uses adaptive precoding.
- MIMO mode 5: Uses non-adaptive precoding with $M_t = 1$ stream.

	Number of transmit antennas	STC rate per MIMO layer	Number of MIMO streams	Number of subcarriers	Number of MIMO layers
	N_t	R	M_t	N_F	L
MIMOMode 0	2	1	2	2	1
	4	1	2	2	1
	8	1	2	2	1
MIMOMode 1 and MIMOMode 2	2	1	1	1	1
	2	2	2	1	1
	4	1	1	1	1
	4	2	2	1	1
	4	3	3	1	1
	4	4	4	1	1
	8	1	1	1	1
	8	2	2	1	1
	8	3	3	1	1
	8	4	4	1	1
	8	5	5	1	1
	8	6	6	1	1
	8	7	7	1	1
	8	8	8	1	1
	8	8	8	1	1
MIMOMode 3 and MIMOMode 4	2	1	2	1	2
	4	1	2	1	2
	4	1	3	1	3
	4	1	4	1	4
	8	1	2	1	2
	8	1	3	1	3
	8	1	4	1	4

Figure 3.5: DL MIMO parameters (from [10, Table 845]).

3.5.2 Encoding and Precoding of MU-MIMO

Multi-user MIMO schemes are used to enable a resource allocation to communicate data to two or more AMSs. Multi-user transmission with one or two MIMO streams per AMS is

	Number of transmit antennas	STC rate per MIMO layer	Number of MIMO streams	Number of subcarriers	Number of MIMO layers
	N_t	R	M_t	N_F	L
MIMO mode 4	4	2 and 1*	3	1	2
	4	2 and 1**	4	1	3
	4	2	4	1	2
	8	2 and 1*	3	1	2
	8	2 and 1*	4	1	3
	8	2	4	1	2
MIMO mode 5	2	1/2	1	2	1
	4	1/2	1	2	1
	8	1/2	1	2	1

Figure 3.6: DL MIMO parameters (from [10, Table 845]).

supported for MU-MIMO. MU-MIMO includes the MIMO configuration of 2Tx antennas to support up to two AMSs, and 4Tx or 8Tx antennas to support up to four AMSs, with one MIMO stream per AMS. Both OL MU-MIMO (mode 3) and CL MU-MIMO (mode 4) are supported.

Encoding of MU-MIMO Modes

- MIMO mode3: Uses multi-layer encoding.
- MIMO mode4: Uses multi-layer encoding.

Precoding of MU-MIMO Modes

- MIMO mode 3: Uses non-adaptive precoding. With OL MU MIMO inside the OL region, the precoder \mathbf{W} with two MIMO streams is predefined and fixed over time. With OL MU MIMO outside the OL region, the precoder \mathbf{W} is an $N_t \times M_t$ sub-matrix

of a predefined $N_t \times \max M_t$ matrix. The precoding matrix \mathbf{W} used by the ABS is given by

$$\mathbf{W}(k) = [v_1(k) \quad v_2(k) \quad \cdots \quad v_{M_t}(k)] \quad (3.13)$$

where $v_i(k)$ is the precoding vector for the i th AMS on the k th subcarrier, which shall also be used for precoding the pilot symbols on the i th pilot MIMO stream on the k th subcarrier.

- MIMO mode 4: Uses adaptive precoding. In CL MU MIMO, the precoder \mathbf{W} is an $N_t \times M_t$ matrix for each subcarrier. It is used to communicate to up to M AMSs simultaneously. The form and derivation of the precoding matrix does not need to be known at the AMS. The ABS determines the precoding matrix based on the feedback received from the AMS. The ABS shall construct the precoding matrix \mathbf{W} as

$$\mathbf{W}(k) = [v_1(k) \quad v_2(k) \quad \cdots \quad v_{M_t}(k)] \quad (3.14)$$

where $v_i(k)$ is the precoding vector for the i th MIMO stream on the k th subcarrier, which shall also be used for precoding the pilot symbols on the i th pilot MIMO stream on the k th subcarrier.

3.5.3 Mapping of Data and Pilot Subcarriers

Consecutive symbols for each antenna at the output of the MIMO precoder are mapped in a frequency domain-first order across LRUs of the allocation, starting from the data subcarrier with the smallest OFDM symbol index and smallest subcarrier index, and continuing to subcarrier index with increasing subcarrier index. When the edge of the allocation is reached, the mapping is continued in the next OFDM symbol.

	DLRU	NLRU	SLRU
MIMO mode 0	Yes	Yes	No
MIMO mode 1	Yes, with $M_t=2$	Yes, with $M_t \leq 4$	Yes
MIMO mode 2	No	Yes, with $M_t \leq 4$	Yes
MIMO mode 3	No	No	Yes
MIMO mode 4	No	Yes	Yes
MIMO mode 5	No	No	No

Figure 3.7: Supported Permutation for each DL MIMO mode outside the OL region (from [10, Table 846]).

	DLRU	NLRU	SLRU
MIMO mode 0	Yes, with $\text{Max}M_t = 2$	No	No
MIMO mode 1	Yes, with $\text{Max}M_t = 2$	No	Yes, with $\text{Max}M_t = 2$
MIMO mode 2	No	No	No
MIMO mode 3	No	No	Yes, with $\text{Max}M_t = 2$
MIMO mode 4	No	No	No
MIMO mode 5	No	Yes, with $\text{Max}M_t = 1$	Yes, with $\text{Max}M_t = 1$

Figure 3.8: Supported Permutation for each DL MIMO mode in the OL region (from [10, Table 847]).

3.5.4 Usage of MIMO Modes

Fig. 3.7 shows permutations supported for each MIMO mode outside the OL region. All pilots are precoded regardless of the number of transmit antennas and allocation type.

3.6 Feedback Mechanisms and Operation [10]

Again this section is mainly taken from [10].

3.6.1 Open-Loop Region

An OL region with $\max M_t$ MIMO streams is defined as a time-frequency resource using the $\max M_t$ MIMO streams pilot pattern and a given OL MIMO mode with $M_t = \max M_t$ without rank adaptation. The OL region allows base stations to coordinate their OL MIMO transmissions, in order to offer a stable interference environment where the precoders and numbers of MIMO streams are not time-varying. The LRUs used for the OL region are indicated in the AAI SCD message. These LRUs shall be aligned across cells. Only a limited set of OL MIMO modes are allowed for transmission in the OL region, as specified in Fig. 3.8. All OL MIMO modes can also be used outside the OL region except for MIMO mode 5, as specified in Fig. 3.7. An OL region is associated with a specific set of parameters:

- type (number of MIMO streams $\max M_t$, MIMO mode, MIMO feedback mode, type of permutation), and
- LRUs.

There are three types of OL regions, as specified in Fig. 3.9. Dynamic switching between MIMO modes 1 and 3 in downlink transmissions in OL region type 2 is allowed. The rank-2 precoders for transmission with MIMO mode 1 or 3 in OL region type 2 are the same on a given subband. All BSs that are coordinated over the same OL region should use the same number of MIMO streams, in order to guarantee low interference fluctuation and thus improve the CQI prediction at the AMS. All pilots are precoded by non-adaptive precoding with $\max M_t$ MIMO streams in the OL region. CQI measurements should be taken by the AMS on the precoded demodulation pilots rather than on the DL midamble. The $\max M_t$ precoded pilots streams shall be transmitted in all the LRUs in the OL region even if data are not being transmitted by the ABS on some or all of the LRUs.

	MaxMt	MIMO mode	MIMO feedback mode	Supported permutation
OL region type 0	2 MIMO streams	MIMO mode 0 MIMO mode 1 (Mt = 2 MIMO streams)	MFM 0	DLRU
OL region type 1	1 MIMO streams	MIMO mode 5 (Mt = 1 MIMO streams)	MFM 1	NLRU
			MFM 2	SLRU
OL region type 2	2 MIMO streams	MIMO mode 0 (Mt = 2 MIMO streams) MIMO mode 3 (Mt = 2 MIMO streams)	MFM 5	SLRU

Figure 3.9: Types of open-loop regions (from [10, Table 848]).

3.6.2 MIMO Feedback Mode Selection

An AMS may send an unsolicited event-driven report to indicate its preferred MIMO feedback mode to the ABS. Event-driven reports for MIMO feedback mode selection may be sent on the P-FBCH during any allowed transmission interval for the allocated P-FBCH.

3.6.3 MIMO Feedback Modes

Each MIMO transmission mode can be supported by one or several MIMO feedback modes. When allocating a feedback channel, the MIMO feedback mode shall be indicated to the AMS, and the AMS will feedback information accordingly. The description of MIMO feedback modes and corresponding supported MIMO transmission modes is shown in Fig. 3.10. Some detailed description of feedback and AMS processing are in the following subsections.

The feedback of the quantized wideband correlation matrix shall be requested by the ABS for operation with transformation codebook-based feedback mode using the Feedback Polling A-MAP IE. The ABS may request the feedback of the quantized wideband correlation matrix independently of the MIMO feedback mode requested in the Feedback Allocation A-MAP

IE. The quantized wideband correlation matrix may be used for wideband beamforming.

MIMO feedback mode 0 is used for the OL-SU SFBC and SM adaptation in diversity permutation. The AMS estimates the wideband CQI for both SFBC and SM, and reports the CQI and STC Rate. STC Rate 1 means SFBC with precoding and STC Rate 2 means rank-2 SM with precoding. MIMO feedback mode 0 may also be used for CQI feedback for sounding based beamforming. The AMS shall estimate the wideband CQI for SFBC mode ($\max M_t = 0b00$), and report the CQI.

MIMO feedback mode 1 is used for the OL-SU CDR with STC rate 1/2 in diversity permutation. MIMO feedback mode 2 is used for the OL-SU SM in localized permutation for frequency selective scheduling. The STC Rate indicates the preferred number of MIMO streams for SM. The subband CQI shall correspond to the selected rank. MIMO feedback mode 3 is used for the CL-SU SM in localized permutation for frequency selective scheduling. The STC Rate indicates the preferred number of MIMO streams for SM. The subband CQI shall correspond to the selected rank.

MIMO feedback mode 4 is used for the CL SU MIMO using wideband beamforming with rank 1. In this mode, AMS shall feedback the wideband CQI. The wideband CQI shall be estimated at the AMS assuming short-term or long-term precoding at the ABS, according to the feedback period. The channel state information may be obtained at the ABS via the feedback of the correlation matrix, or via the feedback of the wideband PMI.

MIMO feedback mode 5 is used for OL MU MIMO in localized permutation with frequency selective scheduling. In the mode, AMS shall feedback the subband selection, MIMO stream indicator and the corresponding CQI.

MIMO feedback mode 6 is used for CL MU MIMO in localized permutation with frequency selective scheduling. In this mode, AMS shall feedback the subband selection, corresponding CQI and subband PMI. The subband CQI refers to the CQI of the best PMI

in the subband. Rank-1 base codebook (or its subset) is used to estimate the PMI in one subband.

MIMO feedback mode 7 is used for CL MU MIMO in diversity permutation using wideband beamforming MU MIMO. In this mode, AMS shall feedback the wideband CQI. The wideband CQI shall be estimated at the AMS assuming short-term or long-term precoding at the ABS, according to the feedback period. The channel state information may be obtained at the ABS via the feedback of the correlation matrix. or via the feedback of the wideband PMI.

3.6.4 Downlink Signaling Support of DL-MIMO Modes

The BS shall send some parameters necessary for DL MIMO operation in a broadcast message. The broadcast information is carried in the S-SFH SP3 IE or in the additional broadcast information such as AAI SCD or AAI DL IM messages. The BS shall send some parameters necessary for DL MIMO operation in a unicast message. The unicast information is carried in the DL Basic Assignment A-MAP IE, DL Subband Assignment A-MAP IE, DL Persistent A-MAP IE, Feedback Polling A-MAP IE, and Feedback Allocation A-MAP IE. Figure 3.12 specifies the DL control parameters required for MIMO operation. When CS indication indicates the use of a codebook subset and MFM indicates a CL SU MIMO mode (MFM = 3 and 4), the MS shall use the SU base codebook subset of Fig. 3.13 when $N_t = 4$. When CS indication indicates the use of a codebook subset and MFM indicates a CL MU MIMO mode (MFM = 6 and 7), the MS shall use the MU base codebook subset of Fig. 3.13 when $N_t = 4$.

MIMO Feedback Mode	Description and Type of RU	Feedback Content	Support MIMO Mode Outside the OL region	Support MIMO Mode Inside the OL region
0	OLSU MIMO SFBC/SM (Diversity: DLRU, NLRU) Sounding based CL SU and MU MIMO	1. STCrate 2. Wideband CQI	MIMO mode 0 and MIMO mode 1 Flexible adaptation between the two modes STC rate=1:SFBC CQI 2<=STC rate<=4:SM CQI In DLRU: $M_t=2$ for SM In NLRU: $M_t \geq 2$ for SM For sounding based CL SU MU MIMO, STC rate =1:SFBC CQI	MIMO mode 0 and MIMO mode 1 Flexible adaptation between the two modes STC rate=1:SFBC CQI STC rate=2:SM CQI In DLRU only
1	OLSU MIMO SM (Diversity: NLRU)	1. Wideband CQI	n.a	MIMO mode 5 STC rate = 1/2
2	OLSU MIMO SM (localized: SLRU)	1. STCrate 2. Subband CQI 3. Subband selection	MIMO Mode 1 1<=STC rate<=8	MIMO mode 5 STC rate = 1/2
3	CLSU MIMO (localized: SLRU)	1. STCrate 2. Subband CQI 3. Subband PMI 4. Subband selection 5. Wideband correlation matrix	MIMO mode 2 1<=STC rate<=8	n.a
4	CLSU MIMO (Diversity: NLRU)	1. Wideband CQI 2. Wideband PMI 3. Wideband correlation matrix	MIMO mode 2 ($M_t \leq 4$)	n.a
5	OLMU MIMO (localized: SLRU)	1. Subband CQI 2. Subband selection 3. MIMO stream indicator	MIMO mode 3	MIMO mode 3
6	CLMU MIMO (localized: SLRU)	1. Subband CQI 2. Subband PMI 3. Subband selection 4. Wideband correlation matrix	MIMO mode 4	n.a
7	CLMU MIMO (Diversity: NLRU)	1. Wideband CQI 2. Wideband PMI 3. Wideband correlation	MIMO mode 4	n.a

Figure 3.10: MIMO feedback modes (from [10, Table 849]).

Parameter	Description	Value	Notes
Broadcast Information			
N_t	Number of transmit antennas at the BS	2,4,8	Indicated in S-SFH (system information) SP3 IE
OL Region	OL MIMO region, which signaling is used to indicate MS where is the predefined OL MIMO region and number of MIMO streams (1 or 2)	OL-Region-ON (1 bit): Signal the existence of OL region. OL-Rank1-Config (3 bit): to signal the combination of sub-band and mini-band in OL region type 1. Refer to Table 848. SB-OL-Region-2-Size (4 bit): signal the number of sub-bands in OL region type 2	Indicated in AAI_SCD Message
BS SI	Rank-1 base codebook subset indication for interference mitigation with PMI coordination	BitMAP: 8 bits if $N_t = 2$ 16 bits if $N_t = 4, 8$	Rank-1 codebook element restriction or recommendation information It shall be ignored if Codebook mode = 0b00, 0b01 or 0b10 It is indicated in AAI DL IM Message Its usage is enabled by Codebook mode or Codebook coordination
Unicast Information			
MEF	MIMO Encoder format	SFBC Vertical encoding Horizontal encoding	MIMO encoder format. Indicated in DL Basic Assignment A-MAP IE, DL Subband Assignment A-MAP IE, DL Persistent A-MAP IE

Figure 3.11: DL MIMO control parameters (from [10, Table 850]).

Parameter	Description	Value	Notes
M_t	Number of MIMO streams in transmission	1 to 8	Number of MIMO streams in the transmission. Indicated in DL Basic Assignment A-MAP IE, DL Subband Assignment A-MAP IE, DL Persistent A-MAP IE
SI	Index of allocation pilot MIMO stream	1 to 4	SI shall be indicated if MEF is HE Indicated in DL Basic Assignment A-MAP IE, DL Subband Assignment A-MAP IE, DL Persistent A-MAP IE
MFM	MIMO feedback mode	Refer to Table 849	To decide the feedback content and related MS processing Indicated in Feedback Allocation A-MAP IE, Feedback Polling A-MAP IE
$MaxM_t$	Maximum number of MIMO streams	If $N_t=2$ (any MFM): 0b0: 1 0b1: 2 If $N_t=4$ (any MFM): 0b00: 1 0b01: 2 0b10: 3 0b11: 4 If $N_t=8$ (SU-MIMO MFM 0, 1, 2, 3, 4): 0b00: 1 0b01: 2 0b10: 4 0b11: 8 If $N_t=8$ (MU-MIMO MFM 5, 6, 7): 0b00: 1 0b01: 2 0b10: 3 0b11: 4	If MFM indicates a SU feedback mode: the maximum STCrate scheduled for each user If MFM indicates a MU feedback mode: the maximum number of users scheduled on each RU Indicated in Feedback Allocation A-MAP IE, Feedback Polling A-MAP IE
CS indication	Codebook subset type for CL MIMO mode 2 and 4	Base codebook or codebook subset	Depending on the MFM and CS indication, the MS shall feedback a PMI from the SU or MU base codebook, or from a subset of the SU or MU of the base codebook. Indicated in Feedback Allocation A-MAP IE, Feedback Polling A-MAP IE
CM	Codebook feedback mode for CL MIMO mode 2 and 4	0b00: base mode with codebook coordination disabled 0b01: transformation mode with codebook coordination disabled 0b10: differential mode with codebook coordination disabled 0b11: differential mode with codebook coordination disabled	This field specifies the codebook feedback mode. If codebook coordination is enabled by setting Codebook_mode to 0b11 or by setting Codebook_coordination to 0b1, and if the AMS reports STC rate equal to 1, then the AMS shall find the rate-1 PMI from the codebook entries broadcasted in

Figure 3.12: DL MIMO control parameters (from [10, Table 850]).

Rank	One	Two	Three	Four
Subset selection	$C(4,1,6,m)$ $m = 0 \text{ to } 15$	$C(4,2,6,m)$ $m = 0 \text{ to } 15$	$C(4,3,6,m)$ $m = 0 \text{ to } 15$	$C(4,4,6,m)$ $m = 0 \text{ to } 5$

Figure 3.13: Subset selection of the base codebook for four transmit antennas (from [10, Table 866]).

3.6.5 Quantized MIMO Feedback for Closed-loop Transmit Precoding

An AMS feedbacks a Preferred Matrix Index (PMI) to support DL precoding. There are three types of codebook feedback modes as follows.

- The base mode: the PMI feedback from a AMS shall represent an entry of the base codebook. It shall be sufficient for the ABS to determine a new precoder.
- The transformation mode: the PMI feedback from a AMS shall represent an entry of the transformed base codebook according to long term channel information.
- The differential mode: the PMI feedback from a AMS shall represent an entry of the differential codebook or an entry of the base codebook at PMI reset times. The feedback from a AMS provides a differential knowledge of the short-term channel information. This feedback represents information that is used along with other feedback information known at the ABS for determining a new precoder.

An AMS shall support the base and transformation modes and may support the differential mode. The transformation and differential feedback modes are applied to the base codebook or to a subset of the base codebook.

Base mode for codebook-based feedback

Index	m	$\mathbf{C}(2,1,3,m) = [\mathbf{c}_1; \mathbf{c}_2]$	
		\mathbf{c}_1	\mathbf{c}_2
000	0	0.7071	-0.7071
001	1	0.7071	-0.5000-0.5000i
010	2	0.7071	-0.7071i
011	3	0.7071	0.5000-0.5000i
100	4	0.7071	0.7071
101	5	0.7071	0.5000+0.5000i
110	6	0.7071	0.7071i
111	7	0.7071	-0.5000+0.5000i

Figure 3.14: Base codebook $\mathbf{c}(2,1,3)$ (from [10, Table 851]).

The base codebook is a unitary codebook. That is each of its matrices consists of columns of a unitary matrix. The AMS selects its preferred matrix from the base codebook based on channel measurements. The AMS sends back the index of the preferred codeword, and the ABS determines the precoder \mathbf{W} according to the index. Both ABS and AMS use the same codebook for correct operation. The base codebooks are defined below for two, four, and eight transmit antennas at the ABS, where the notation $\mathbf{C}(N_t, M_t, N_B)$ denote the codebook, which consists of $2N_B$ complex, matrices of dimension N_t by M_t , and M_t denotes the number of MIMO streams. The notation $\mathbf{C}(N_t, M_t, N_B, i)$ denotes the i -th codebook entry of $\mathbf{C}(N_t, M_t, N_B)$.

The base codebook of SU-MIMO with two transmit antennas consist of rank-1 codebook $\mathbf{C}(2,1,3)$ and rank-2 codebook $\mathbf{C}(2,2,3)$, as illustrated in Figs. 3.14 and 3.15, respectively.

The base codebook for MU-MIMO is the same as the rank 1 base codebook for SU-MIMO. The base codebooks of SU-MIMO with four transmit antennas consist of rank-1 codebook $\mathbf{C}(4,1,6)$, rank-2 codebook $\mathbf{C}(4,2,6)$, rank-3 codebook $\mathbf{C}(4,3,6)$ and rank-4 codebook $\mathbf{C}(4,4,6)$.

Index	m	$c(2,2,3,m) = [c_{11} \ c_{12}; c_{21} \ c_{22}]^T$	
		c_{11} c_{21}	c_{12} c_{22}
000	0	0.7071 0.7071	-0.7071 0.7071
001	1	0.7071 0.7071	-0.5000-0.5000i 0.5000+0.5000i
010	2	0.7071 0.7071	-0.7071i 0.7071i
011	3	0.7071 0.7071	0.5000-0.5000i -0.5000+0.5000i
100-111	4-7	-	-

Figure 3.15: Base codebook $c(2,2,3)$ (from [10, Table 852]).

Transformation Codebook Based Feedback Mode

The base codebooks and their subsets of rank 1 for SU and MU MIMO can be transformed as a function of the ABS transmit correlation matrix. A quantized representation of the ABS transmit correlation matrix shall be fed back by the AMS as instructed by the ABS. Both ABS and AMS transform the rank 1 base codebook to a rank 1 transformed codebook using the correlation matrix. The transformation for codewords of rank 1 is of the form

$$\tilde{v}_t = \frac{R_{v_i}}{\|R_{v_i}\|} \quad (3.15)$$

where v_i is the i th codeword of the base codebook, \tilde{v}_t is the i th codeword of the transformed codebook, and \mathbf{R} is the $N_t \times N_t$ transmit correlation matrix. After obtaining the transformed codebook, both AMS and ABS shall use the transformed codebook for the feedback and precoding process of rank 1.

The codebooks of rank > 1 shall be used without transformation when the AMS is operating with the transformation codebook-based feedback mode.

Diagonal Entries	Binary encoding	a	b	q
q_1	0	0.6	0	0.6000
q_2	1	0.9	0	0.9000

Figure 3.16: Quantization parameters for diagonal entries of \mathbf{R} (from [10, Table 867]).

The correlation matrix \mathbf{R} shall be fed back to support the transformation mode of codebook-based precoding. It is fed back periodically and one correlation matrix is valid for whole band. During some time period and in the whole band, the correlation matrix is measured as

$$\mathbf{R} = E[\mathbf{H}_{ij}^H \mathbf{H}_{ij}] \quad (3.16)$$

where \mathbf{H}_{ij} is the correlated channel matrix in the i th OFDM symbol period and j th subcarriers. Because of the symmetry of the correlation matrix, only the upper triangular elements shall be fed back after quantization.

The \mathbf{R} matrix is normalized by the maximum element amplitude, and then quantized to reduce the feedback overhead. The equation of normalization is

$$\tilde{\mathbf{R}} = \frac{\mathbf{R}}{\max(|r_{ij}|)} \quad i, j = 1, \dots, N_t, \quad (3.17)$$

where $r_{i,j}$ denotes the ij th element of \mathbf{R} . The normalized diagonal elements are quantized by 1 bit, and the normalized complex elements are quantized by 4 bits. The equation for quantization is

$$q = a \cdot e^{(j \cdot b \cdot 2\pi)} \quad (3.18)$$

where either $a = [0.6 \quad 0.9]$ and $b = 0$ or $a = [0.1 \quad 0.5]$ and $b = [0 \quad 1/8 \quad 1/4 \quad 3/8 \quad 1/2 \quad 5/8 \quad 3/4 \quad 7/8]$ for diagonal entries. The total number of bits of feedback is 6 for 2 transmit antennas, 28 for 4 transmit antennas, and 120 for 8 transmit antennas. The AMS and ABS shall use the same transformation based on the correlation matrix fed back by the AMS.

Non-Diagonal Entries	Binary encoding	a	b	q
q_1	0000	0.1	0	0.1000
q_2	0001	0.1	1/8	0.0707+0.0707i
q_3	0010	0.1	1/4	0.1000i
q_4	0011	0.1	3/8	-0.0707+0.0707i
q_5	0100	0.1	1/2	-0.1000
q_6	0101	0.1	5/8	-0.0707-0.0707i
q_7	0110	0.1	3/4	-0.1000i
q_8	0111	0.1	7/8	0.0707-0.0707i
q_9	1000	0.5	0	0.5000
q_{10}	1001	0.5	1/8	0.3536+0.3536i
q_{11}	1010	0.5	1/4	0.5000i
q_{12}	1011	0.5	3/8	-0.3536+0.3536i
q_{13}	1100	0.5	1/2	-0.5000
q_{14}	1101	0.5	5/8	-0.3536-0.3536i
q_{15}	1110	0.5	3/4	-0.5000i
q_{16}	1111	0.5	7/8	0.3536-0.3536i

Figure 3.17: Quantization parameters for non-diagonal entries of R (from [10, Table 868]).

Differential Codebook-Based Feedback Mode

The differential feedbacks exploit the correlation between precoding matrices adjacent in time or frequency. The feedback shall start initially and restart periodically by sending a one-shot feedback that fully depicts the precoder by itself. At least one differential feedback shall follow the start and restart feedback. The start and restart feedback employs the codebook defined for the base mode and is sent through long term report defined in Feedback Allocation A-MAP IE for MFM 3 and 6. The differential feedback is sent through short term report defined in Feedback Allocation A-MAP IE for MFM 3 and 6.

Denote the feedback index, the corresponding feedback matrix, and the corresponding

precoder by t , $\mathbf{D}(t)$, and $\mathbf{V}(t)$, respectively. The sequential index is reset to 0 at $T_{max} + 1$. The index for the start and restart feedbacks are 0. Let \mathbf{A} be a vector or a matrix and \mathbf{Q}_A be the rotation matrix determined by \mathbf{A} . The precoder corresponding to each index is given by

$$\mathbf{V}(t) = \mathbf{Q}_{\mathbf{V}(t-1)} \mathbf{D}(t), \quad t = 0, 1, 2, \dots, T_{max}, \quad (3.19)$$

where the rotation matrix $\mathbf{Q}_{\mathbf{V}(t-1)}$ is a unitary matrix $N_t \times N_t$ computed from the previous precoder $\mathbf{V}(t-1)$ with N_t is the number of transmit antennas. The dimension of the feedback matrix $\mathbf{D}(t)$ is , where M_t is the number of spatial streams. $\mathbf{Q}_{\mathbf{V}(t-1)}$ has the form $\mathbf{Q}_{\mathbf{V}(t-1)} = [\mathbf{V}(t-1) \quad \mathbf{V}^\perp(t-1)]$, where $\mathbf{V}^\perp(t-1)$ consists of columns each of which has a unit norm and is orthogonal to the other columns of $\mathbf{Q}_{\mathbf{V}(t-1)}$. For $M_t = 1$, where $\mathbf{V}(t-1)$ is a vector,

$$\mathbf{Q}_{\mathbf{V}(t-1)} = \begin{cases} \mathbf{I} - \frac{2}{\|\omega\|^2} \omega \omega^H, & \text{for } \|\omega\| > 0, \\ \mathbf{I}, & \text{otherwise,} \end{cases} \quad (3.20)$$

where $\|\mathbf{V}(t-1)\| = 1$ and $\omega = e^{-j\theta} \mathbf{V}(t-1) - \mathbf{e}_1$; θ is the phase of the first entry of $\mathbf{V}(t-1)$, and $\mathbf{e}_1 = [1 \ 0 \dots 0]^T$. For $M_t > 1$, let $L = N_t - M_t$ for computing $\mathbf{Q}_{\mathbf{V}(t-1)}$. L columns are appended to $\mathbf{V}(t-1)$ forming a square matrix $\mathbf{M} = [\mathbf{V}(t-1) \mathbf{E}]$ and the appended columns are

$$\mathbf{E} = [\mathbf{e}_{\tau_1} \dots \mathbf{e}_{\tau_L}] \quad (3.21)$$

where \mathbf{e}_{τ_j} is the $N_t \times 1$ vector whose τ_j th entry is one and whose other entries are zeros. $\mathbf{Q}_{\mathbf{V}(t-1)}$ is computed by orthogonalizing and normalizing the columns of \mathbf{M} . The indexes τ_j for $j = 1, \dots, L$ are selected for the numerical stability of the orthogonalization and normalization process. Let

$$\mathbf{g} = (|\Re(\mathbf{V}(t-1))| + |\Im(\mathbf{V}(t-1))|) \mathbf{a} \quad (3.22)$$

where \mathbf{a} is the $1 \times M_t$ vector with all entries equal to one; $\Re()$ and $\Im()$ take the real and imaginary parts of the inputs, respectively; $||$ takes the absolute values of the input matrix

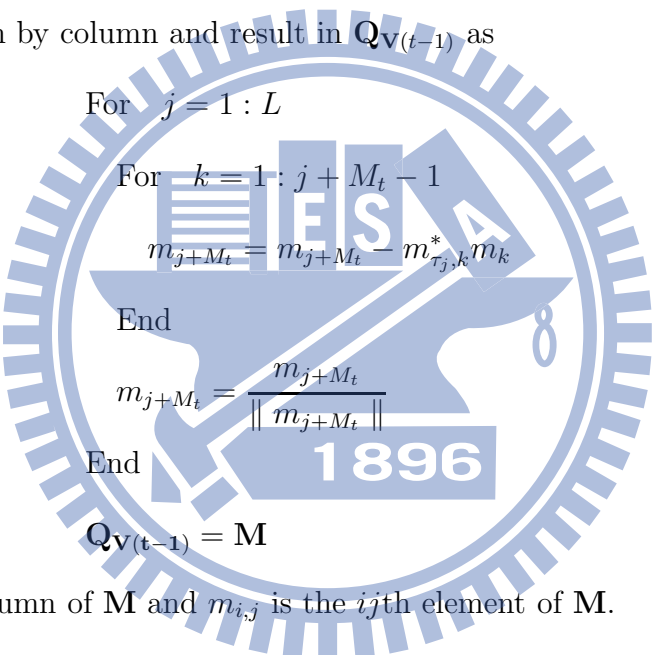
entry by entry. The i th element of the vector \mathbf{g} is the sum of the absolute values of all the real and imaginary parts of $\mathbf{V}(t-1)$ on the same row. The entries of \mathbf{g} are stored in an increasing numerical order. If $\mathbf{g}_i = \mathbf{g}_j$ and $i < j$, then $\mathbf{g}_i < \mathbf{g}_j$ is used in the order list. The order list is

$$\mathbf{g}_{k_1} < \dots < \mathbf{g}_{k_{N_t}} \quad (3.23)$$

where k_i for $i = 1, \dots, N_t$ are row indexes of \mathbf{g} . The first L indexes in the list are assigned to the indexes τ_j in \mathbf{E} as

$$\tau_j = k_j, \quad \text{for } j = 1, \dots, L. \quad (3.24)$$

The Gram-Schmidt orthogonalization and a normalization process are applied to the last L columns of \mathbf{M} column by column and result in $\mathbf{Q}_{\mathbf{V}(t-1)}$ as



```

For  $j = 1 : L$ 
  For  $k = 1 : j + M_t - 1$ 
     $m_{j+M_t} = m_{j+M_t} - m_{\tau_j, k}^* m_k$ 
  End
   $m_{j+M_t} = \frac{m_{j+M_t}}{\|m_{j+M_t}\|}$ 
End
 $\mathbf{Q}_{\mathbf{V}(t-1)} = \mathbf{M}$ 

```

(3.25)

where m_k is the k th column of \mathbf{M} and $m_{i,j}$ is the ij th element of \mathbf{M} .

The feedback matrix $\mathbf{D}(t)$ is selected from a differential codebook. Denote the codebook by $D(N_t, M_t, N_w)$, where N_w is the number of codewords in the codebook. The codebooks $D(2, 1, 4)$ and $D(2, 2, 4)$ are listed in Figs. 3.18 and 3.19, respectively. Denote $D_i(N_t, M_t, N_w)$ the i th codeword of $D(N_t, M_t, N_w)$. The rotation matrices $\mathbf{Q}_{D_i(N_t, M_t, N_w)}$ s of the $D(N_t, M_t, N_w)$ s comprise a set of N_t by N_t matrices that is denoted by $\mathbf{Q}_{D(N_t, M_t, N_w)}$.

The differential codebook $D(4, 3, N_w)$ is computed from $\mathbf{Q}_{D(4, 1, N_w)}$. The i th codeword of

$D(4, 3, N_w)$, denoted by $\mathbf{D}_i(4, 3, N_w)$,

$$\mathbf{D}_i(4, 3, N_w) = \begin{bmatrix} 0 & 1 & 0 & 0 \\ 0 & 0 & 1 & 0 \\ 0 & 0 & 0 & 1 \\ 1 & 0 & 0 & 0 \end{bmatrix} \tilde{\mathbf{Q}}_i(4, 1, N_w) \quad (3.26)$$

where $\tilde{\mathbf{Q}}_i(4, 1, N_w)$ consists of the last three columns of the i th matrix in $\mathbf{Q}_{D(4,1,N_w)}$. The differential codebook $D(4, 4, N_w)$ is computed from $\mathbf{Q}_{D(4,2,N_w)}$. The i th codeword of $D(4, 4, N_w)$ is the i th matrix in $\mathbf{Q}_{D(4,2,N_w)}$. The differential codebooks $D(8, 5, N_w)$, $D(8, 6, N_w)$, $D(8, 7, N_w)$ are computed from $D(8, 3, N_w)$, $D(8, 2, N_w)$, and $D(8, 1, N_w)$, respectively. The i th codewords $\mathbf{D}_i(8, 5, N_w)$, $\mathbf{D}_i(8, 6, N_w)$, and $\mathbf{D}_i(8, 7, N_w)$ of $D(8, 5, N_w)$, $D(8, 6, N_w)$, and $D(8, 7, N_w)$, respectively, are given by

$$\mathbf{D}_i(8, 5, N_w) = \begin{bmatrix} 0 & 0 & 0 & 1 & 0 & 0 & 0 & 0 \\ 0 & 0 & 0 & 0 & 1 & 0 & 0 & 0 \\ 0 & 0 & 0 & 0 & 0 & 1 & 0 & 0 \\ 0 & 0 & 0 & 0 & 0 & 0 & 1 & 0 \\ 0 & 0 & 0 & 0 & 0 & 0 & 0 & 1 \\ 1 & 0 & 0 & 0 & 0 & 0 & 0 & 0 \\ 0 & 1 & 0 & 0 & 0 & 0 & 0 & 0 \\ 0 & 0 & 1 & 0 & 0 & 0 & 0 & 0 \end{bmatrix} \tilde{\mathbf{Q}}_i(8, 3, N_w), \quad (3.27)$$

$$\mathbf{D}_i(8, 6, N_w) = \begin{bmatrix} 0 & 0 & 1 & 0 & 0 & 0 & 0 & 0 \\ 0 & 0 & 0 & 1 & 0 & 0 & 0 & 0 \\ 0 & 0 & 0 & 0 & 1 & 0 & 0 & 0 \\ 0 & 0 & 0 & 0 & 0 & 1 & 0 & 0 \\ 0 & 0 & 0 & 0 & 0 & 0 & 1 & 0 \\ 0 & 0 & 0 & 0 & 0 & 0 & 0 & 1 \\ 1 & 0 & 0 & 0 & 0 & 0 & 0 & 0 \\ 0 & 1 & 0 & 0 & 0 & 0 & 0 & 0 \end{bmatrix} \tilde{\mathbf{Q}}_i(8, 2, N_w), \quad (3.28)$$

$$\mathbf{D}_i(8, 7, N_w) = \begin{bmatrix} 0 & 1 & 0 & 0 & 0 & 0 & 0 & 0 \\ 0 & 0 & 1 & 0 & 0 & 0 & 0 & 0 \\ 0 & 0 & 0 & 1 & 0 & 0 & 0 & 0 \\ 0 & 0 & 0 & 0 & 1 & 0 & 0 & 0 \\ 0 & 0 & 0 & 0 & 0 & 1 & 0 & 0 \\ 0 & 0 & 0 & 0 & 0 & 0 & 1 & 0 \\ 0 & 0 & 0 & 0 & 0 & 0 & 0 & 1 \\ 1 & 0 & 0 & 0 & 0 & 0 & 0 & 0 \end{bmatrix} \tilde{\mathbf{Q}}_i(8, 1, N_w), \quad (3.29)$$

Index	Codeword	Index	Codeword
1	$[1 \ 0]^T$	3	$[\cos(15^\circ) \ \sin(15^\circ)\exp(j120)]^T$
2	$[\cos(15^\circ) \ \sin(15^\circ)]^T$	4	$[\cos(15^\circ) \ \sin(15^\circ) \ \exp(-j120)]^T$

Figure 3.18: D(2,1,4) codebook (from [10, Table 869]).

Index	Codeword	Index	Codeword
1	$[1 \ 0; 0 \ 1]^T$	3	$[\cos(15^\circ) \ \sin(15^\circ)\exp(j120); \sin(15^\circ)\exp(j120) \ \cos(15^\circ)]^T$
2	$[\cos(15^\circ) \ \sin(15^\circ); \sin(15^\circ) \ -\cos(15^\circ)]^T$	4	$[\cos(15^\circ) \ \sin(15^\circ) \ \exp(-j120); \sin(15^\circ) \ \exp(-j120) \ -\cos(15^\circ)]^T$

Figure 3.19: D(2,2,4) codebook (from [10, Table 870]).

where $\tilde{\mathbf{Q}}_i(8, k, N_w)$ consists of the last 8 columns of the i th matrix in $\tilde{\mathbf{Q}}_{D(8,k,N_w)}$. The differential codebook $D(8, 8, N_w)$ is computed from $D(8, 4, N_w)$. The i th codeword of $D(8, 8, N_w)$ is the i th matrix in $\tilde{\mathbf{Q}}_{D(8,k,N_w)}$.

3.7 Uplink MIMO Transmission Schemes [10]

Again this section is mainly taken from [10].

3.7.1 Uplink MIMO Architecture and Data Processing

The architecture of uplink MIMO at the transmitter side is shown in Fig. 3.1. The MIMO encoder block maps a single MIMO layer ($L = 1$) onto M_t ($M_t \geq L$) MIMO streams, which are fed to the precoder block. For SU-MIMO and collaborative spatial multiplexing (MU-MIMO), only one FEC block exists in the allocated RU (vertical MIMO encoding at transmit side).

The precoder block maps MIMO stream(s) to antennas by generating the antenna-specific

data symbols according to the selected MIMO mode. The MIMO encoder and precoder blocks shall be omitted when the AMS has one transmit antenna. The subcarrier mapping blocks map antenna-specific data to the OFDM symbol.

3.7.2 MIMO Layer to MIMO Stream Mapping

MIMO layer to MIMO stream mapping is performed by the MIMO encoder. The uplink MIMO encoder is identical to the downlink MIMO encoder.

Horizontal encoding (MEF = 0b10) is not supported for uplink transmissions. Collaborative spatial multiplexing (CSM) is achieved with vertical encoding (MEF = 0b01) at the AMS. The STC rate per AMS for uplink SU-MIMO and MU-MIMO (CSM) transmissions is defined as $R = M/N_F$. An AMS with 1 transmit antenna shall use vertical encoding (MEF = 0b01) for uplink transmissions.

Uplink SFBC encoding is identical to the downlink SFBC encoding. SFBC encoding format shall not be allocated to an AMS with 1 transmit antenna.

Uplink vertical encoding is identical to the downlink vertical encoding. Vertical encoding with 1 MIMO stream ($M_t = 1$) format shall be allocated to an AMS with 1 transmit antenna.

3.7.3 MIMO Stream to Antenna Mapping

MIMO stream to antenna mapping is performed by the precoder. The uplink mapping is identical to the downlink mapping.

Non-adaptive Precoding

There is no precoding if there is only one transmit antenna at the MS. With non-adaptive precoding, the precoding matrix is an $N_t \times M_t$ matrix $\mathbf{W}(k)$, where N_t is the number of transmit antennas, M_t is the numbers of MIMO streams, and k is the physical index of

MEF	RU with M_t pilot MIMO streams
SFBC	$C_{UL,OL,SU}(N_t, M_t, N_w)$, $M_t = 2$
VE	$C_{UL,OL,SU}(N_t, M_t, N_w)$, $M_t = 1, \dots, 4$

Figure 3.20: Codebook subsets used for non-adaptive precoding in UL DLRU and NLRU (from [10, Table 921]).

MEF	RU with M_t pilot MIMO streams
SFBC	Na
VE	$N_t = 2$: $C_{base, UL}(2, M_t, 4)$, $M_t = 1, 2$ $N_t = 4$: $C_{base, UL}(4, M_t, 6)$, $M_t = 1, 2, 3, 4$

Figure 3.21: Codebook subsets used for non-adaptive precoding in UL SLRU (from [10, Table 922]).

the subcarrier where $\mathbf{W}(k)$ is applied. The matrix \mathbf{W} is selected from a subset of size N_w precoders of the base codebook for a given rank. \mathbf{W} belongs to one of the subsets of the base codebook, according to the type of allocation, MEF, N_t and M_t , as specified in Figs. 3.20 and 3.21.

In an RU allocated in an AAI subframe and non-adaptive precoding, the matrix \mathbf{W} changes every $N_1 P_{SC}$ contiguous physical subcarriers according to Equation, and it does not depend on the AAI subframe number. The $N_t \times M_t$ precoding matrix $\mathbf{W}(k)$ applied on subcarrier k in physical subband s is selected as the codeword of index i in the open-loop codebook subset of rank M_t , where i is given by

$$i = s \mod N_w, \quad s = 0, \dots, N_{sub} - 1, \quad (3.30)$$

with N_{sub} denoting the number of physical subbands across the entire system bandwidth.

Adaptive Precoding

There is no precoding if there is only one transmit antenna at the AMS. With adaptive precoding, the precoder \mathbf{W} is derived at the ABS or at the AMS, as instructed by the ABS. With 2Tx or 4Tx at the AMS in FDD and TDD systems, unitary codebook based adaptive precoding is supported. In this mode, an AMS transmits a sounding signal on the uplink to assist the precoder selection at the ABS. The ABS then signals the uplink precoding matrix index to be used by the AMS. With 2Tx or 4Tx at the AMS in TDD systems, adaptive precoding based on the measurements of downlink reference signals is supported. The AMS chooses the precoder based on the downlink measurements. The form and derivation of the precoding matrix does not need to be known at the ABS.

3.7.4 Uplink MIMO Transmission Modes

There are five MIMO transmission modes for UL MIMO transmission as listed in Fig. 3.22 and where the allowed values of the parameters for each UL MIMO mode are shown in Fig. 3.23. M_t refers to the number of MIMO streams transmitted from one AMS. In modes 3 and 4, N_t refers to the number of transmit antennas at one AMS involved in CSM.

Mode Index	Description	MIMO encoding format (MEF)	MIMO Precoding
Mode 0	OL SU-MIMO	SFBC	Non-adaptive
Mode 1	OL SU-MIMO (SM)	VE	Non-adaptive
Mode 2	CL SU-MIMO (SM)	VE	Adaptive
Mode 3	OL Collaborative spatial multiplexing (MU-MIMO)	VE	Non-adaptive
Mode 4	CL Collaborative spatial multiplexing (MU-MIMO)	VE	Adaptive

Figure 3.22: Uplink MIMO modes (from [10, Table 923]).

	Number of transmit antennas	STC rate per MIMO layer	Number of MIMO streams	Number of subcarriers	Number of MIMO layers
	N_t	R	M_t	N_F	L
MIMO mode 0	2	1	2	2	1
	4	1	2	2	1
MIMO mode 1	1	1	1	1	1
MIMO mode 1 and MIMO mode 2	2	1	1	1	1
	2	2	2	1	1
	4	1	1	1	1
	4	2	2	1	1
	4	3	3	1	1
	4	4	4	1	1
MIMO mode 3 and MIMO mode 4	1	1	1	1	1
	2	1	1	1	1
	2	2	2	1	1
	4	1	1	1	1
	4	2	2	1	1
	4	3	3	1	1

Figure 3.23: UL MIMO parameters (from [10, Table 924]).

	DLRU	NLRU	SLRU
MIMO mode 0	Yes	Yes	No
MIMO mode 1	Yes, with $M_t \leq 2$	Yes	Yes
MIMO mode 2	Yes, with $M_t \leq 2$	Yes	Yes
MIMO mode 3	Yes, with $M_t = 1$	Yes	Yes
MIMO mode 4	Yes, with $M_t = 1$	Yes	Yes

Figure 3.24: Supported permutation for each UL MIMO mode (from [10, Table 925]).

Consecutive symbols for each antenna at the output of the MIMO precoder are mapped in a frequency domain first order across LRUs of the allocation, starting from the data subcarrier with the smallest OFDM symbol index and smallest subcarrier index, and continuing to subcarrier index with increasing subcarrier index. When the edge of the allocation is reached, the mapping is continued on the next OFDM symbol.

Fig. 3.24 shows the permutations supported for each MIMO mode.

Downlink Signaling Support of UL-MIMO Modes

The ABS shall send parameters necessary for UL MIMO operation in a unicast message. The parameters may be transmitted depending on the type of operation. The unicast information is carried in the UL basic Assignment A-MAP IE, UL Subband Assignment A-MAP IE, and UL Persistent A-MAP IE. Fig. 3.25 specifies the DL control parameters required for UL MIMO operation.

Codebooks for Closed-Loop Transmit Precoding

The notation $C_{base,UL}(N_t, M_t, NB)$ denotes the rank- M_t uplink base codebook, which consists of 2^{NB} complex matrices of dimension N_t by M_t , and M_t denotes the number of MIMO streams. The notation $C_{base,UL}(N_t, M_t, NB, i)$ denotes the i^{th} codebook entry of

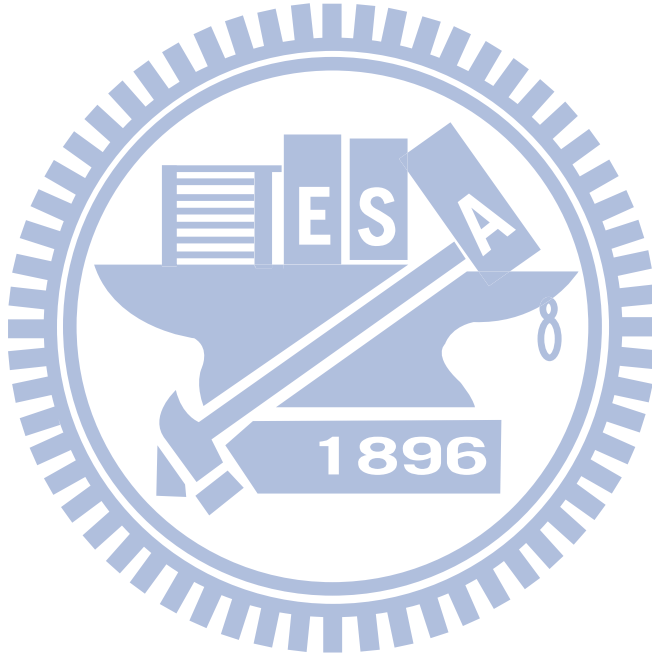
Parameter	Description	Value	Notes
MEF	MIMO encoding format	SFBC Vertical encoding	MIMO encoding format
CSM	Collaborative Spatial Multiplexing	Disabled or enabled	SU MIMO if CSM is disabled MU MIMO if CSM is enabled
Mt	Number of MIMO streams	1 to 4	Number of MIMO streams in the AMS transmission
TNS	Total number of MIMO streams in the LRU	1 to 4	Enabled when CSM is enabled Indication of the total number of MIMO streams in the LRU
SI	First pilot index	1 to 4	Enabled when CSM is enabled. 1 bit for 2Tx, 2bit for 4Tx
PF	Precoding flag	non adaptive precoding or adaptive codebook precoding	Cannot be applied to AMS with 1 transmit antenna
PMI Indicator	PMI indicator	0b0: the AMS shall use the precoder of rank M_t of its choice 0b1: the indicated PMI of rank M_t shall be used by the AMS for precoding	This field is relevant only when PF indicates adaptive codebook precoding. PMI indication = 0b0 may be used in TDD When PMI indication = 0b1, the ABS selects the precoder to use at the AMS
PMI	Precoding matrix index in the UL base codebook	0 to 9 when $N_t = 2$ 0 to 63 when $N_t = 4$	Enabled when PF indicates adaptive codebook precoding, and PMI indication = 0b1.

Figure 3.25: UL MIMO control parameters (from [10, Table 926]).

$$C_{base,UL}(N_t, M_t, NB).$$

The base codebooks of SU-MIMO with two transmit antennas consist of rank-1 codebook $C_{base,UL}(2, 1, 4)$ and rank-2 codebook $C_{base,UL}(2, 2, 3)$. Fig. 3.15 is included to illustrate the rank-1 base codebooks. The rank-2 base codebook $C_{base,UL}(2, 2, 3)$ for uplink 2 Tx is the same as the downlink 2 Tx rank-2 base codebook

The base codebook for UL collaborative spatial multiplexing MIMO is the same as the base codebook for SU-MIMO.



Chapter 4

Equalization and Closed-Loop MIMO Technology

In this chapter, we first introduce the system model and focus on precoding and equalization. Then we include the feedback processing block. We propose two feedback processing method and compare it with three other methods.

4.1 System Model

Fig. 4.1 depicts the considered system model. Information bits for subcarrier k are first passed through the modulator and sent into the encoder. There are four different types of encoder, but we will not discuss them. After passing through the encoder, there are M streams. Let \mathbf{s} be the symbol vector at the encoder output as

$$\mathbf{s}_k = [s_{k,1} s_{k,2} \dots s_{k,M}]^T. \quad (4.1)$$

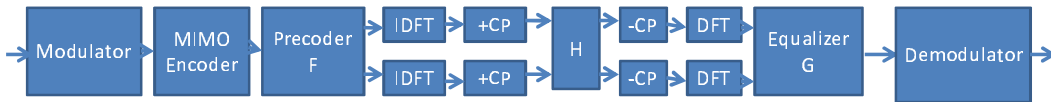


Figure 4.1: System model.

For convenience, we assume that the M data streams are equally-powered and independent to each other. That is, $E[\mathbf{s}_k \mathbf{s}_k^*] = \mathbf{I}_M$ which \mathbf{A}^* denotes complex-conjugate of matrix \mathbf{A} . We denote the precoder by \mathbf{F} . \mathbf{F} is an $N_t \times M$ matrix. There are several precoder codebook sets. The signal after precoding can be expressed as

$$\mathbf{x}_k = \mathbf{F} \mathbf{s}_k. \quad (4.2)$$

where \mathbf{x}_k is a length N_t vector and N_t is the number of transmit antennas. We assume that $N_t > M$. Then we transform the signal vector to the time domain using IDFT and add CP. Let the number of the receive antenna be N_r . We consider a multipath channel, whose input-output relation in the frequency domain can be written as

$$\mathbf{y}_k = \mathbf{H} \mathbf{F} \mathbf{x}_k + \mathbf{n}_k. \quad (4.3)$$

where \mathbf{y}_k is the received symbol vector, \mathbf{H} is the $N_t \times N_r$ channel matrix and \mathbf{n}_k is the $N_r \times 1$ noise vector. We assume that the entries of \mathbf{H} are independent and identically distributed (i.i.d.) and their distributions are complex normal with zero mean and unit variance, denoted by $CN(0, 1)$. Similarly, the entries of \mathbf{n}_k are also i.i.d. and the distribution is $CN(0, N_0)$. After passing the signal over the channel, we remove the CP and transform the result back to frequency domain. We consider two different kinds of equalizer, zero-forcing (ZF) and minimum mean-square error (MMSE). Let \mathbf{G} be the $M \times N_r$ equalizer matrix.

4.1.1 Linear Equalizer Matrix

Let \mathbf{F}_k be the precoder matrix for multicarrier k and let \mathbf{G}_k be the corresponding equalizer matrix for the same subcarrier. The MSE matrix at the k th subcarrier is given by

$$\mathbf{E}_k(\mathbf{F}_k, \mathbf{G}_k) \triangleq E[(\hat{\mathbf{x}}_k - \mathbf{x}_k)(\hat{\mathbf{x}}_k - \mathbf{x}_k)^H] = \mathbf{G}_k^H \mathbf{R}_{yk} \mathbf{G}_k + \mathbf{I} - \mathbf{G}_k^H \mathbf{H}_k \mathbf{F}_k - \mathbf{F}_k^H \mathbf{H}_k^H \mathbf{G}_k \quad (4.4)$$

where $\mathbf{R}_{yk} \triangleq E[\mathbf{y}_k \mathbf{y}_k^H] = \mathbf{H}_k \mathbf{F}_k \mathbf{F}_k^H \mathbf{H}_k^H + \mathbf{R}_{n_k}$. The MSE of the i th substream at subcarrier

k is the i th diagonal element of \mathbf{E}_k , as given by

$$MSE_{k,i}(\mathbf{F}_k, \mathbf{g}_{k,i}) = [\mathbf{E}_k]_{ii} = \mathbf{g}_{k,i}^H \mathbf{R}_{y_k} \mathbf{g}_{k,i} + 1 - \mathbf{g}_{k,i}^H \mathbf{H}_k \mathbf{f}_{k,i} - \mathbf{f}_{k,i}^H \mathbf{H}_k^H \mathbf{g}_{k,i} \quad (4.5)$$

where $\mathbf{g}_{k,i}$ is the i th column of \mathbf{G}_k . To obtain the optimal receive matrix \mathbf{G}_k^{opt} , it suffices to find \mathbf{G}_k such that each diagonal element of \mathbf{E}_k is minimized. It follows that [11]

$$\mathbf{G}_k^{opt} = (\mathbf{H}_k \mathbf{F}_k \mathbf{F}_k^H \mathbf{H}_k^H + \mathbf{R}_{n_k})^{-1} \mathbf{H}_k \mathbf{F}_k. \quad (4.6)$$

We set each symbol has the same precoder so the optimum equalizer for the MMSE equalizer is given by

$$\mathbf{G} = (\mathbf{H} \mathbf{F} \mathbf{F}^H \mathbf{H}^H + \mathbf{R}_n)^{-1} \mathbf{H} \mathbf{F}. \quad (4.7)$$

On the other hand, the ZF equalizer can be derived as

$$\mathbf{G} = (\mathbf{H} \mathbf{F})^\dagger. \quad (4.8)$$

In either case, the signal vector at the equalizer output is given by

$$\hat{\mathbf{x}} = \mathbf{G} \mathbf{H} \mathbf{F} \mathbf{x} + \mathbf{G} \mathbf{n}. \quad (4.9)$$

4.2 Precoder Selection Methods

We introduce several feedback-based methods for precoder selection in this section. Fig. 4.2 depicts the considered system model. Reference [14] proposed SVD-based search method and [17] proposed optimal precoder selection method. We propose max minSNR-based search method and MMSE-based exhaustive search method.

4.2.1 MaxminSNR-Based Search Method

In this method, We maximize the minimum SNR at the receiver antennas under MMSE or ZF equalization. It can be thought as minimize the maximum symbol error rate (SER) at

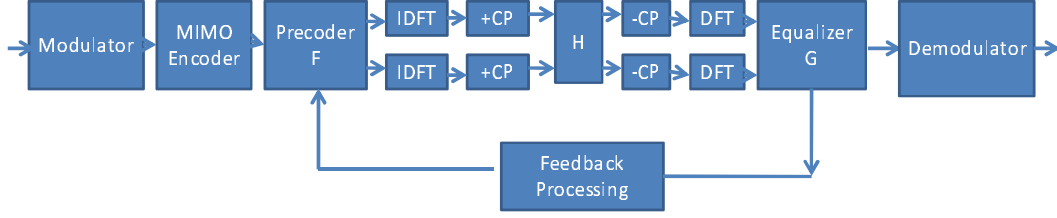


Figure 4.2: System model with feedback.

the receive antennas. The signal power per receive antenna can be expressed as

$$| \mathbf{g}_k^T \mathbf{H} \mathbf{F}_i \mathbf{x} |^2. \quad (4.10)$$

The noise power is

$$\sigma_n^2 | \mathbf{g}_k^T \mathbf{g}_k |. \quad (4.11)$$

The optimum precoding matrix \mathbf{F} selected from the codebook \mathbf{C} maximizes the minimum SNR of at the receive antennas as

$$\begin{aligned} \mathbf{F} &= \arg \max_{\mathbf{F}_i} \min_{k | \mathbf{F}_i} \text{SNR}_k \\ &= \arg \max_{\mathbf{F}_i} \min_{k | \mathbf{F}_i} \frac{| \mathbf{g}_k^T \mathbf{H} \mathbf{F}_i \mathbf{x} |^2}{\sigma_n^2 | \mathbf{g}_k^T \mathbf{g}_k |} \end{aligned} \quad (4.12)$$

where k is the index of the receive antennas, i is the index of the precoder, and \mathbf{g}_k is the equalizer for k th receive antenna.

4.2.2 MMSE-Based Exhaustive Search Method

In this method, we minimize the mean square error (MSE) between $\hat{\mathbf{X}}$ and \mathbf{X} under the ZF or the MMSE equalizer. We compare all possible precoders to find the best one in the source that

$$\min MSE = \arg \min_{F_i} \| \hat{\mathbf{X}} - \mathbf{X} \|^2. \quad (4.13)$$

For ZF equalizer, therefore,

$$\min MSE = \arg \min_{F_i} \| (\mathbf{H} \mathbf{F}_i)^\dagger \mathbf{H} \mathbf{F}_i \mathbf{X} + (\mathbf{H} \mathbf{F}_i)^\dagger \mathbf{n} - \mathbf{X} \|^2, \quad (4.14)$$

and for the MMSE equalizer,

$$\min MSE = \arg \min_{F_i} \|(\mathbf{H}\mathbf{F}_i\mathbf{F}_i^H\mathbf{H}^H + \mathbf{R}_n^{-1})\mathbf{H}\mathbf{F}_i\mathbf{H}\mathbf{F}_i\mathbf{X} + (\mathbf{H}\mathbf{F}_i\mathbf{F}_i^H\mathbf{H}^H + \mathbf{R}_n^{-1})\mathbf{H}\mathbf{F}_i\mathbf{n} - \mathbf{X}\|^2. \quad (4.15)$$

Then we will transmit the precoder index i back to the transmitter. The transmitter will use this precoder to allocate the power. In this method, the computation of complexity is high, because we have to evaluate all the precoders.

4.2.3 SVD-Based Search Method [14]

It was proved in [14] that for the ZF receiver, the optimum precoding matrix \mathbf{F} selected from the codebook \mathbf{C} maximizes the minimum singular value of $\mathbf{H}\mathbf{F}$. Reference [14] calls this the minimum singular value selection criterion (MSV-SC), i.e.,

$$\mathbf{F} = \arg \max_{\mathbf{F}_i \in \mathbf{C}} \lambda_{\min}\{\mathbf{H}\mathbf{F}_i\} \quad (4.16)$$

The optimum un-quantized precoder for MSV-SC has also been shown in [14], [18]. Let the singular value decomposition (SVD) of the channel matrix \mathbf{H} be represented by

$$\mathbf{H} = \mathbf{V}_L \Sigma \mathbf{V}_R^H. \quad (4.17)$$

Then, the optimum un-quantized precoding matrix for MSV-SC is

$$\mathbf{F}_{opt} = \bar{\mathbf{V}}_R, \quad (4.18)$$

which is the first M columns of the right singular matrix \mathbf{V}_R . In practice, the optimum precoder shown in (4.18) is difficult to feedback. Using the criterion in (4.16), we can select a precoding matrix from a codebook, and feed back the index to the transmitter. The exhaustive search can be used to find the optimum precoding matrix in the codebook. If the codebook size is L and the number of the subcarriers is N , we then have to conduct the operation in (4.16) for LN times. The required computational complexity can be very high.

We will attempt to minimize the degradation in channel power introduced by quantizing the precoder $\|\mathbf{H}\mathbf{F}_{opt}\|_F^2 - \|\mathbf{H}\mathbf{F}\|_F^2$ where $\|\cdot\|_F$ is the Frobenius matrix norm. Note that

$$\begin{aligned}
\|\mathbf{H}\mathbf{F}_{opt}\|_F^2 - \|\mathbf{H}\mathbf{F}\|_F^2 &= \text{tr}(\overline{\Sigma\Sigma}^T) - \text{tr}(\Sigma\mathbf{V}_R^H\mathbf{F}\mathbf{F}^H\mathbf{V}_R\Sigma^T) \\
&\leq \text{tr}(\overline{\Sigma\Sigma}^T) - \text{tr}(\overline{\Sigma}\overline{\mathbf{V}}_R^H\mathbf{F}\mathbf{F}^H\overline{\mathbf{V}}_R\overline{\Sigma}^T) \\
&\leq \lambda_{max}^2\{\mathbf{H}\}\text{tr}(\mathbf{I}_M - \overline{\mathbf{V}}_R^H\mathbf{F}\mathbf{F}^H\overline{\mathbf{V}}_R) \\
&= \lambda_{max}^2\{\mathbf{H}\}\frac{1}{2}\|\overline{\mathbf{V}}_R\overline{\mathbf{V}}_R^H - \mathbf{F}\mathbf{F}^*\|_F^2
\end{aligned} \tag{4.19}$$

where the second line follows from setting $\overline{\Sigma}$ equal to the first M columns of Σ , the third line results from substituting $\lambda_{max}\{\mathbf{H}\}$ for the other nonzero singular values, and the last line cover from an alternative representation for subspace distance [14]. We will therefore design codebook \mathbf{F} by attempting to minimize the distortion metric

$$E_{\overline{\mathbf{V}}_R}[\min_{i \in \{1,2,\dots,N\}} \frac{1}{2}\|\overline{\mathbf{V}}_R\overline{\mathbf{V}}_R^H - \mathbf{F}\mathbf{F}^H\|_F^2] \tag{4.20}$$

where $\overline{\mathbf{V}}_R$ is isotropically distributed on $\mathcal{U}(M_t, M)$. Matrices in $\mathcal{U}(M_t, M)$ can be characterized as representing M -dimensional subspaces of the complex M_t -dimensional vector space. Thus [14] will adopt the common Grassmannian packing notation and define the set of all column spaces of the matrices in $\mathcal{U}(M_t, M)$ to be the complex Grassmannian space $\mathcal{G}(M_t, M, \mathcal{C})$. Thus if $\mathbf{F}_1, \mathbf{F}_2 \in \mathcal{U}(M_t, M)$ then column spaces of \mathbf{F}_1 and \mathbf{F}_2 , \mathcal{P}_1 and \mathcal{P}_2 respectively, are contained in $\mathcal{G}(M_t, M, \mathcal{C})$. The chordal distance between two subspaces \mathcal{P}_1 and \mathcal{P}_2 is [1]

$$\begin{aligned}
d_{chordal}(\mathbf{F}_1, \mathbf{F}_2) &= \frac{1}{\sqrt{2}}\|\mathbf{F}_1\mathbf{F}_1^H - \mathbf{F}_2\mathbf{F}_2^H\| \\
&= \sqrt{M - \sum_{i=1}^M \lambda_i^2\{\mathbf{F}_1^H\mathbf{F}_2\}}.
\end{aligned} \tag{4.21}$$

Reference [14] use this sub-optimum codeword selection criterion which minimizes the chordal distance between the chosen codeword and the ideal (un-quantized) optimum pre-

coder, i.e.,

$$\mathbf{F} = \arg \min_{\mathbf{F}_i \in \mathbf{C}} d_{chordal}(\mathbf{F}_i, \mathbf{F}_{opt}). \quad (4.22)$$

Simulation results show that this criterion can perform comparably to the MSV-SC criterion.

4.2.4 Optimum Precoder Selection [17]

To obtain the set of transmit matrices $\{\mathbf{F}_k\}$, reference [17] now consider the minimization of an arbitrary objective function of the diagonal elements of MSE. The MSE can be expressed as

$$\begin{aligned} MSE_{k,i} &= [(\mathbf{I} + \mathbf{F}_k^H \mathbf{H}_k^H \mathbf{R}_{n_k}^{-1} \mathbf{H}_k \mathbf{F}_k)^{-1}]_{ii} \\ &= \frac{1}{1 + \mathbf{f}_{k,i}^H \mathbf{H}_k^H \mathbf{R}_{n_k}^{-1} \mathbf{H}_k \mathbf{f}_{k,i}}. \end{aligned} \quad (4.23)$$

The minimization of arithmetic mean of the MSEs was considered in few papers. The objective function is

$$f_0(\{MSE_{k,i}\}) = \sum_{k,i} (MSE_{k,i}). \quad (4.24)$$

When f_0 is Schur-concave, then precoder \mathbf{F} is

$$\mathbf{F} = \mathbf{U}_{H,1} \Sigma_{F,1} \quad (4.25)$$

where $\mathbf{U}_{H,1} \in C^{n_T \times L}$ has as columns the eigenvectors of \mathbf{R}_H corresponding to the L largest eigenvalues in increasing order, and $\Sigma_{F,1} = [0 \text{diag}(\{\sigma_{F,i}\})] \in C^{L \times L}$ has zero elements, except along the rightmost main diagonal. This objective function is Schur-concave on each carrier k . Therefore, the diagonal structure is optimal. The problem in convex form is

$$\min_{\{z_{k,i}\}} \sum_{k,i} \frac{1}{1 + \lambda_{k,i} z_{k,i}} \text{ s.t. } \sum_{k,i} z_{k,i} \leq P_T \text{ and } z_{k,i} \geq 0, 1 \leq k \leq N, 1 \leq i \leq L_k. \quad (4.26)$$

For simplicity of notation, reference [17] define $z_{k,i} \triangleq \sigma_{F_{k,i}^2}$ and $\lambda_{k,i} \triangleq \lambda_{H_{k,i}}$. This particular problem can be solved very efficient by because the solution has a nice water-filling

interpretation (from the KKT optimality conditions):

$$z_{k,i} = (\mu^{-1/2} \lambda_{k,i}^{-1/2} - \lambda_{k,i}^{-1})^+ \quad (4.27)$$

where $\mu^{-1/2}$ is the waterlevel chosen to satisfy the power constraint with equality.

4.2.5 Matrix Computation Complexity

In the design of signal processing algorithms, an analysis of the required number of flops is often derivable. Where a flop means a floating point operation. In this regard, a dot product of length n vectors is considered to require $2n$ flops because there are n multiplications and n adds. We derive the expressions for the number of needed flops that the equalization in the CL MIMO requires. Fig. 4.3 gives the flop counts of some common matrix operations [16].

In an order of magnitude study, we often throw away the lower order terms since their inclusion does not contribute to the overall flop count. But if the n is small, we have to keep the all the terms. This happens to be our case. We list the total flop counts per subcarrier in Fig. 4.4.

We can see that optimum precoder performs well in complexity because it does not have a complex computation flow. Also we can see that ZF equalizer is much easier than

Method	Flop
Matrix multiplication	$2mnr$
Golub-Reinsch SVD (U, Σ, V)	$4m^2n + 8mn^2 + 9n^3$
Golub-Reinsch SVD (Σ, V)	$4m^2n + 8n^3$
Inverse matrix (Gaussian Elimination)	$2n^3/3$
Eigenvalue	$2n^3/3$

Figure 4.3: Number of flops of different matrix operations [16].

MMSE equalizer. SVD-based and maxminSNR-based search method have less complexity in high order matrix. We can have a conclusion that if the matrix size is low, we can use the MMSE-based search method. When the matrix size is high, we use SVD-based and maxminSNR-based search method.

	Total flop per subcarrier	Total flop (n=2)	Total flop (n=4)	Total flop (n=8)
ZF	$8n^3/3$	64/3	512/3	4096/3
ZF, SVD-Based	$116n^3/3+4n^2$	976/3	7616/3	60160/3
ZF, MMSE-Based	$136n^3/3+8n^2$	1300/3	9088/3	71168/3
ZF, MaxminSNR	$128n^3/3+16n^2+24n+32$	1456/3	9344/3	69280/3
ZF, Optimum precoder	$44n^3/3+n^2$	364/3	2864/3	22720/3
MMSE	$20n^3/3+n^2$	172/3	1328/3	10432/3
MMSE, SVD-Based	$128n^3/3+5n^2$	1084/3	8432/3	66496/3
MMSE, MMSE-Based	$196n^3/3+13n^2$	1724/3	13168/3	102848/3
MMSE, MaxminSNR	$176n^3/3+20n^2+24n+32$	1888/3	12608/3	94624/3
MMSE, Optimum precoder	$50n^3/3+9n^2$	508/3	3632/3	27328/3

Figure 4.4: Number of flops per subcarrier of each method.

Chapter 5

Downlink MIMO Simulation for IEEE 802.16m

In this chapter, we use two different equalizers and four closed-loop MIMO technologies in the downlink transmission for IEEE 802.16m. The two equalizers are ZF and MMSE equalizer. We evaluate the performance of each approach mainly via mean square error (MSE) and symbol error rate (SER).

5.1 System Parameters and Channel Model

Table 5.1 gives the primitive and derived parameters used in our simulation work.

Channel model considers parameters specific to 802.16m including bandwidths, operating frequencies, cell scenario, and multi-antenna configurations. Both system level and link level models are described in detail with a purpose of fulfilling the needs to conduct effective link- and system-level simulations that can generate trustworthy and verifiable results to assess performance related to the 802.16m system requirements. Channel models for evaluation of IMT-Advanced candidate radio interface technologies [6]. We use the Suburban macro-cell model. The parameter are in Fig. 5.1. The root-mean-square (RMS) delay spread of Suburban macrocell channel is 75.7485 ns.

Cluster #	Delay [ns]			Power [dB]			AoD [°]	AoA [°]	Ray power [dB]
1	0	5	10	-3.0	-5.2	-7.0	0	0	-13.0
2	25			-7.5			13	-71	-20.5
3	35			-10.5			-15	-84	-23.5
4	35			-3.2			-8	46	-16.2
5	45	50	55	-6.1	-8.3	-10.1	-12	-66	-16.1
6	65			-14.0			-17	-97	-27.0
7	65			-6.4			12	-66	-19.4
8	75			-3.1			-8	-46	-16.1
9	145			-4.6			-10	-56	-17.6
10	160			-8.0			-13	73	-21.0
11	195			-7.2			12	70	-20.2
12	200			-3.1			8	-46	-16.1
13	205			-9.5			14	-80	-22.5
14	770			-22.4			22	123	-35.4
Cluster AS _{BS} = 2°									
Cluster AS _{MS} = 10°									

Figure 5.1: Suburban macrocell channel model [9].

Table 5.1: OFDMA Downlink Parameters

Parameters	Values
Bandwidth	10 MHz
Central frequency	3.5 GHz
N_{used}	865
Sampling factor n	28/25
G	1/8
N_{FFT}	1024
Sampling frequency	11.2 MHz
Subcarrier spacing	10.94 kHz
Useful symbol time	91.43 μs
CP time	11.43 μs
OFDMA symbol time	102.86 μs
Sampling time	44.65 ns

5.2 Simulation Results for IEEE 802.16m

5.2.1 Simulation Flow

We assume perfect synchronization and omit it in our simulation. For data transmission, we do not do FEC and DeFEC. After equalization, we calculate the MSE between the true signal and the received signal, where the average is taken over all the subcarriers. The symbol error rate (SER) can also be obtained after demapping. Our simulation does not consider IEEE 802.16m frame structure in Fig. 5.2. Precoder changes per frame in 16m, so it changes per 5 ms. We use per symbol simulation in Fig. 5.3, so it changes per 102.67 μs . Therefore the mobile speed 120 km/h in our simulation is equivalent to 4.94 km/h in IEEE 802.16m frame structure. The running time for real IEEE 802.16m frame structure will take very long time so we use the per symbol simulation. We also calculate that per symbol simulation changes channel faster than per frame simulation so the per frame simulation might have better performance than per symbol simulation. For MMSE-based feedback scheme with MMSE equalizer simulation with two transmit antennas and two receive antennas, the simulation

time needs 46000 s.

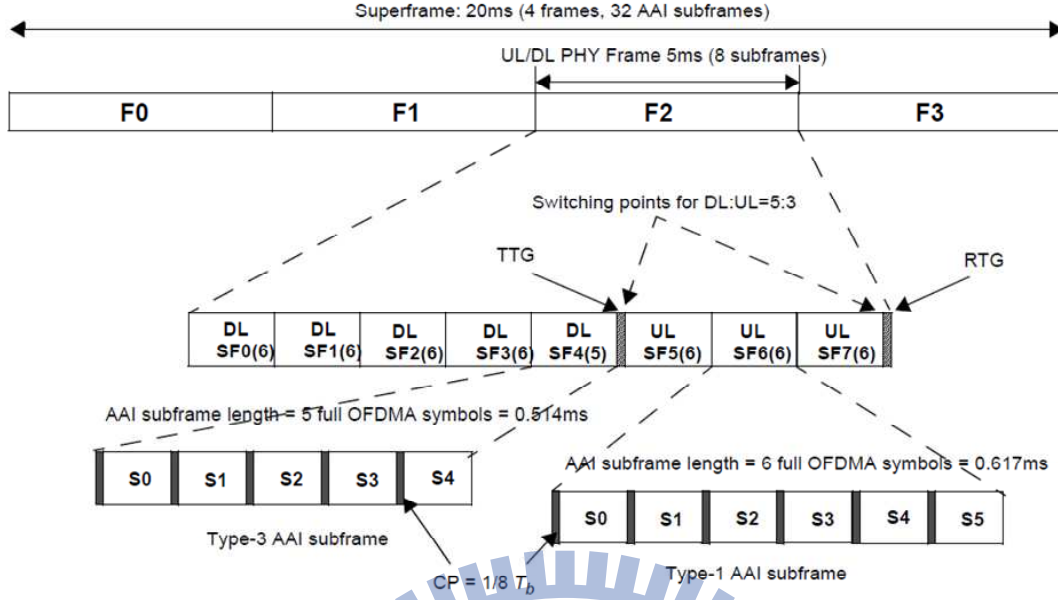


Figure 5.2: IEEE 802.16m TDD frame structure for 10 MHz [9].

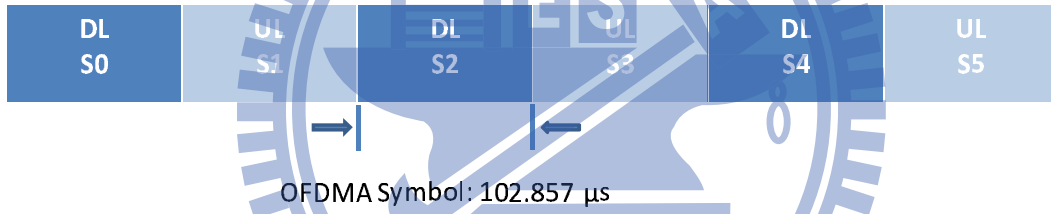


Figure 5.3: TDD structure for 10 MHz.

5.2.2 Validation with AWGN Channel

Before considering multipath channels, we do simulation with an AWGN channel to validate the simulation model. We validate this model by MSE and SER curves resulting from simulation. We simulate a system where FFT size = 1024, bandwidth = 10 MHz, TDD frame length = 5 ms, DL subframe size = 1 preamble + 28 OFDM symbols, and 48 PRUs are used in DL transmission. In Fig. 5.4, the theoretical symbol error rate (SER) curve

versus E_s/N_0 for uncoded QPSK are plotted together with the SER curve resulting from the simulation. We can see the SER curve of our system approaches the theory one. Fig. 5.4 shows the mean square error (MSE) curve resulting from the simulation versus E_s/N_0 , and we can see our system model maintains a close to -1 slope in MSE throughout the simulated range of SNR. Here, the E_s/N_0 means the data power divided by the noise power.

5.3 Simulation Results for Single-Path Channels

Figs. 5.5–5.9 show the MSE and SER with ZF equalizer and different feedback methods at different velocities and SNR values in Suburban channel. Figs. 5.10–5.11 show the performance of ZF equalizer with different feedback methods at velocities of 30 and 120 km/h. We can see that MSE with ZF equalizer are relatively close in different feedback method. This is because ZF equalizer can not cancel the MSE.

Figs. 5.12–5.16 show the MSE and SER with MMSE equalizer and different feedback methods at different velocities and SNR values in Suburban channel.

Figs. 5.17–5.18 show the performance of different feedback methods at velocities of 30 and 120 km/h. We can see that both MSE and SER have the same curve. This is because the MMSE equalizer is finding the minimum mean square error and it also can be seen worked in SER. The optimum precoder method leads all the methods because it use the sounding method to transmit back the best precoder. We also compare all the methods in ZF and MMSE equalizer. MMSE equalizer leads the ZF equalizer both in MSE and SER. This is because ZF equalizer has the noise enhancement problem. Also both ZF and MMSE equalizer can achieve diversity one. We can see in the SER simulation that ZF equalizer with Optimum precoder has better performance in low SNR and MMSE equalizer with Optimum precoder has better performance in high SNR.

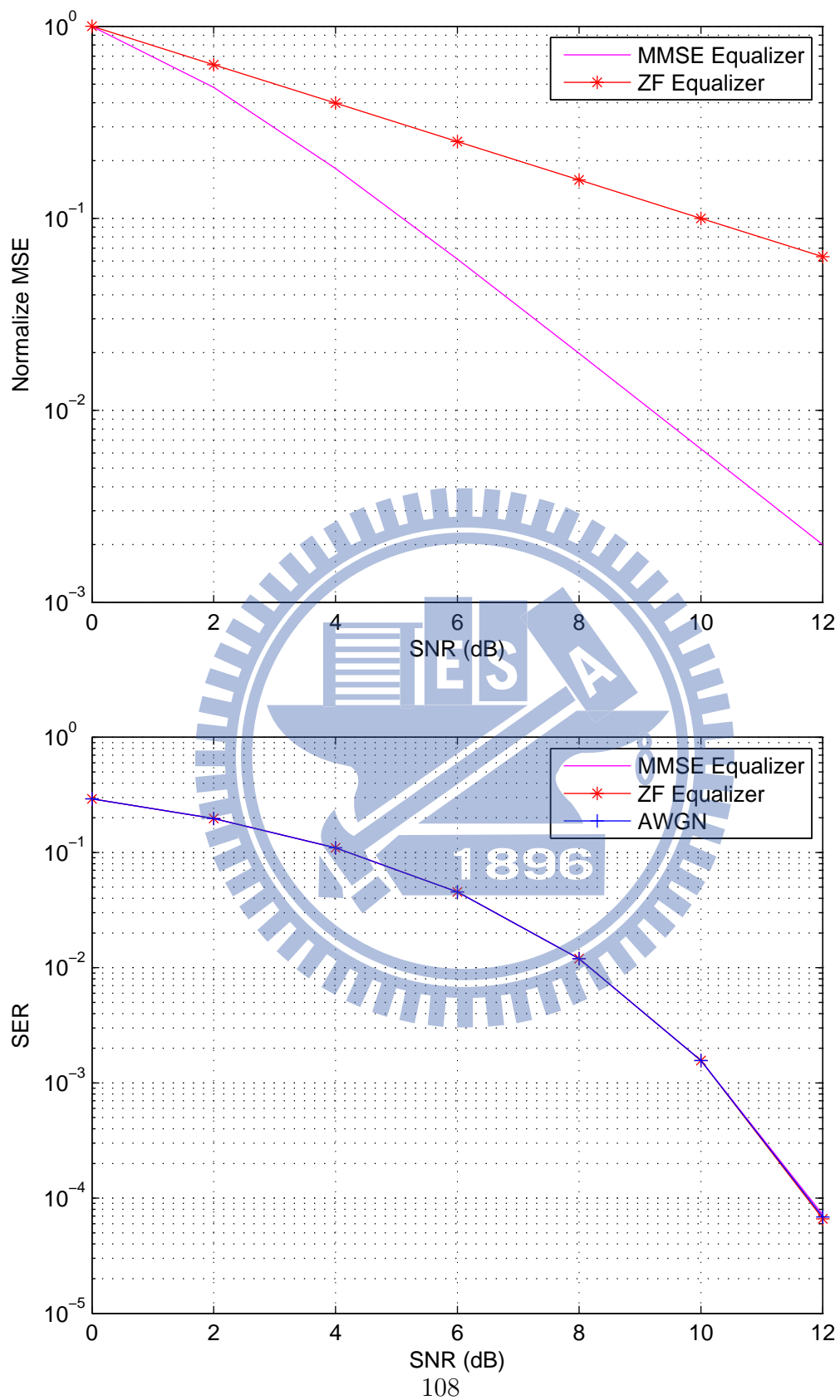


Figure 5.4: MSE and SER for QPSK resulting from simulation compared with theory in AWGN.

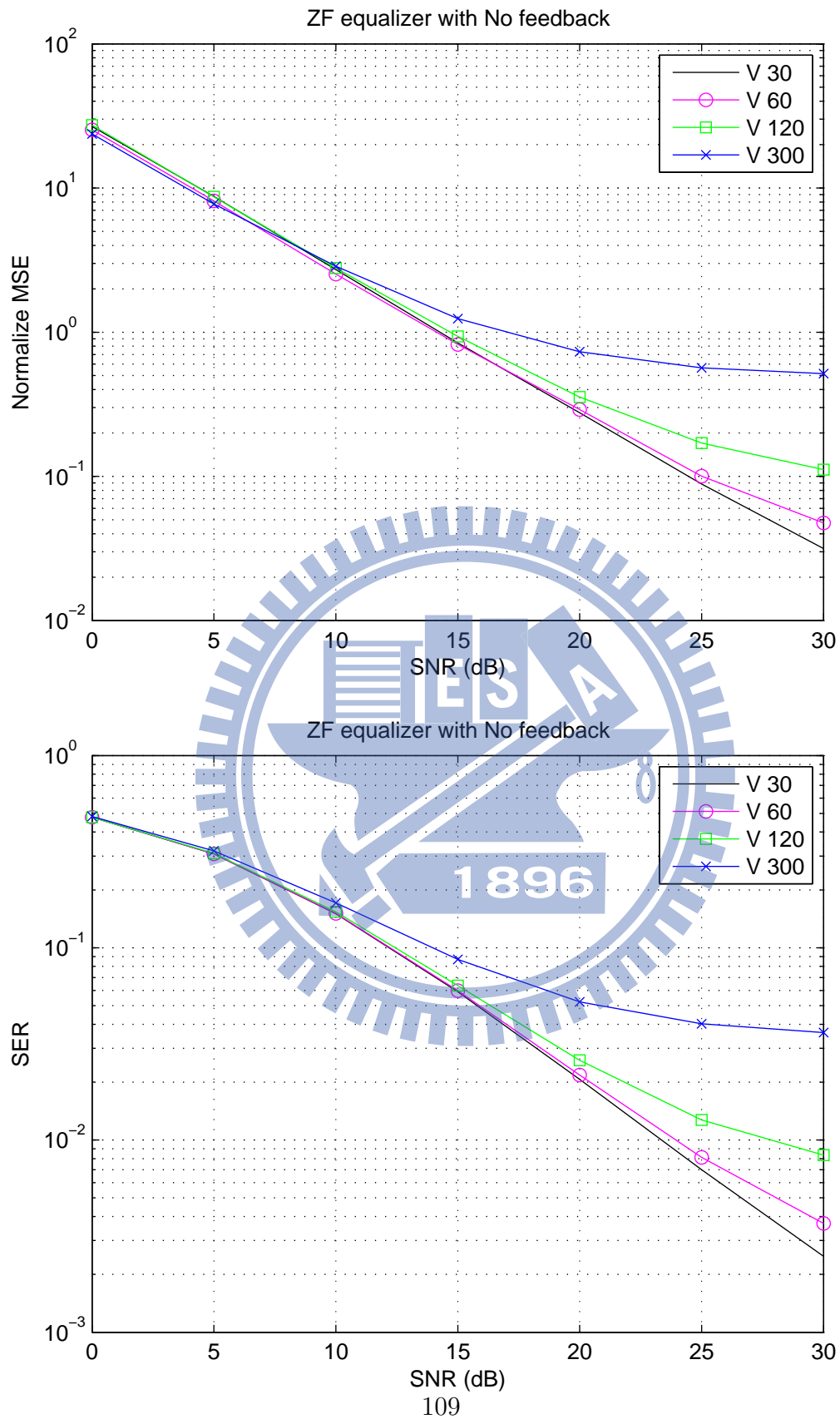


Figure 5.5: MSE and SER for QPSK using ZF equalizer with no feedback in Suburban channel.

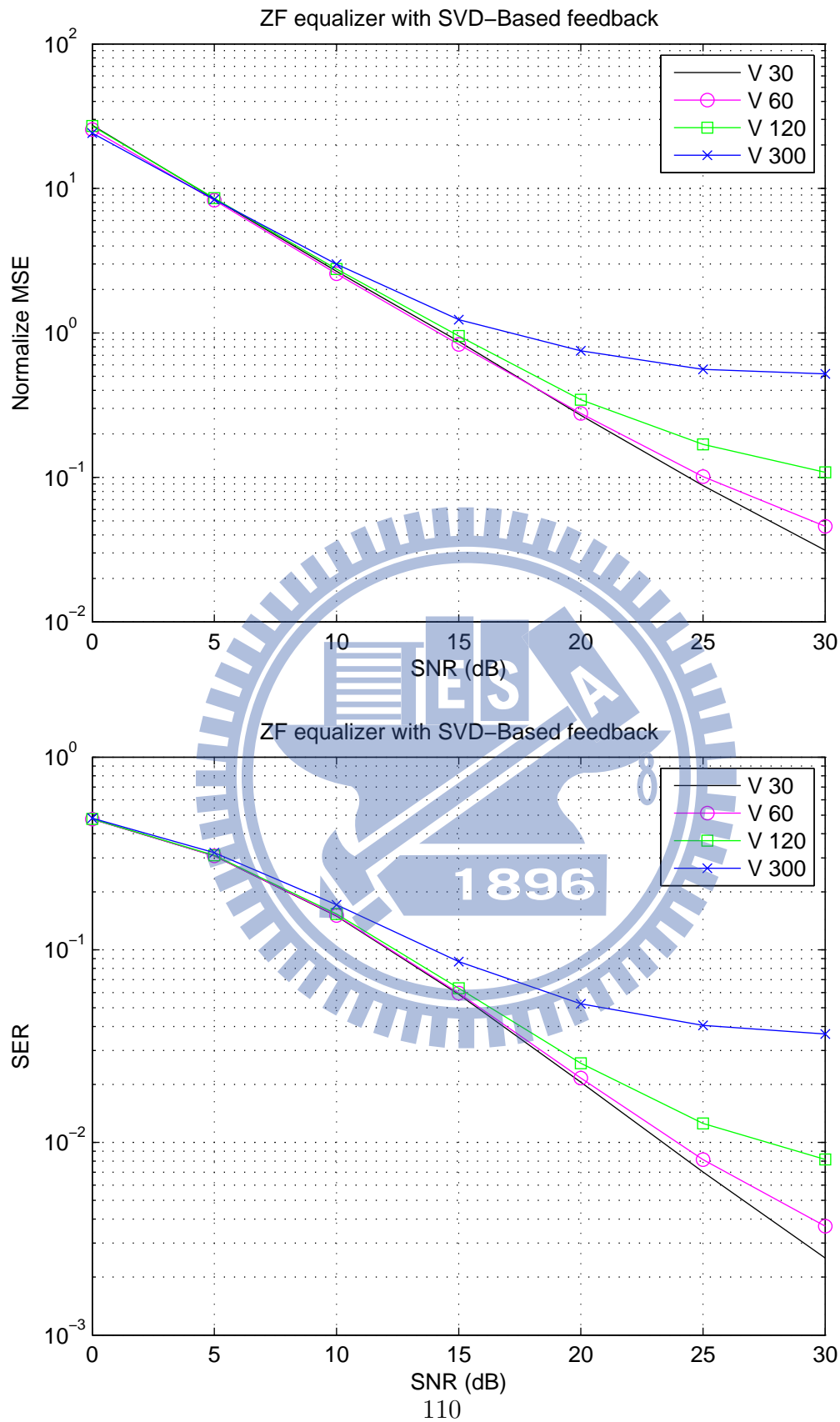


Figure 5.6: MSE and SER for QPSK using ZF equalizer with SVD-Based search feedback in Suburban channel.

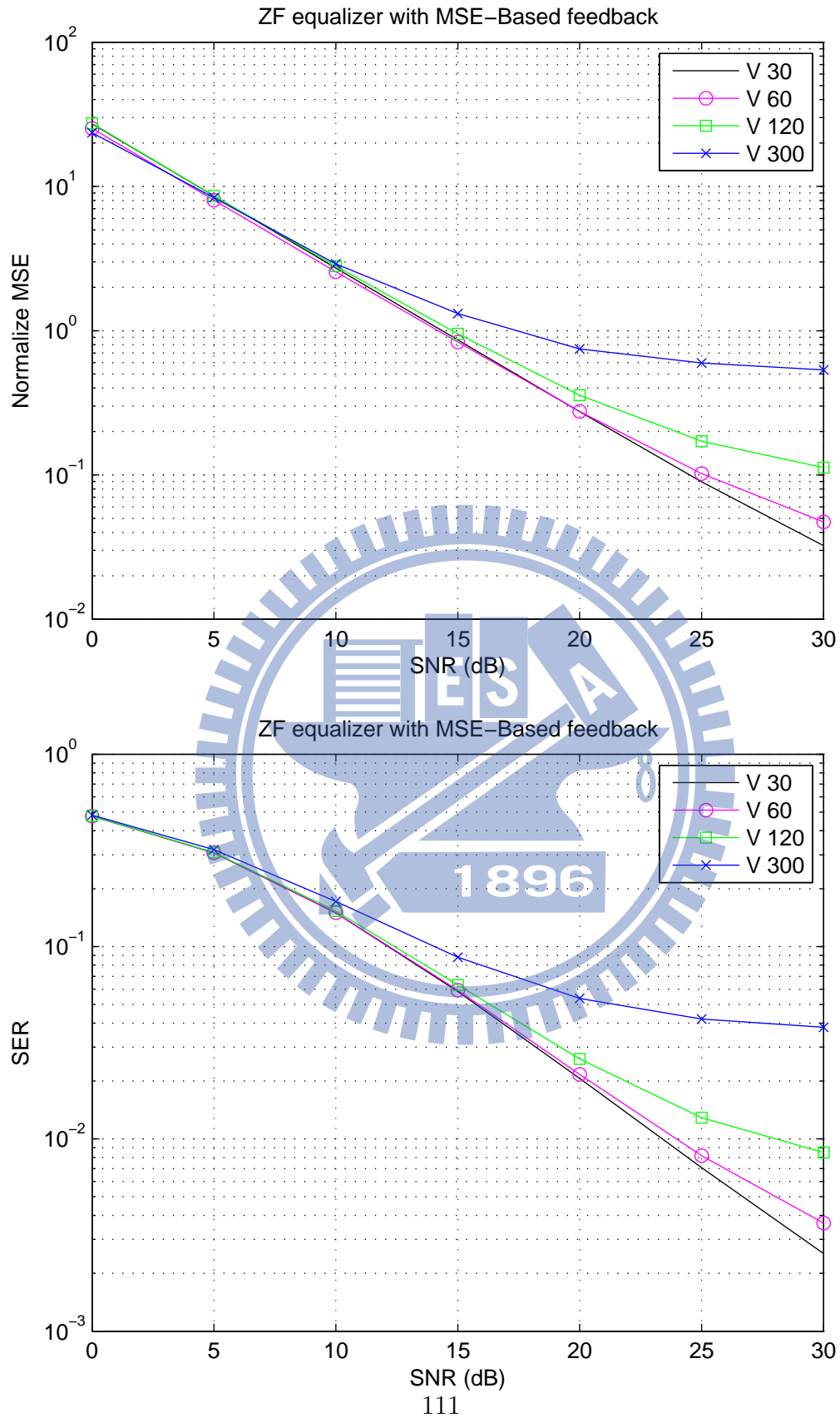


Figure 5.7: MSE and SER for QPSK using ZF equalizer with MMSE-Based exhaustive search feedback in Suburban channel.

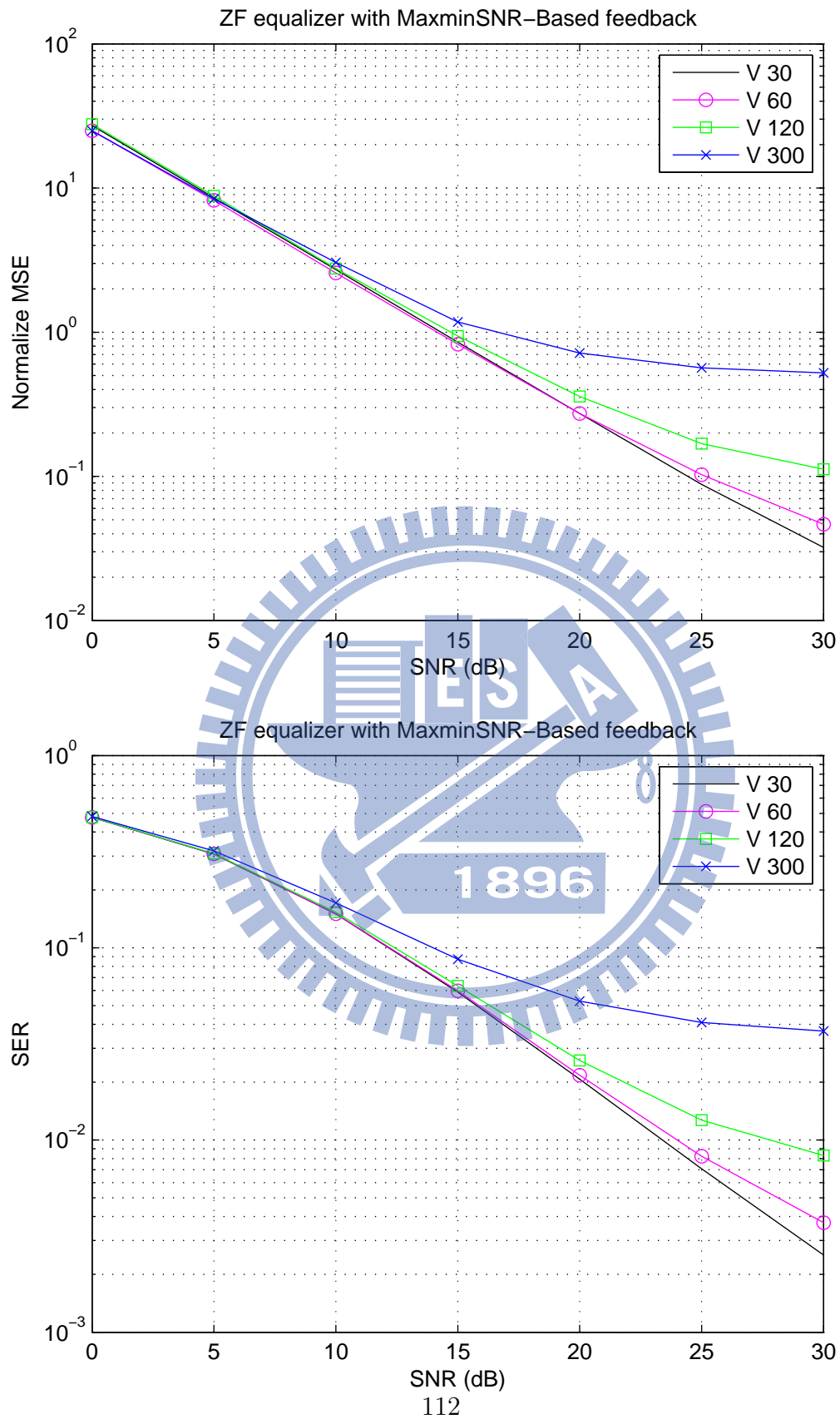


Figure 5.8: MSE and SER for QPSK using ZF equalizer with MaxminSNR-Based search feedback in singlepath Suburban channel.

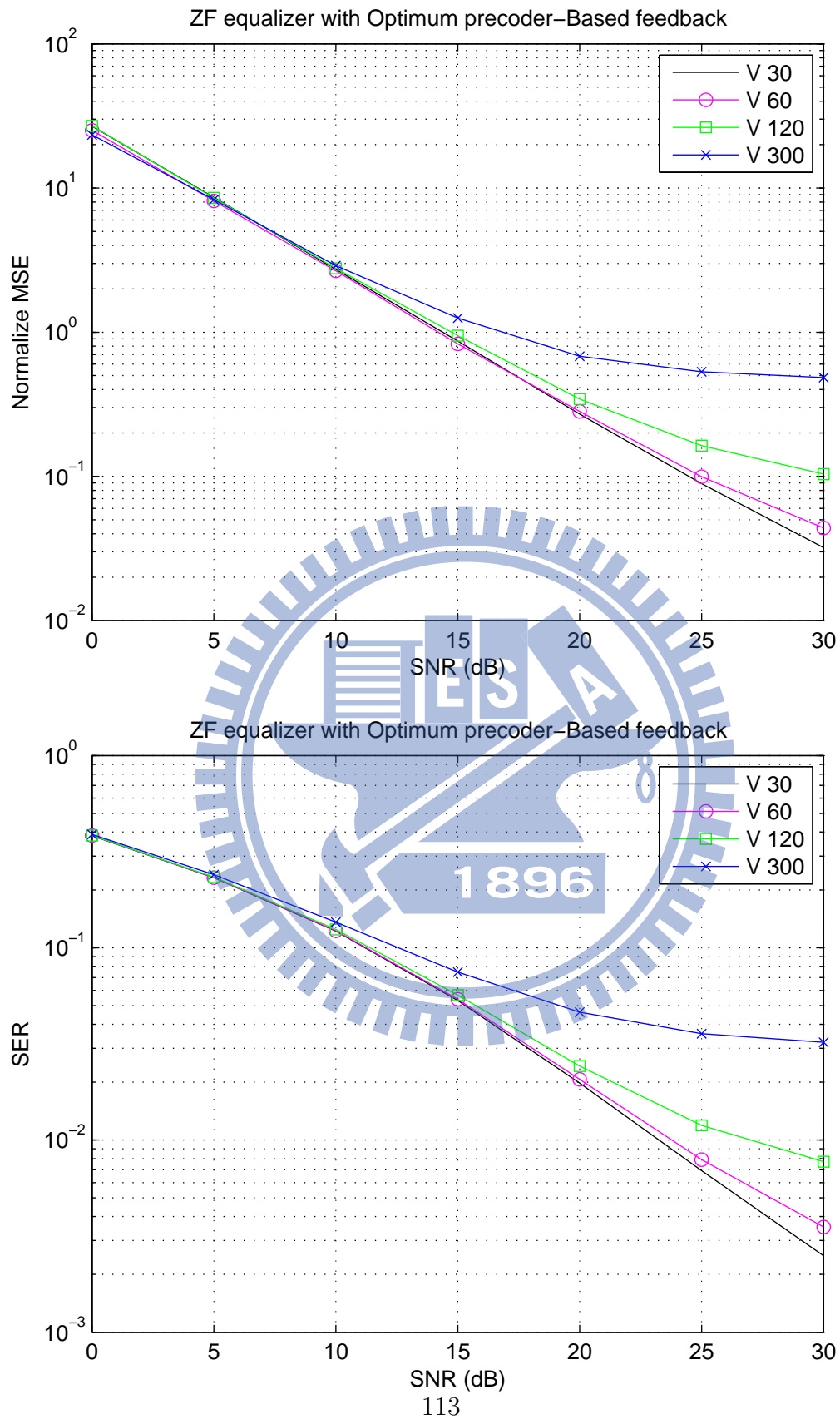


Figure 5.9: MSE and SER for QPSK using ZF equalizer with Optimum precoder feedback in Suburban channel.

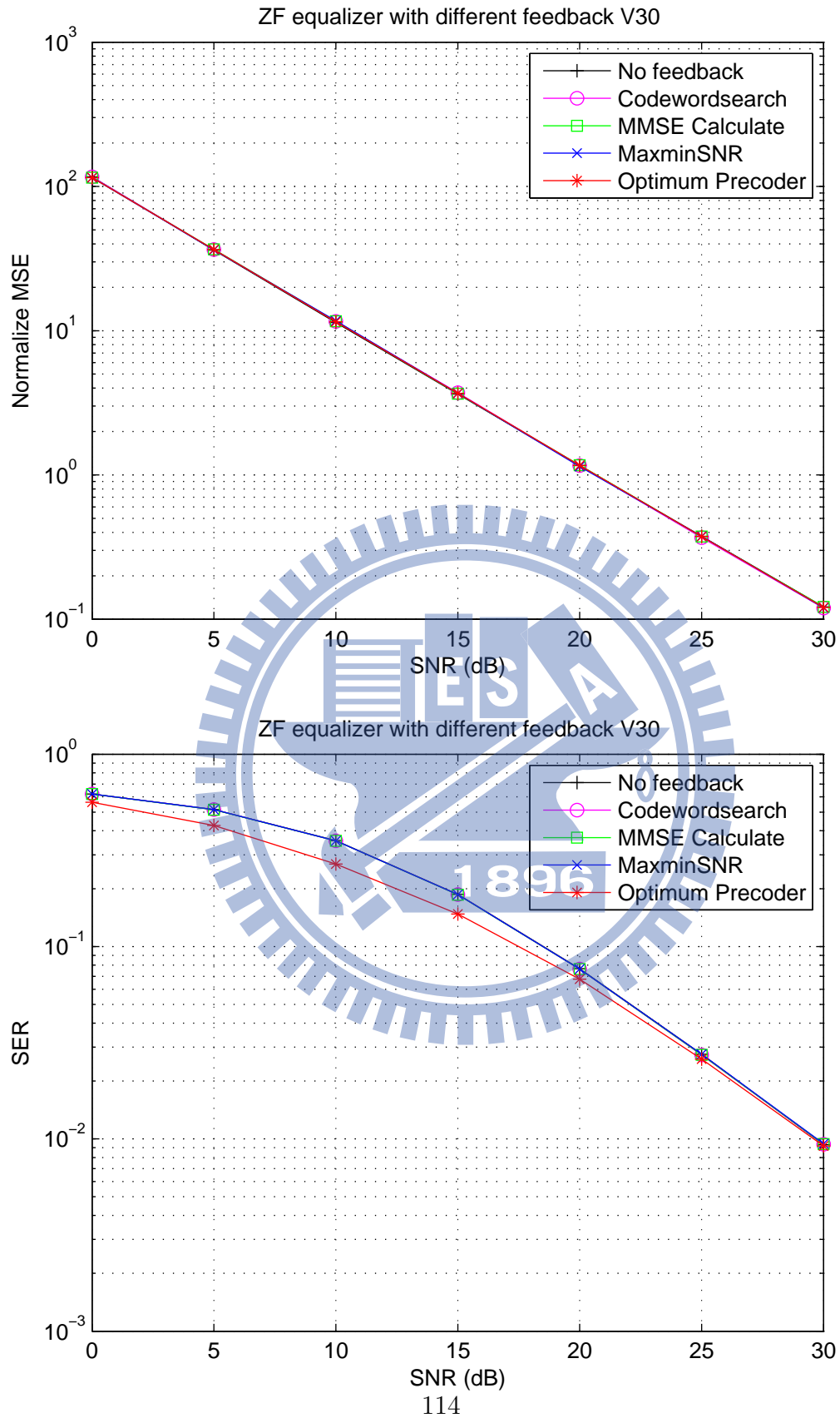


Figure 5.10: MSE and SER for QPSK using ZF equalizer with different feedback methods at 30 km/h in Suburban channel.

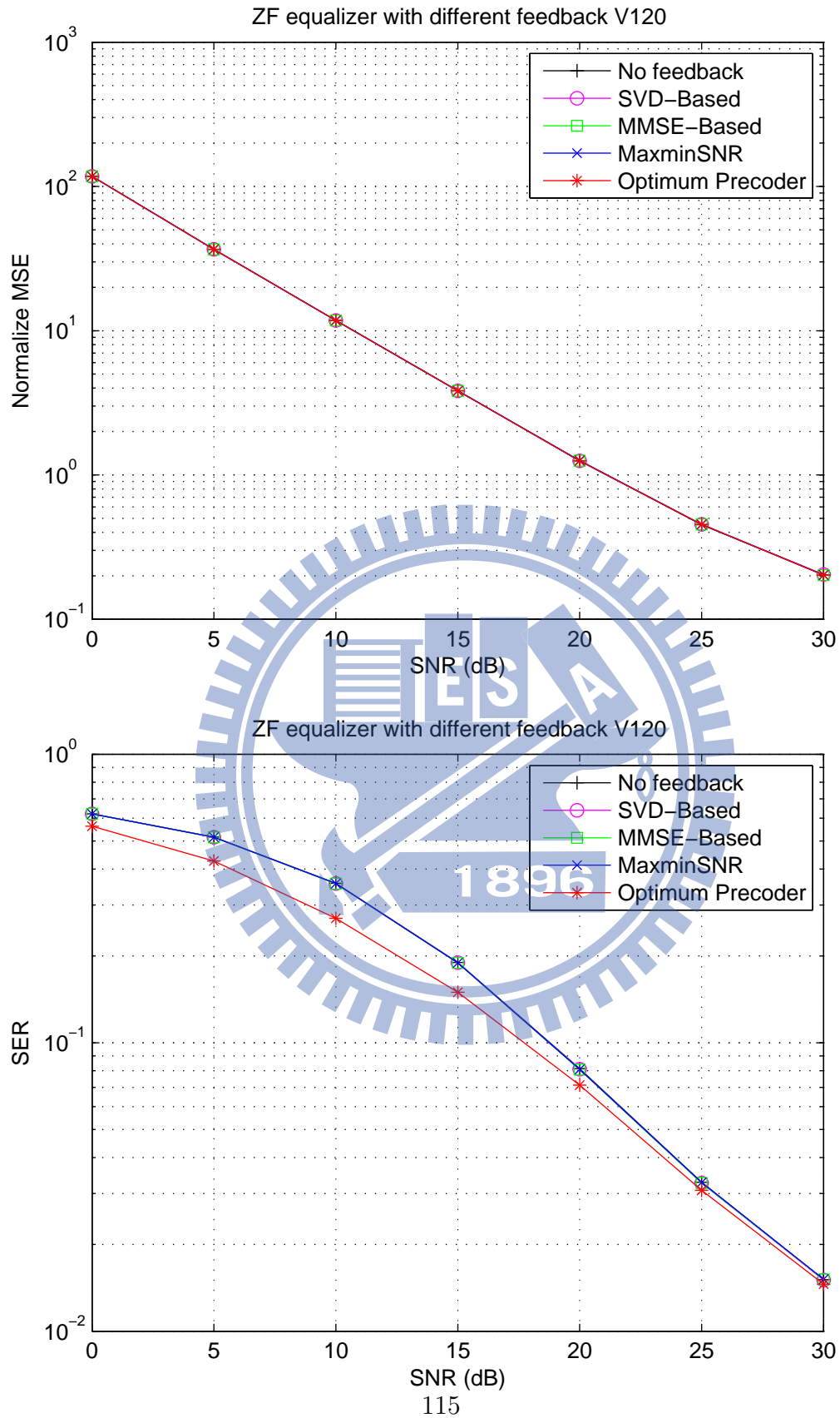


Figure 5.11: MSE and SER for QPSK using ZF equalizer with different feedback methods at 120 km/h in Suburban channel.

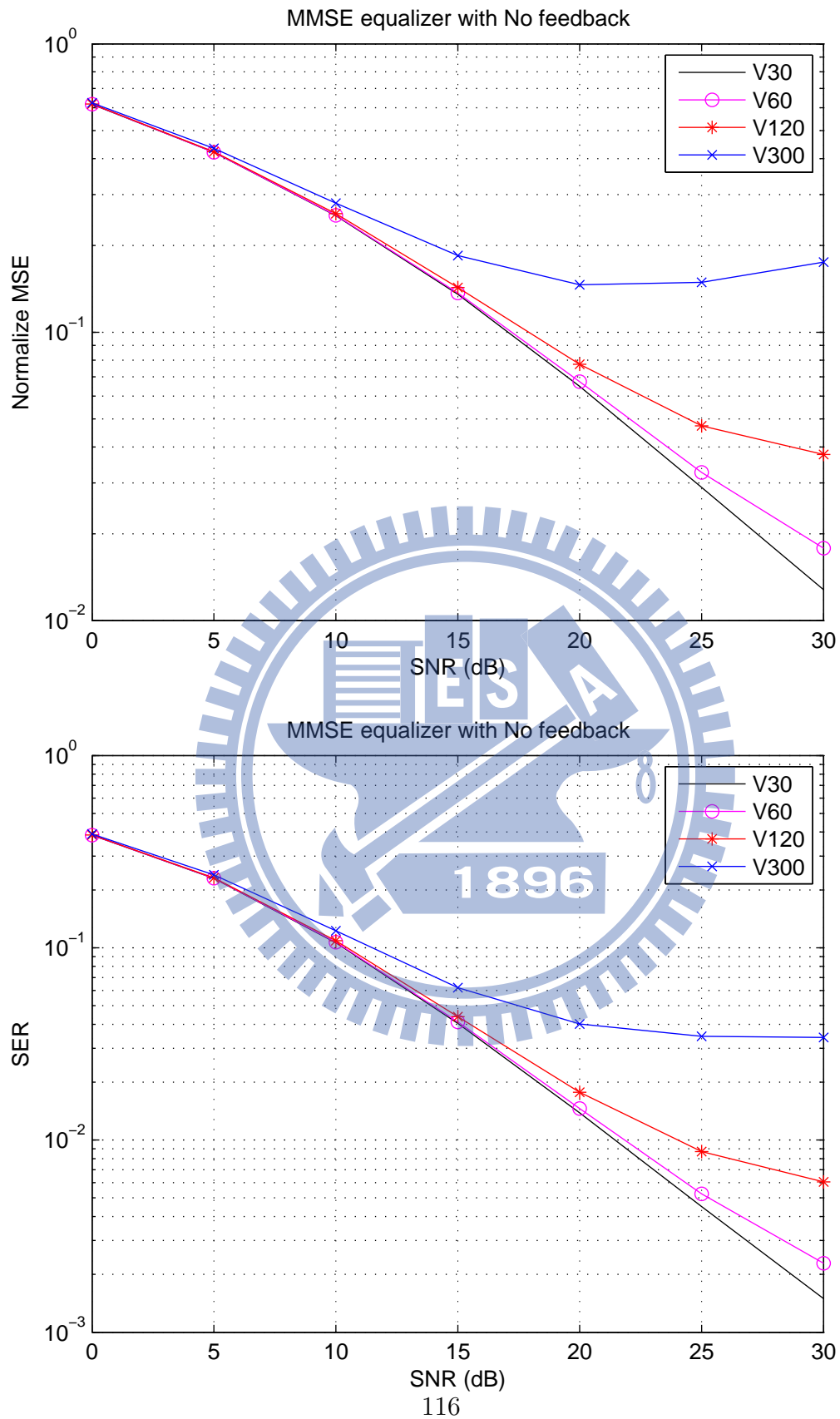


Figure 5.12: MSE and SER for QPSK using MMSE equalizer with no feedback in Suburban channel.

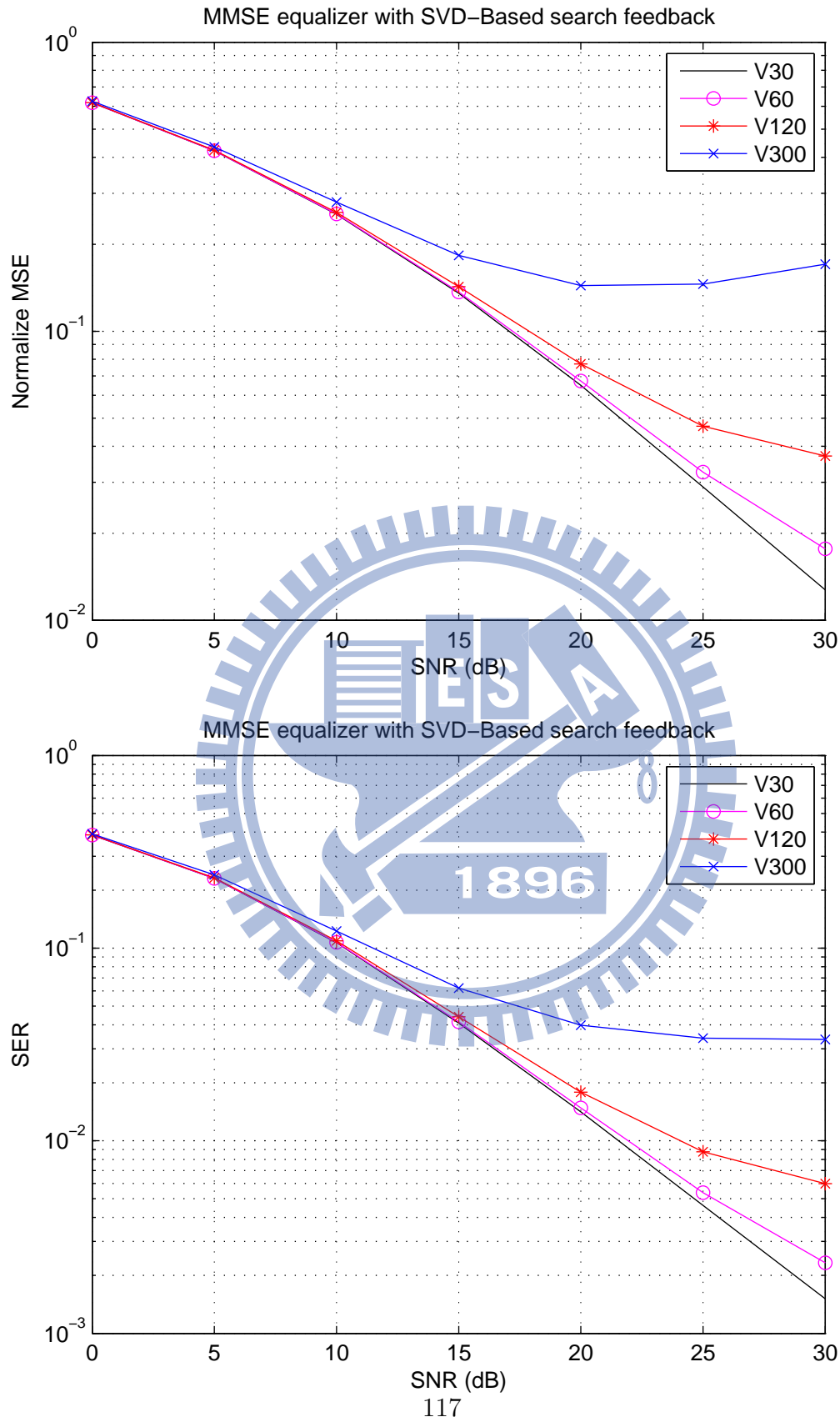


Figure 5.13: MSE and SER for QPSK using MMSE equalizer with SVD-Based search feedback in Suburban channel.

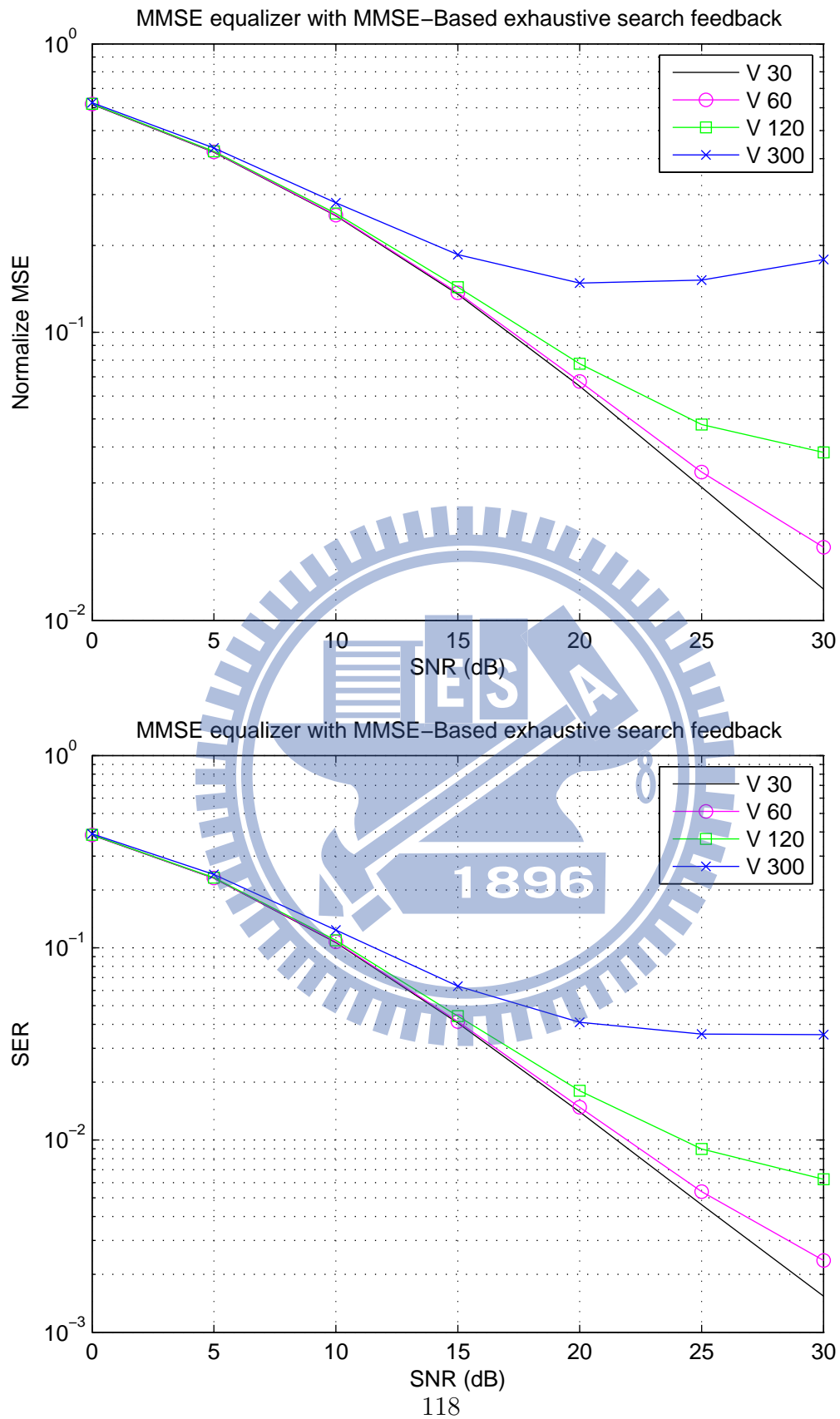


Figure 5.14: MSE and SER for QPSK using MMSE equalizer with MMSE-Based exhaustive search feedback in Suburban channel.

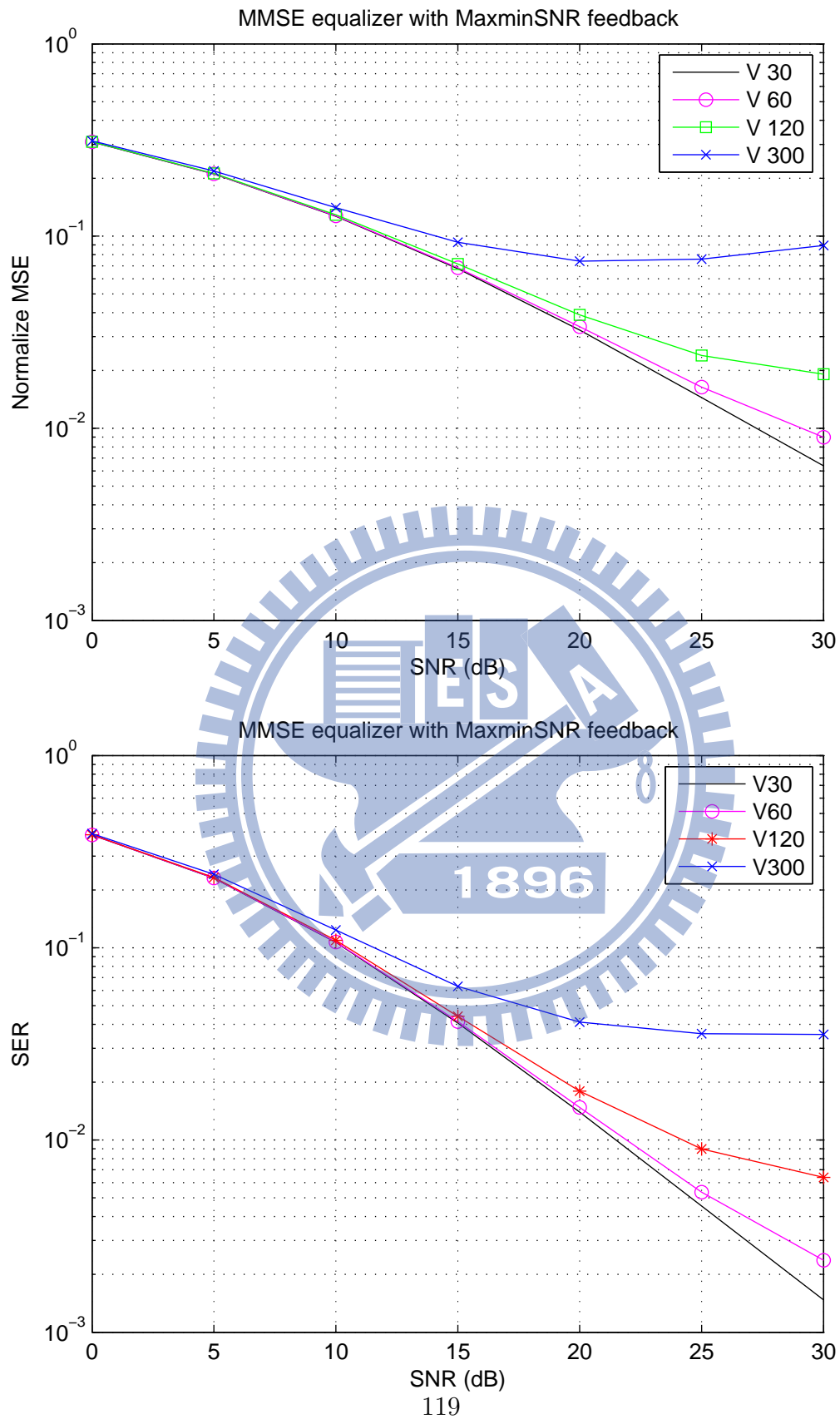


Figure 5.15: MSE and SER for QPSK using MMSE equalizer with MaxminSNR-Based search feedback in Suburban channel.

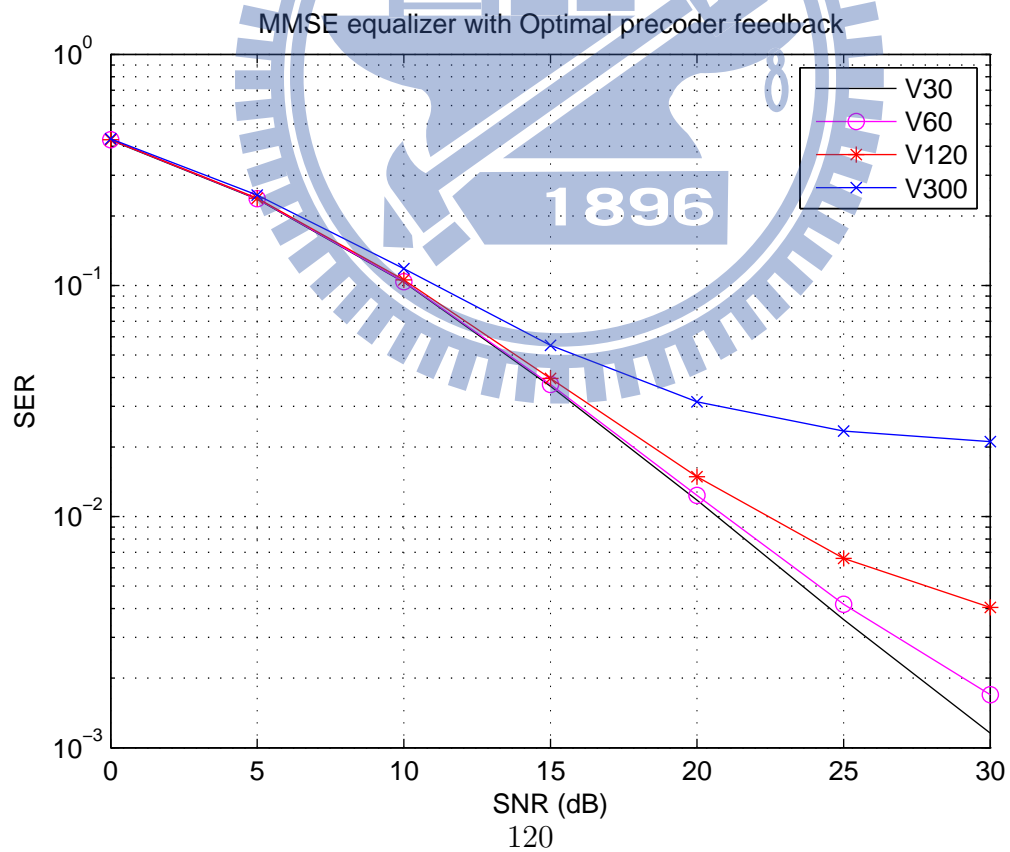
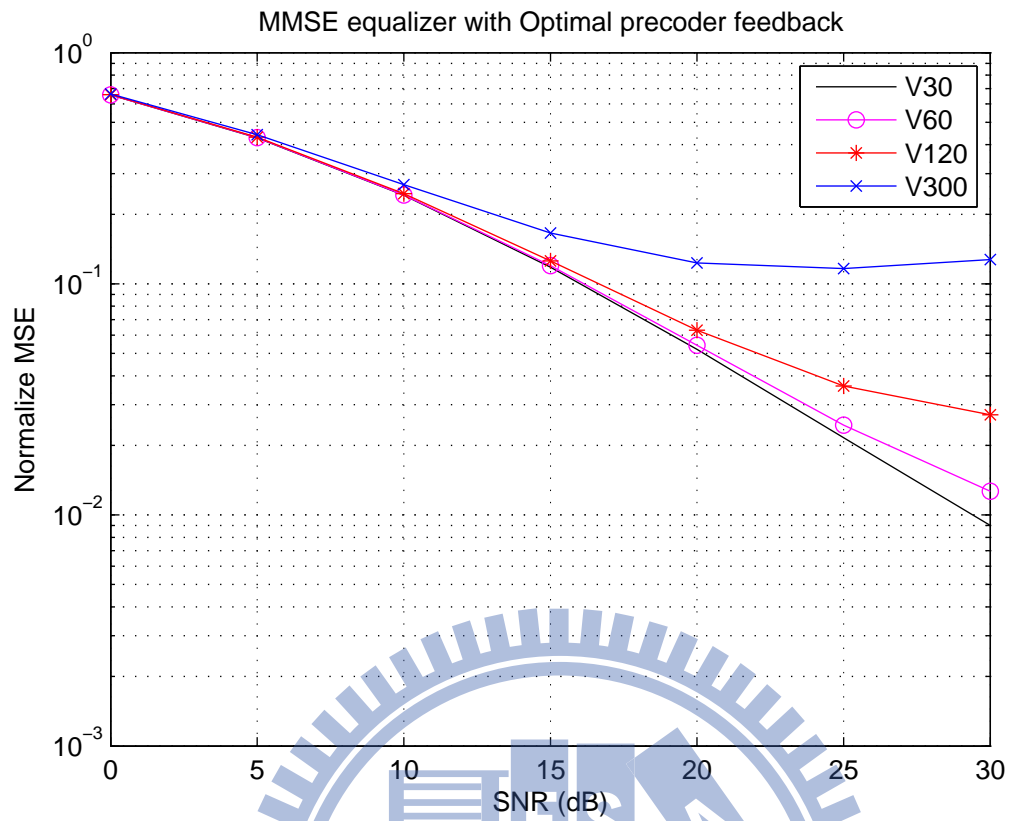


Figure 5.16: MSE and SER for QPSK using MMSE equalizer with Optimum precoder feedback in Suburban channel.

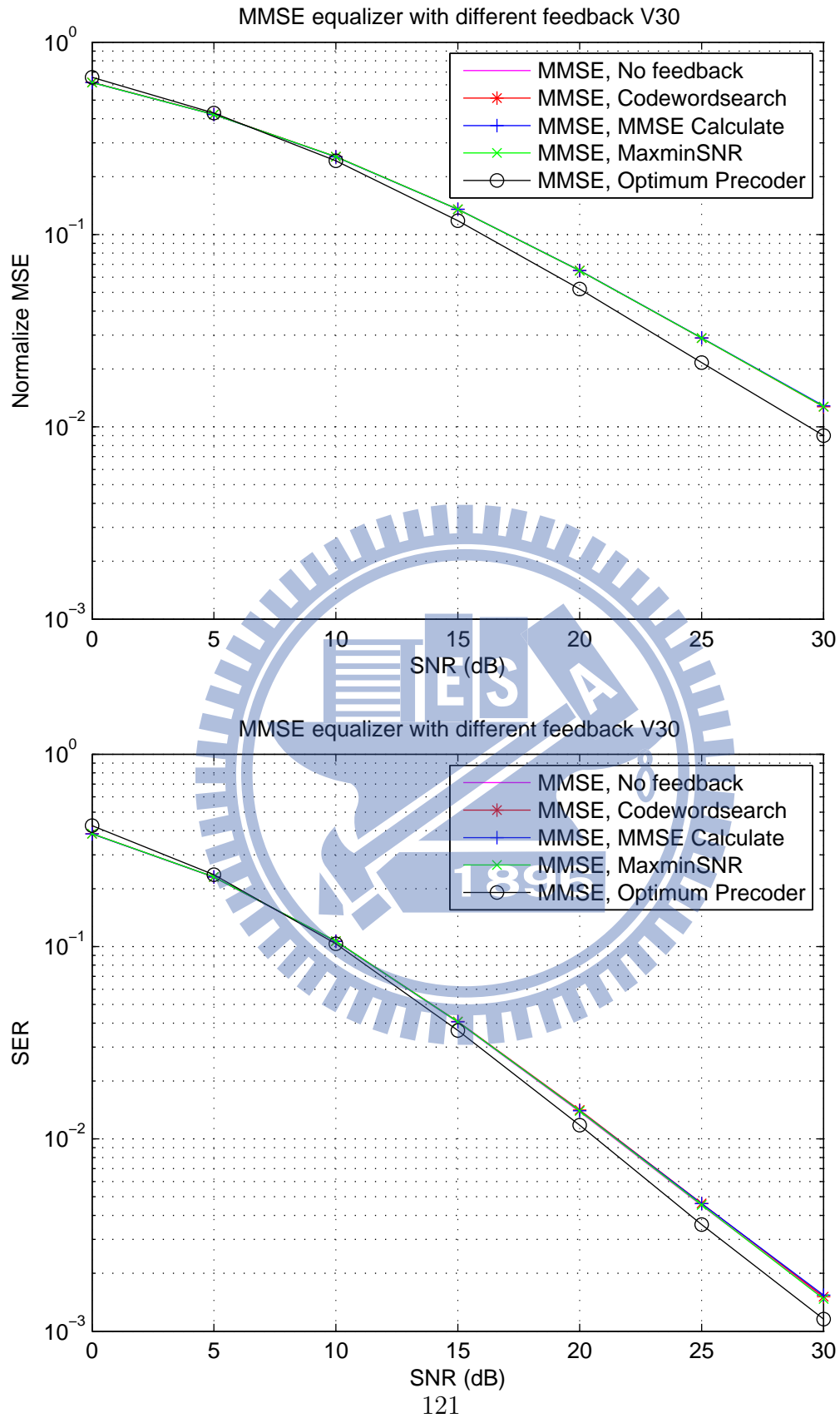


Figure 5.17: MSE and SER for QPSK using MMSE equalizer with different feedback methods at 30 km/h in Suburban channel.

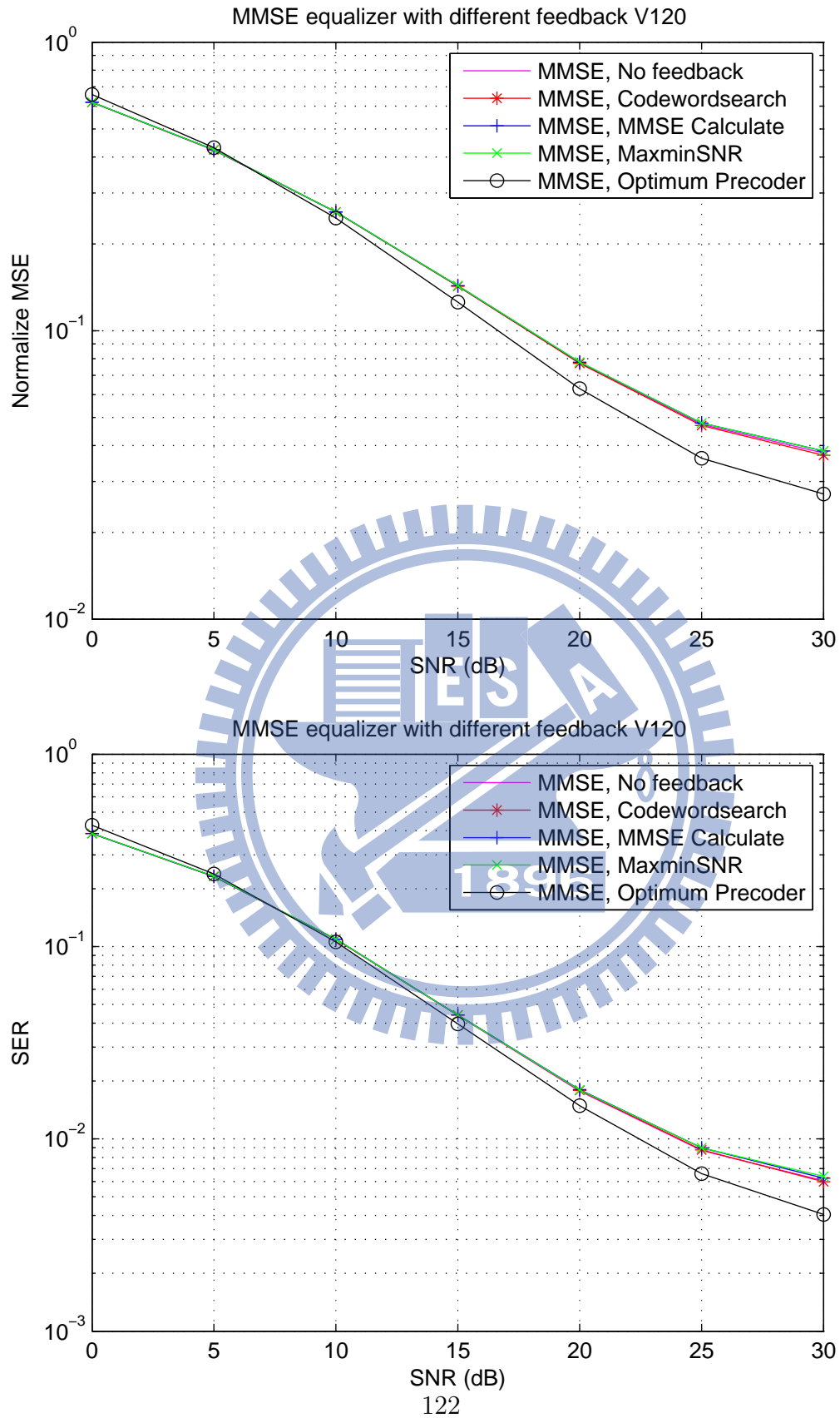


Figure 5.18: MSE and SER for QPSK using MMSE equalizer with different feedback methods at 120 km/h in Suburban channel.

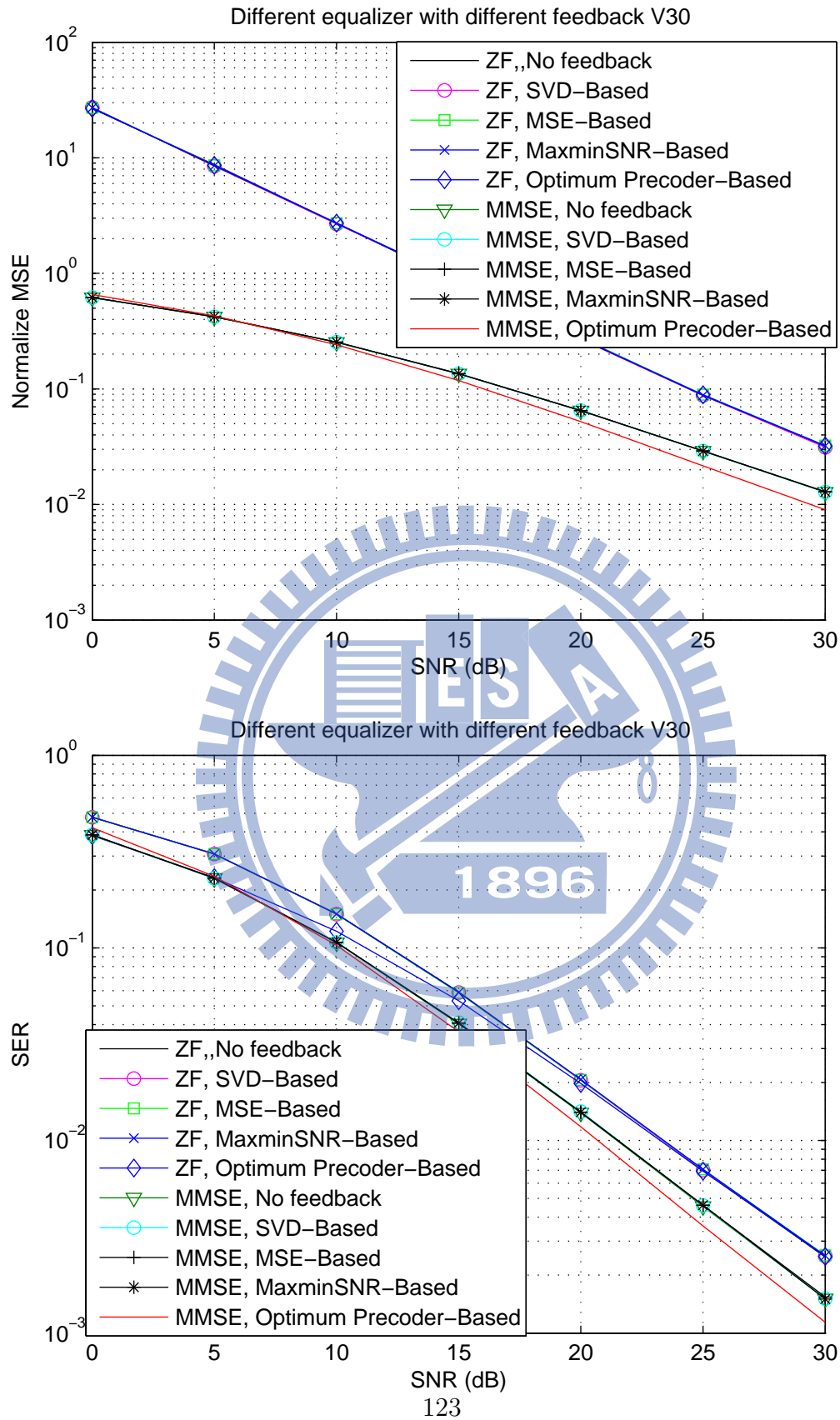


Figure 5.19: MSE and SER for QPSK using ZF and MMSE equalizer with different feedback methods at 30 km/h in Suburban channel.

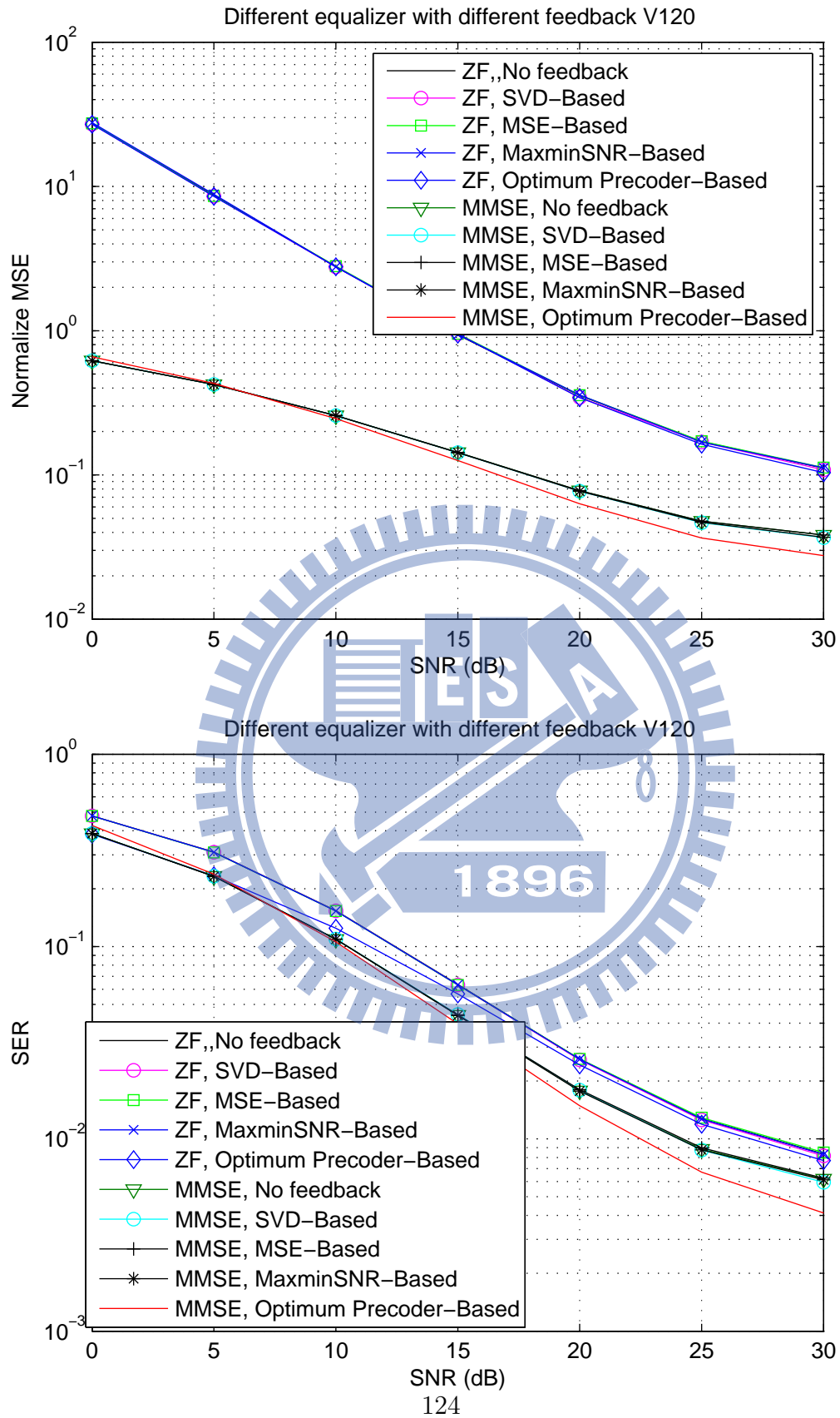


Figure 5.20: MSE and SER for QPSK using ZF and MMSE equalizer with different feedback methods at 120 km/h in Suburban channel.

5.4 Simulation Results for Multipath Channels

Figs. 5.21–5.34 show the simulation with two transmit antennas and two receive antennas. Figs. 5.21–5.25 show the MSE and SER with ZF equalizer and different feedback methods at different velocities and SNR values in Suburban channel. Figs. 5.26–5.27 show the performance of ZF equalizer with different feedback methods at velocities of 30 and 120 km/h. We can see that MSE with ZF equalizer are relatively close in different feedback method. This is because ZF equalizer can't cancel the MSE.

Figs. 5.28–5.32 show the MSE and SER with MMSE equalizer and different feedback methods at different velocities and SNR values in Suburban channel.

Figs. 5.33–5.34 show the performance of different feedback methods at velocities of 30 and 120 km/h. We can see that both MSE and SER have the same curve. This is because the MMSE equalizer is finding the minimum mean square error and it also can be seen worked in SER. The optimum precoder method leads all the methods because it use the sounding method to transmit back the best precoder. Also both ZF and MMSE equalizer can achieve diversity one. We also compare all the methods in ZF and MMSE equalizer. MMSE equalizer leads the ZF equalizer both in MSE and SER. This is because ZF equalizer has the noise enhancement problem.

Figs. 5.37–5.39 show the MSE and SER with ZF equalizer using 4 transmit antennas and 4 receive antennas. We can see that SER can achieve diversity order three.

Figs. 5.40–5.40 show the MSE and SER with ZF equalizer using different antennas and different feedback selection methods. We can see that 4 antennas outperforms 2 antennas. And optimal precoder method with 4 antennas has more coding gain than 2 antennas.

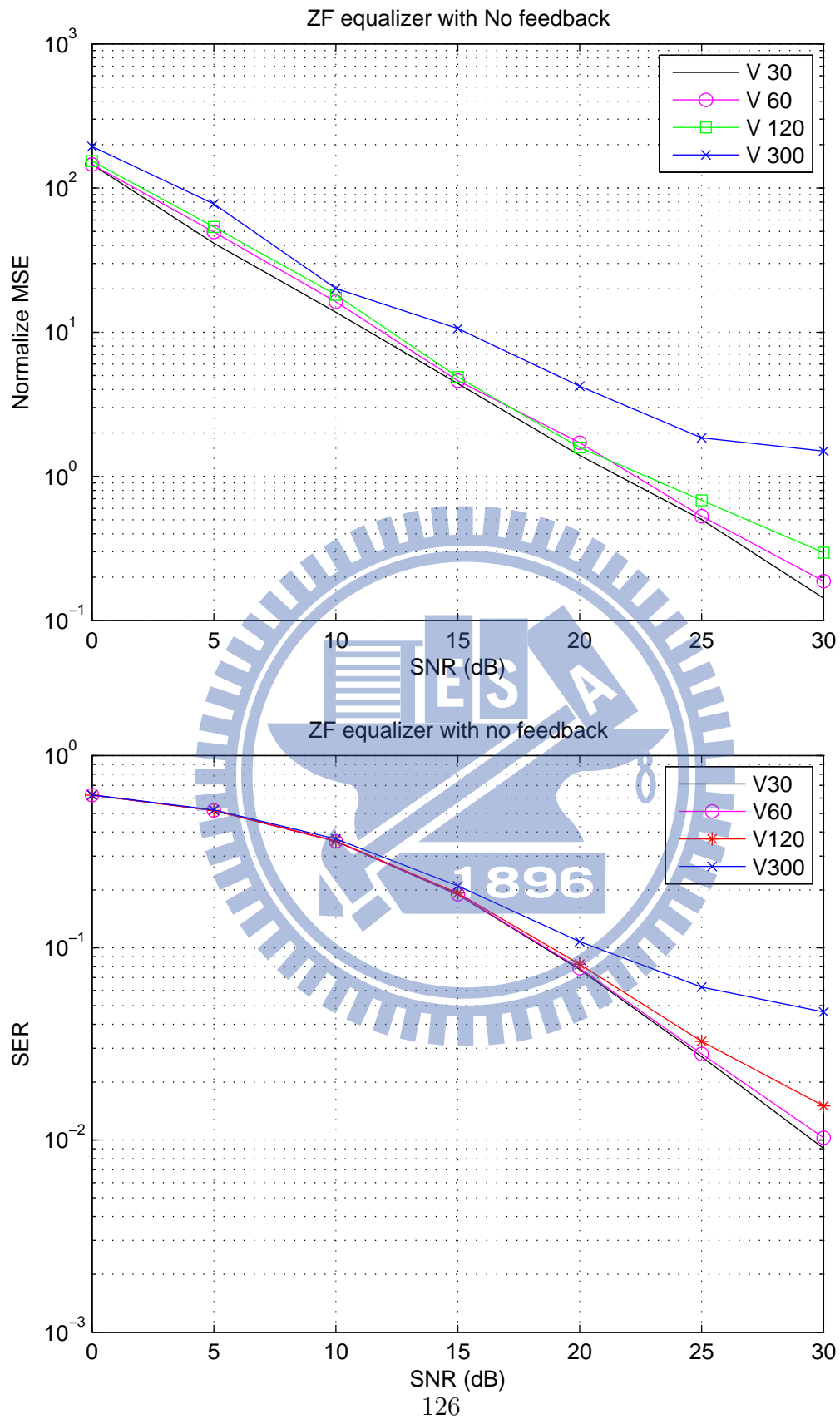


Figure 5.21: MSE and SER for QPSK using ZF equalizer with no feedback in multipath Suburban channel.

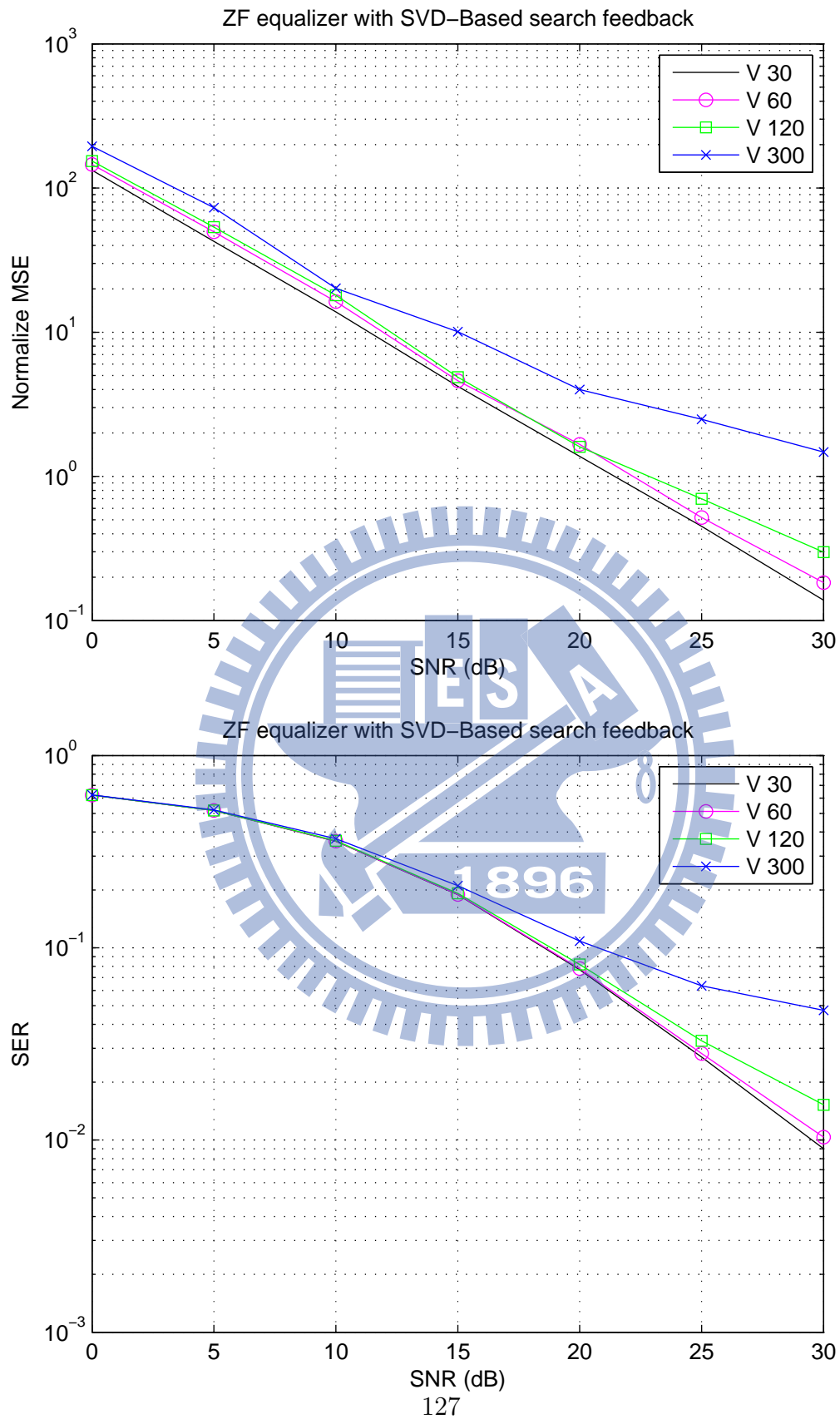


Figure 5.22: MSE and SER for QPSK using ZF equalizer with SVD-Based search feedback in multipath Suburban channel.

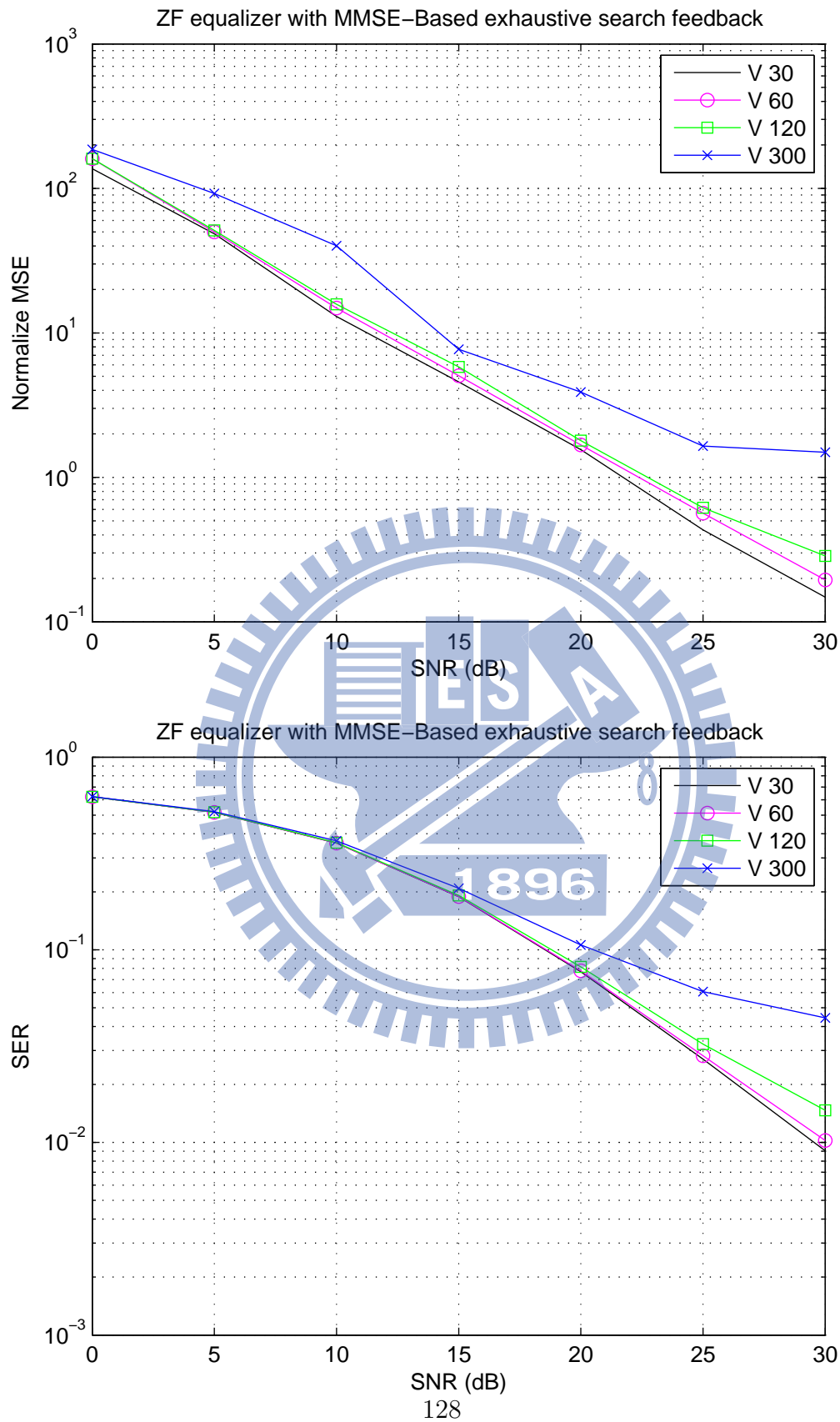


Figure 5.23: MSE and SER for QPSK using ZF equalizer with MMSE-Based exhaustive search feedback in multipath Suburban channel.

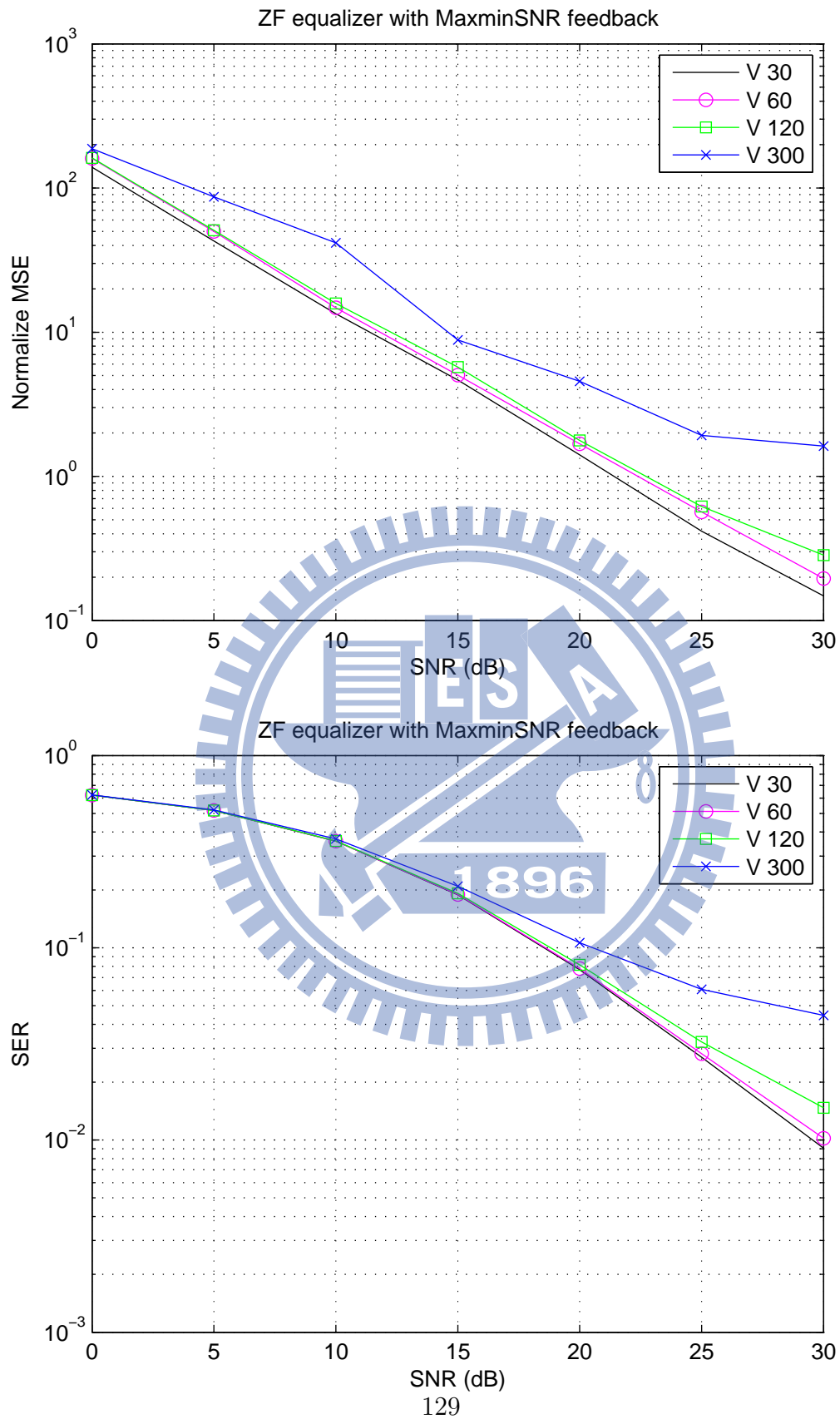


Figure 5.24: MSE and SER for QPSK using ZF equalizer with MaxminSNR-Based search feedback in multipath Suburban channel.

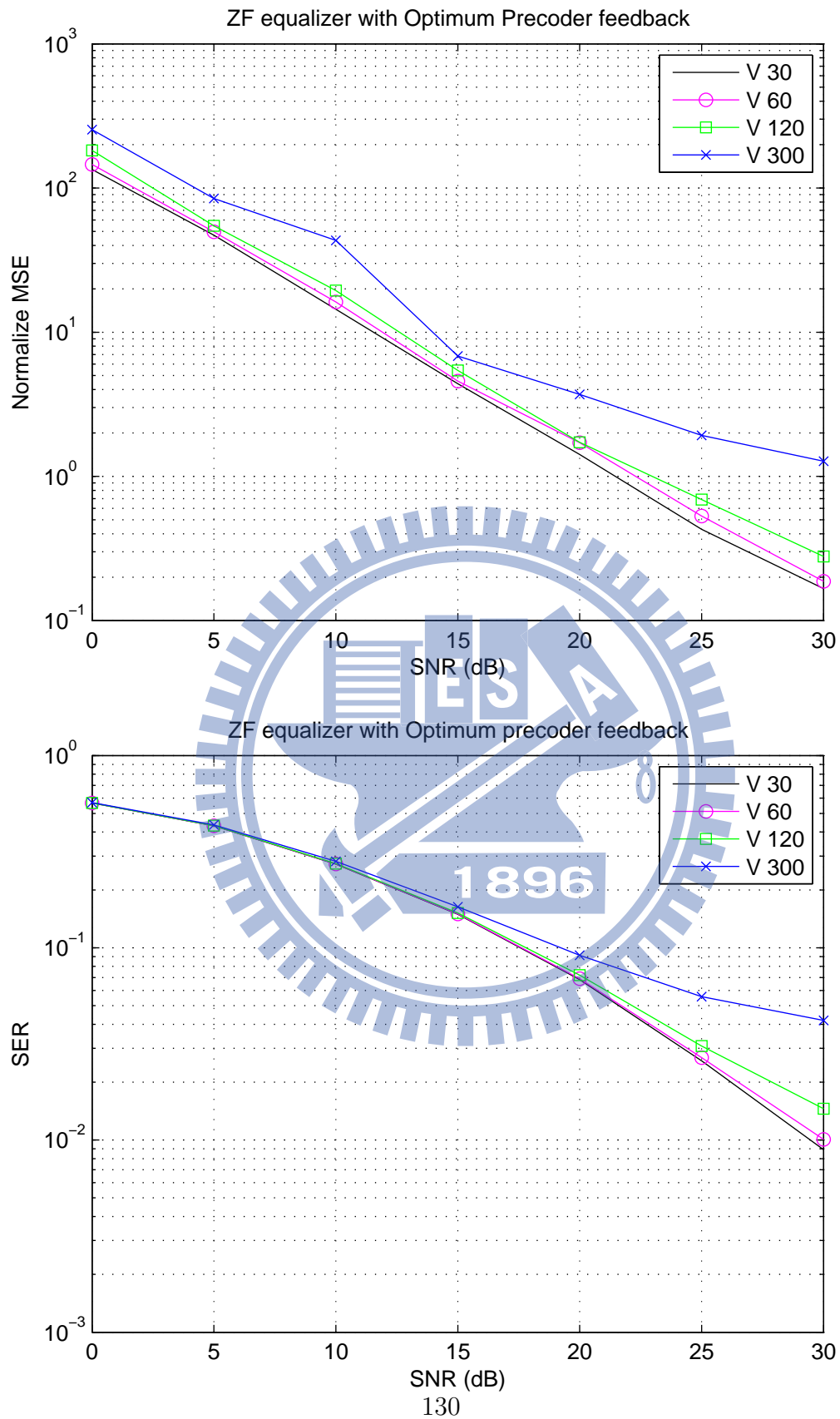


Figure 5.25: MSE and SER for QPSK using ZF equalizer with Optimum precoder feedback in multipath Suburban channel.

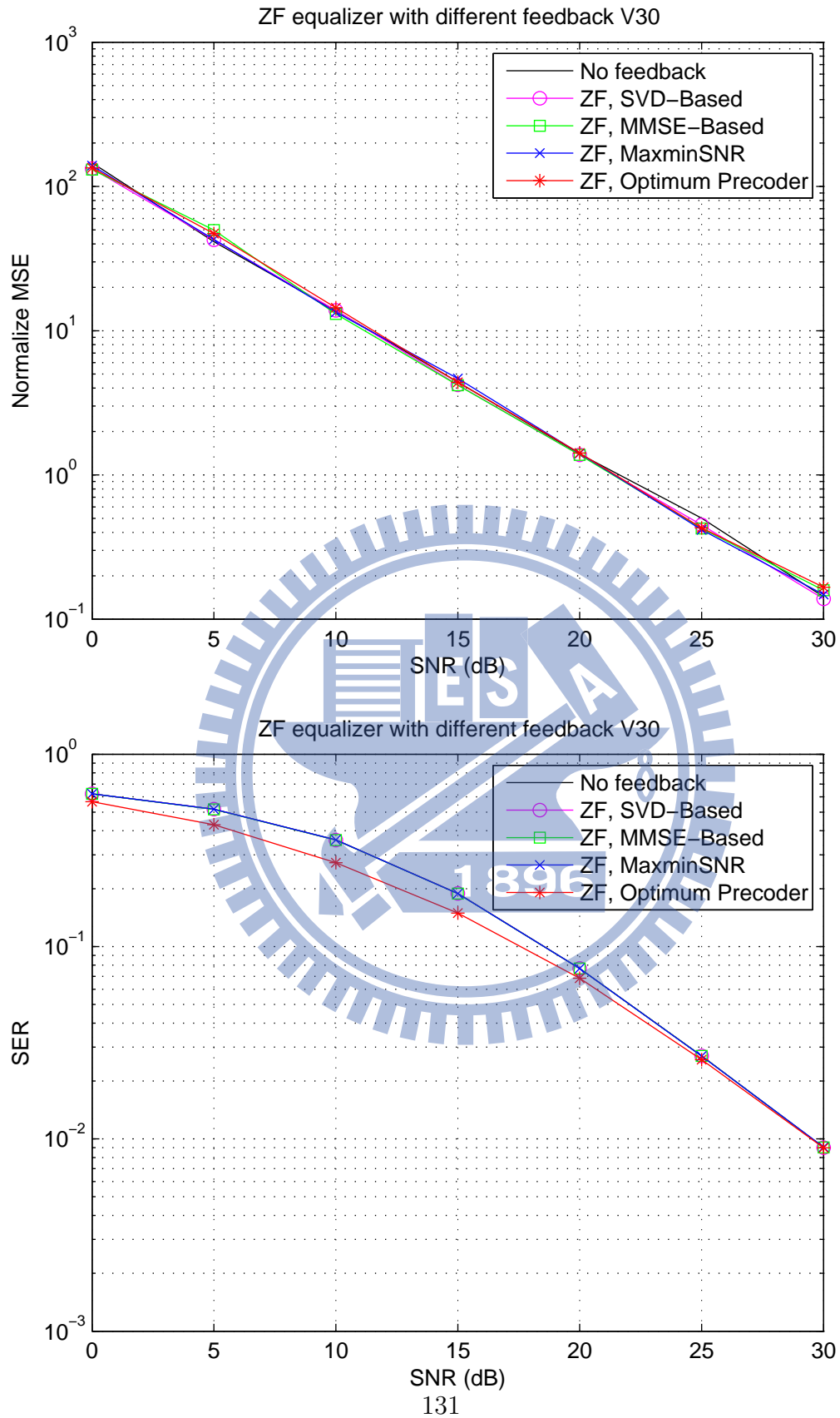


Figure 5.26: MSE and SER for QPSK using ZF equalizer with different feedback methods at 30 km/h in multipath Suburban channel.

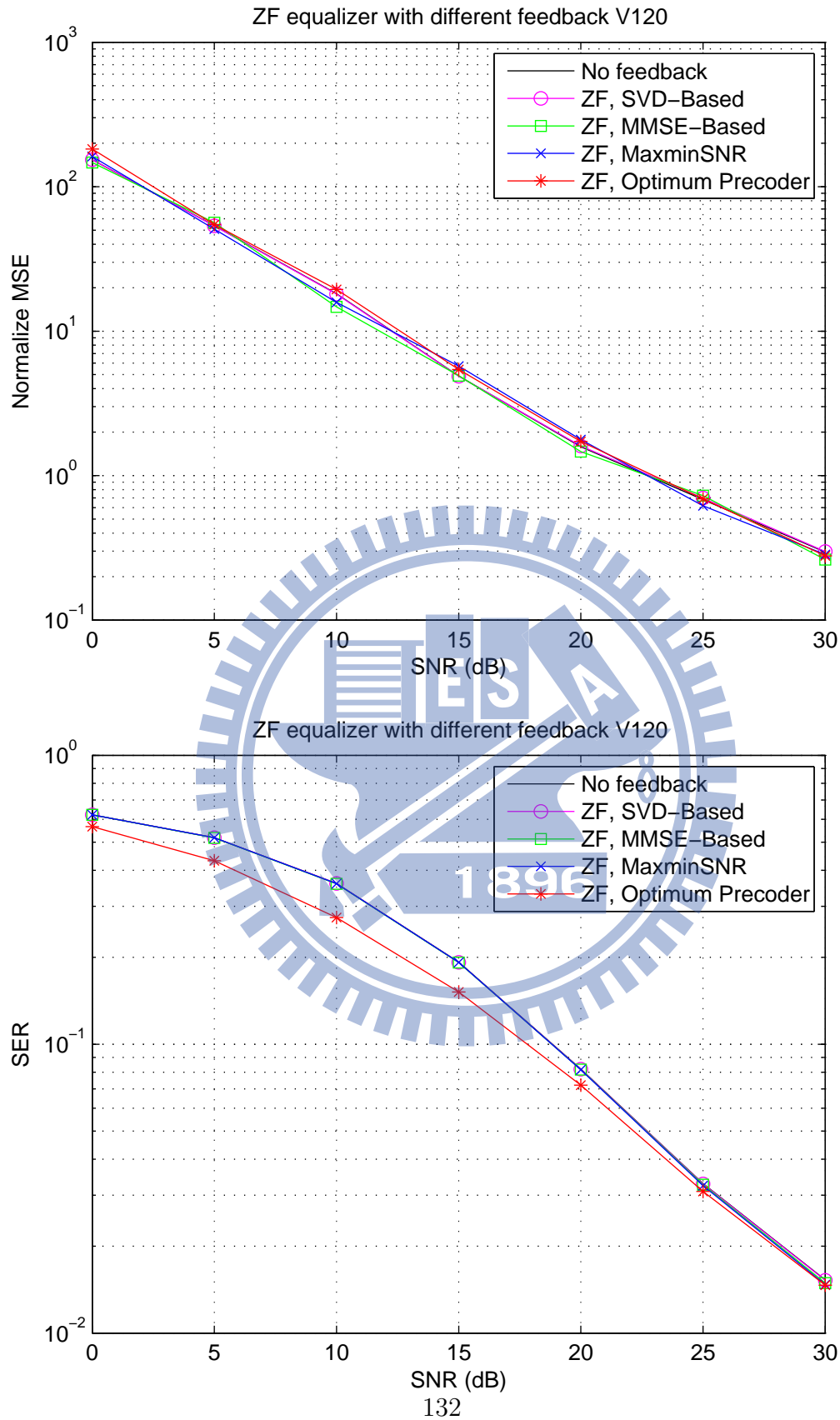


Figure 5.27: MSE and SER for QPSK using ZF equalizer with different feedback methods at 120 km/h in multipath Suburban channel.

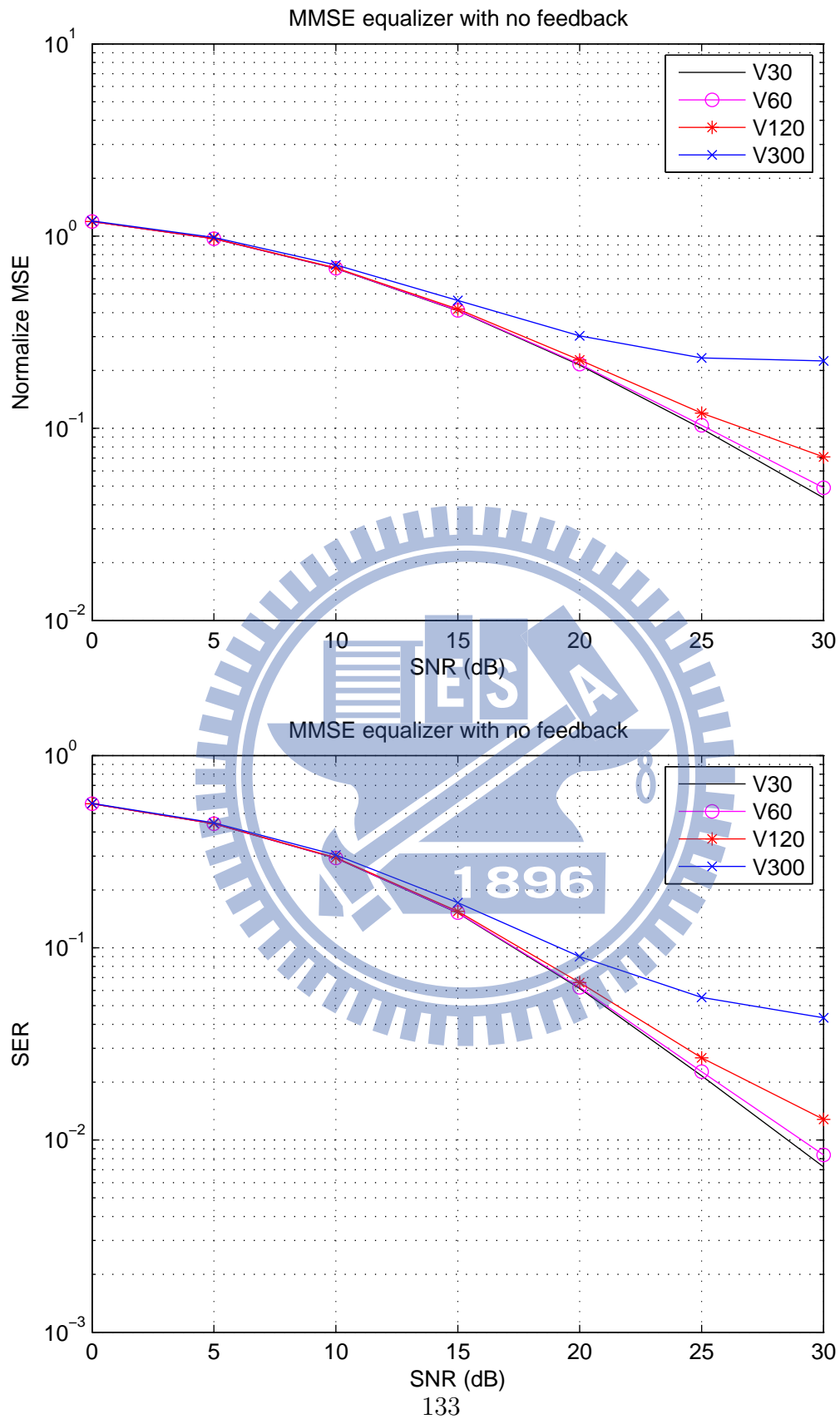


Figure 5.28: MSE and SER for QPSK using MMSE equalizer with no feedback in multipath Suburban channel.

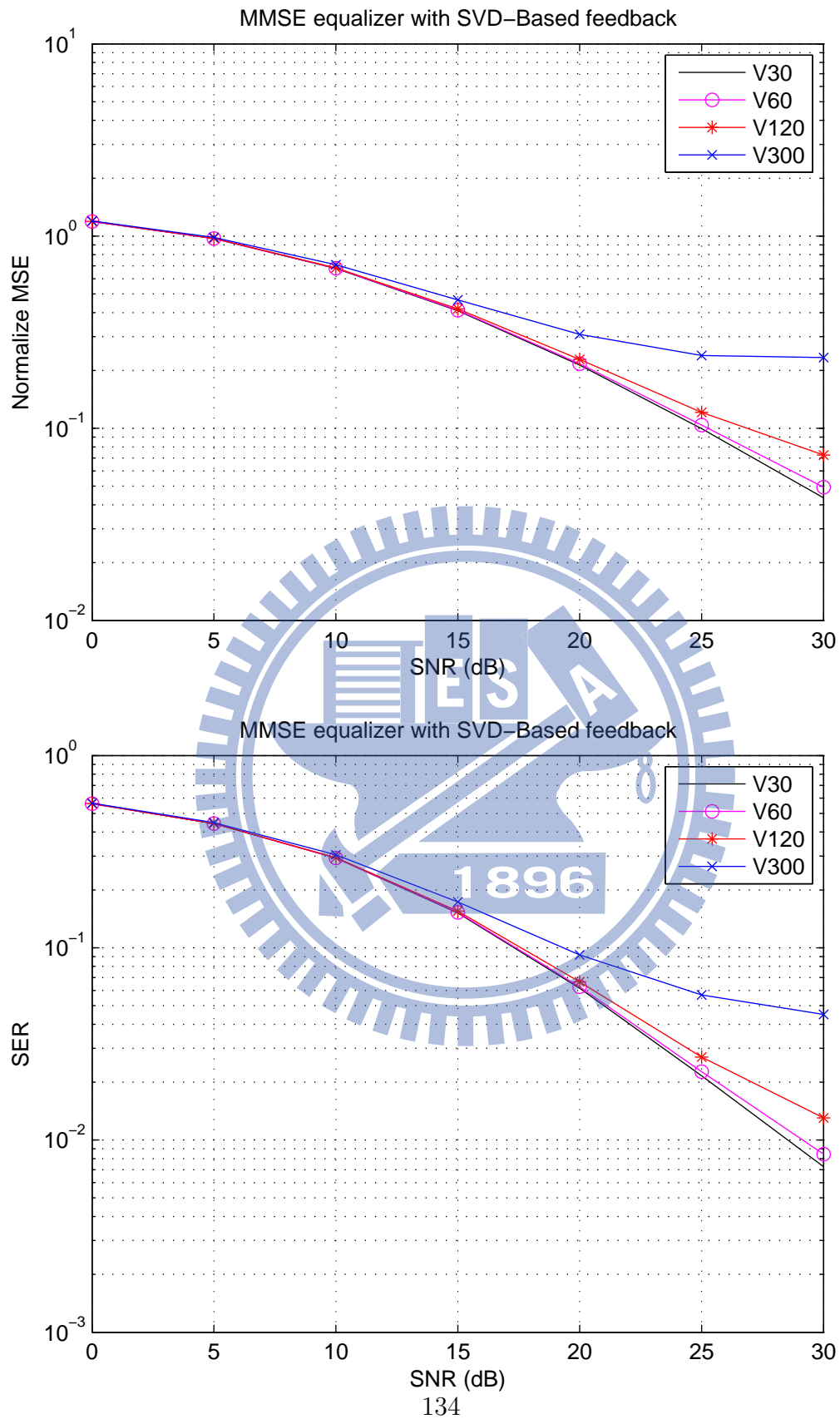


Figure 5.29: MSE and SER for QPSK using MMSE equalizer with SVD-Based search feedback in multipath Suburban channel.

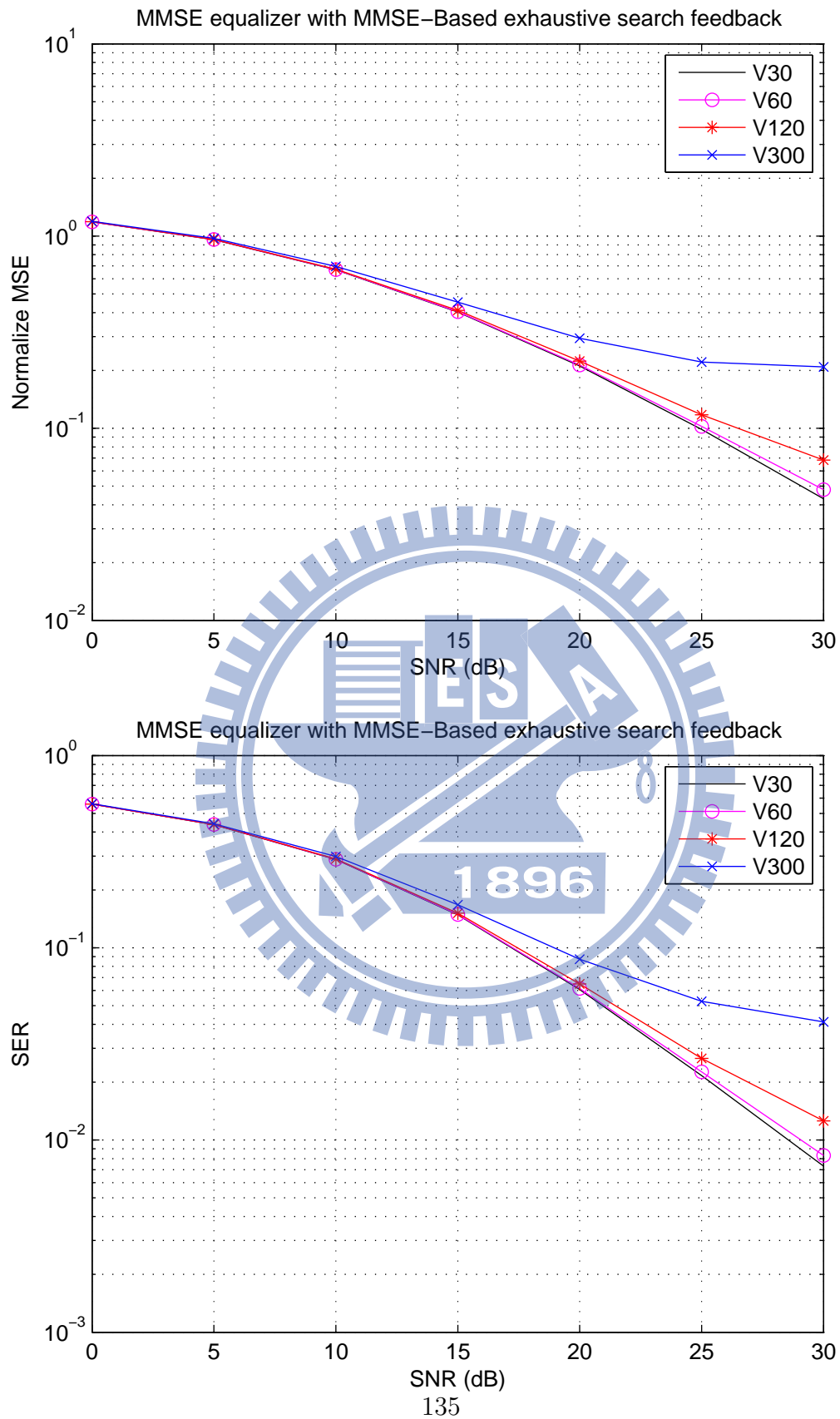


Figure 5.30: MSE and SER for QPSK using MMSE equalizer with MMSE-Based exhaustive search feedback in multipath Suburban channel.

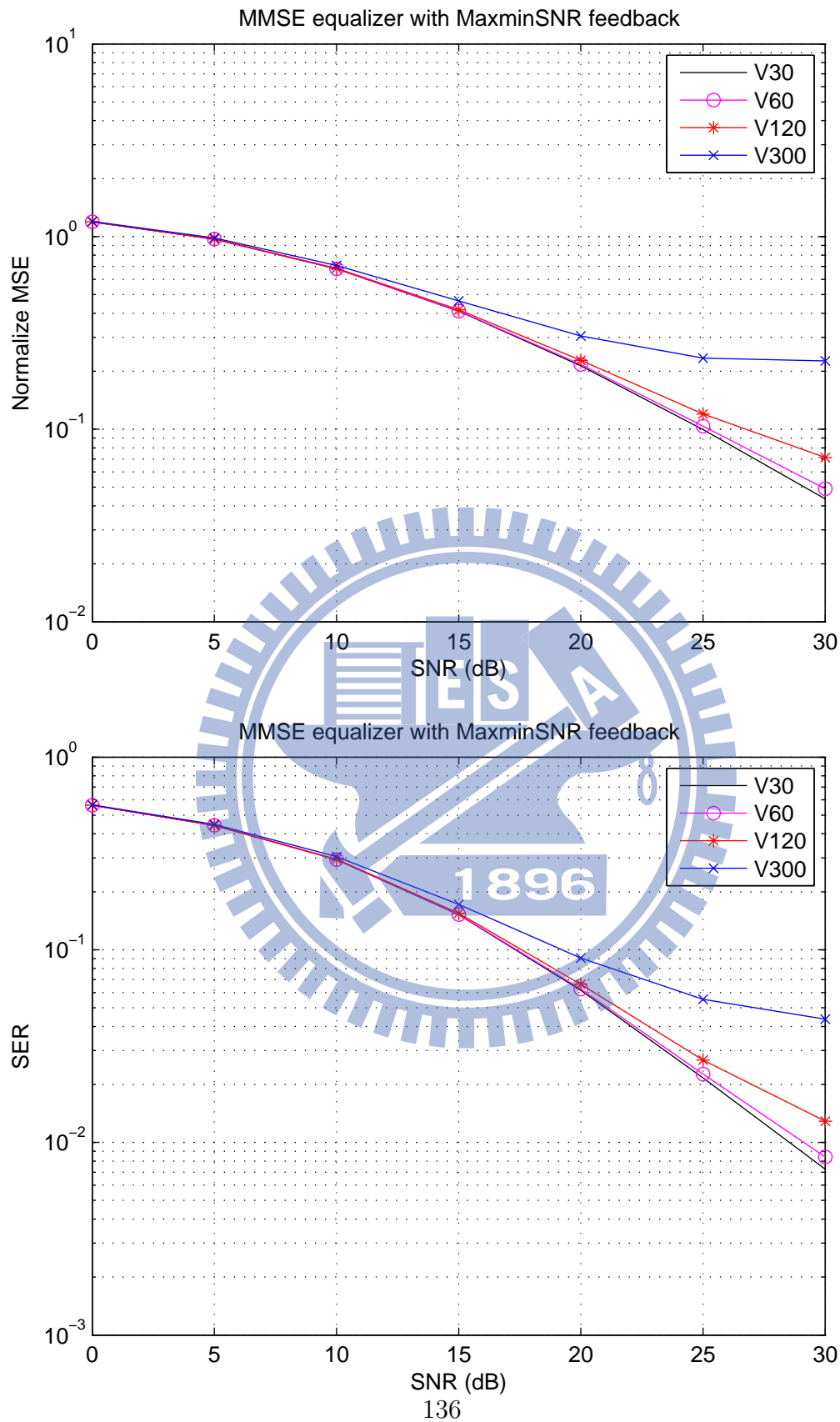


Figure 5.31: MSE and SER for QPSK using MMSE equalizer with MaxminSNR-Based search feedback in multipath Suburban channel.

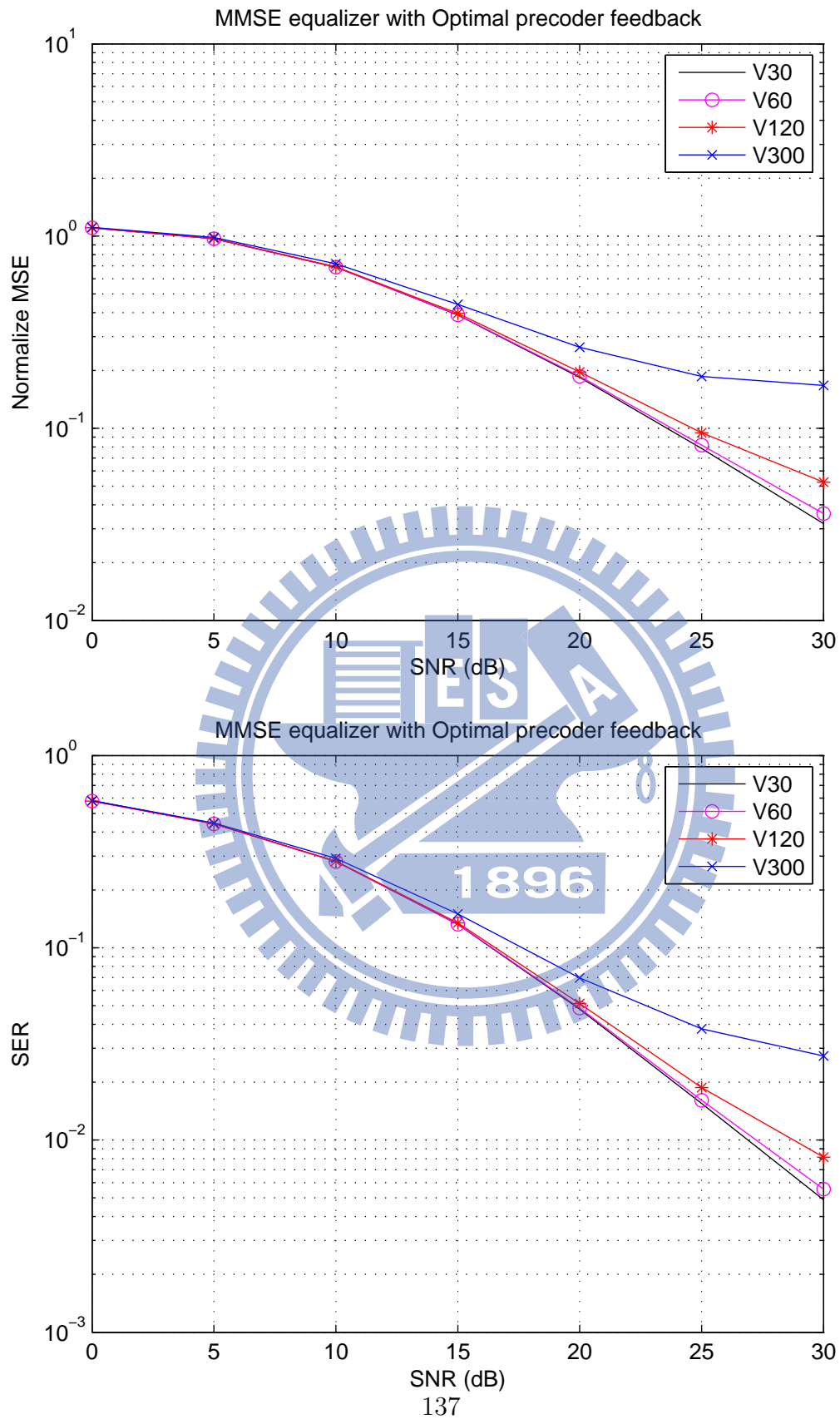


Figure 5.32: MSE and SER for QPSK using MMSE equalizer with Optimum precoder feedback in multipath Suburban channel.

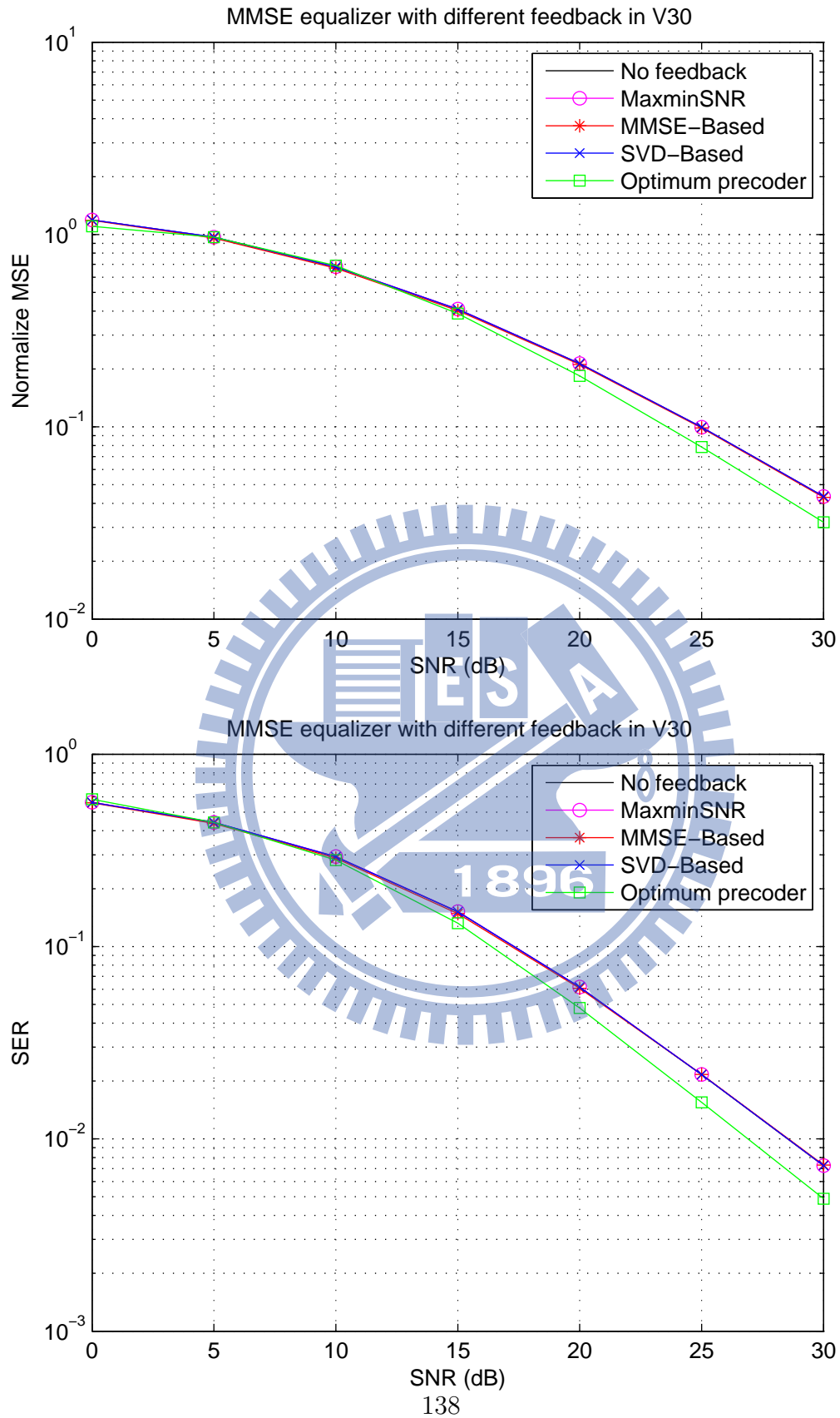


Figure 5.33: MSE and SER for QPSK using MMSE equalizer with different feedback methods at 30 km/h in multipath Suburban channel.

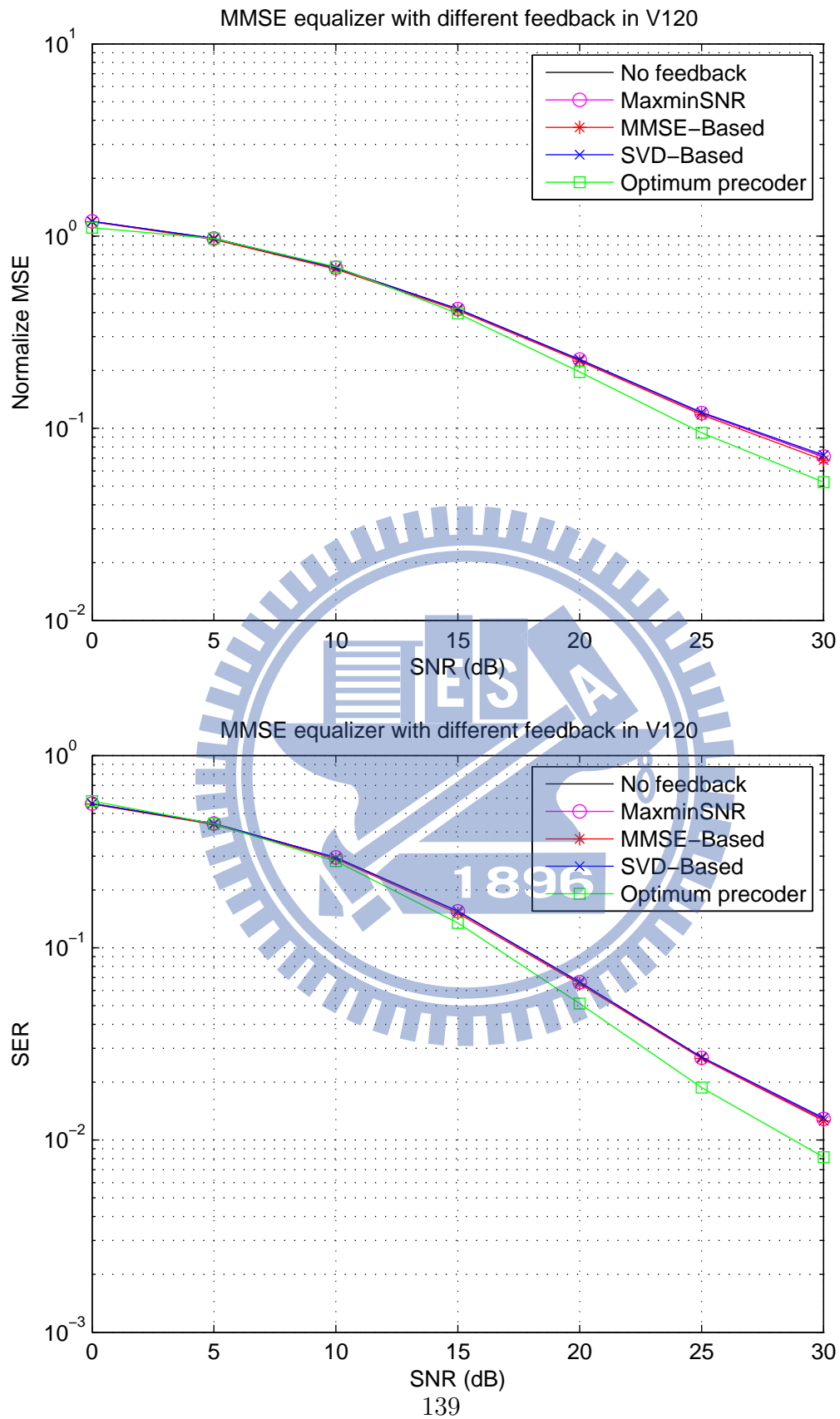


Figure 5.34: MSE and SER for QPSK using MMSE equalizer with different feedback methods at 120 km/h in multipath Suburban channel.

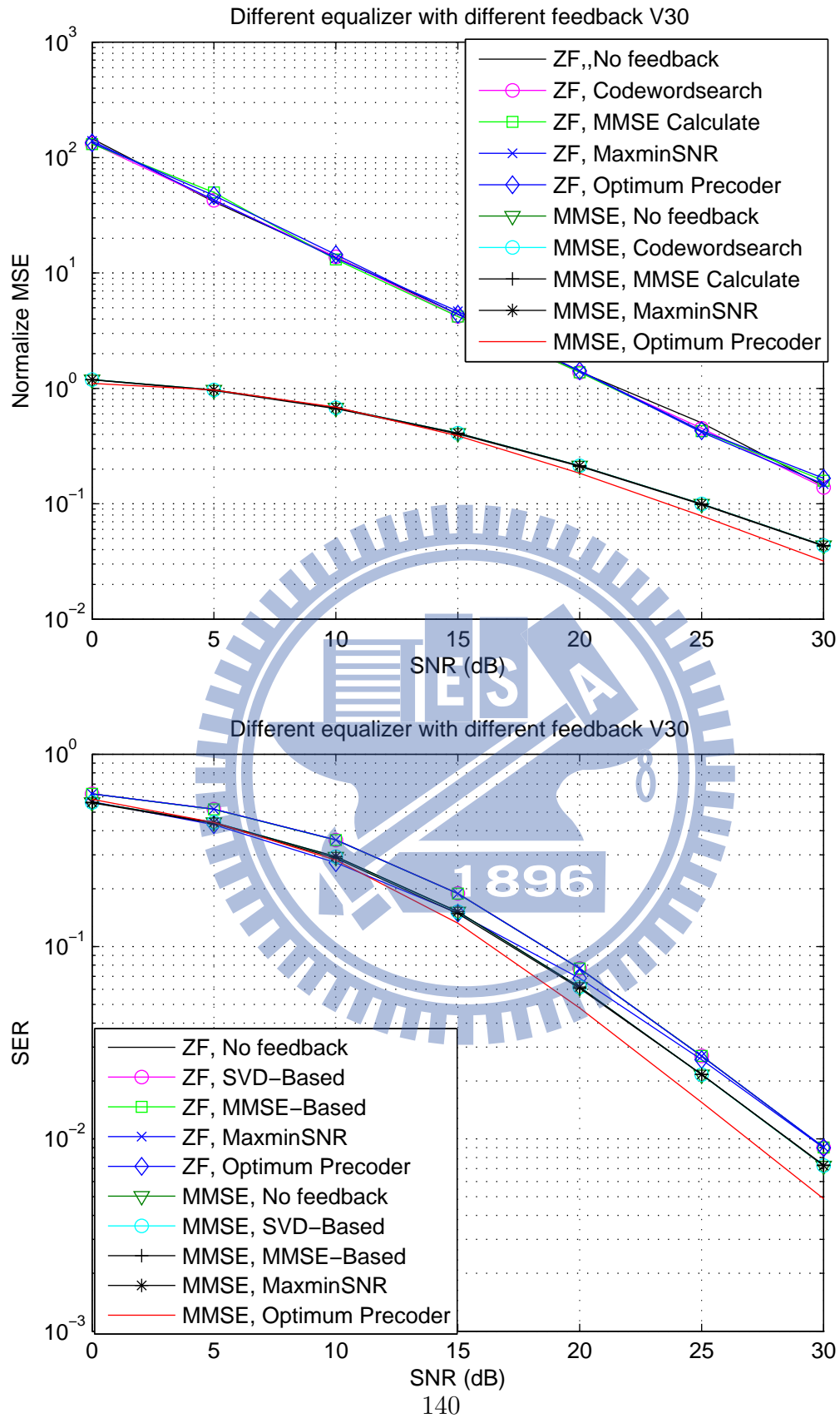


Figure 5.35: MSE and SER for QPSK using ZF and MMSE equalizer with different feedback methods at 30 km/h in multipath Suburban channel.

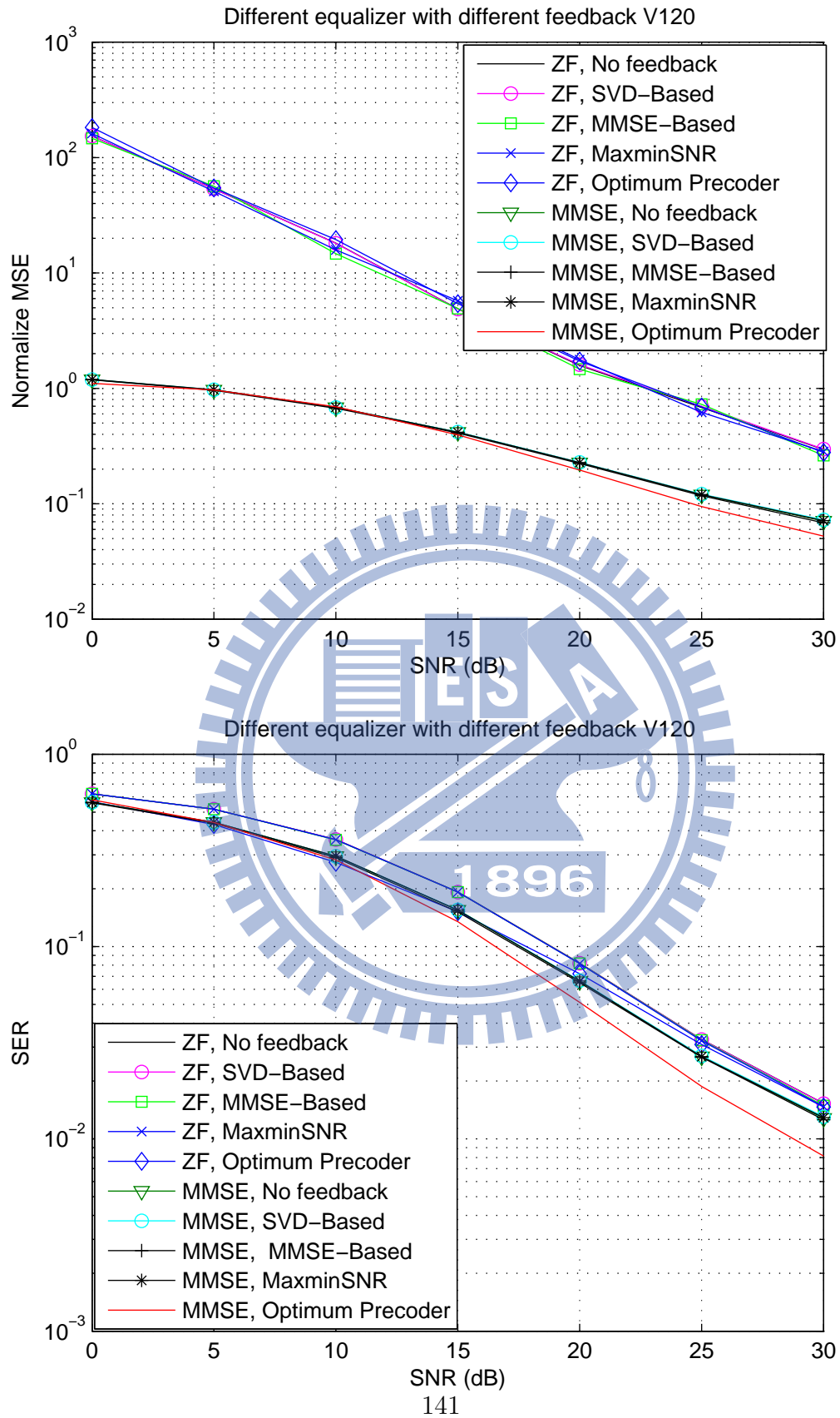


Figure 5.36: MSE and SER for QPSK using ZF and MMSE equalizer with different feedback methods at 120 km/h in multipath Suburban channel.

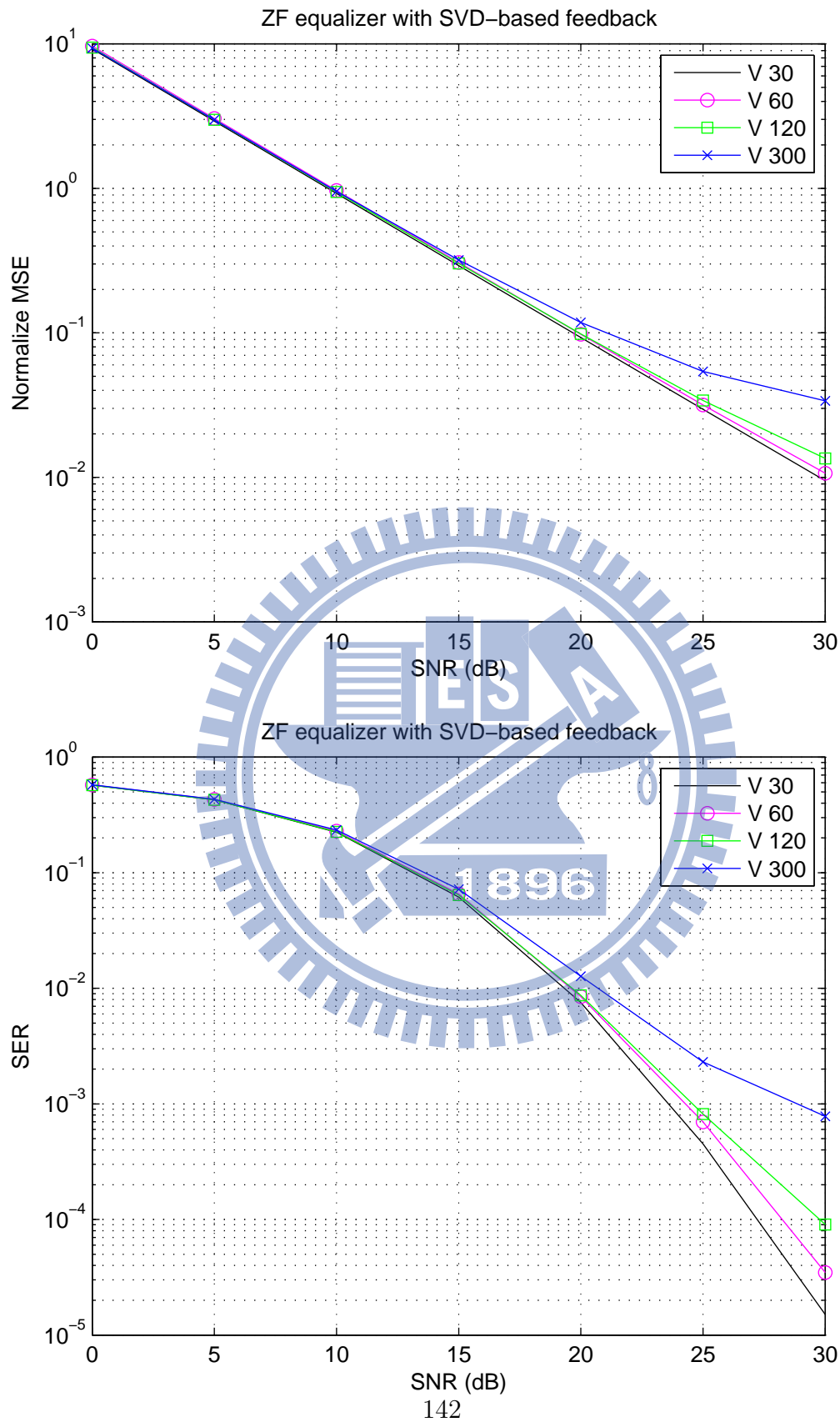


Figure 5.37: MSE and SER for QPSK using ZF equalizer with SVD-Based search feedback in multipath Suburban channel with TX4 RX4 Rank2.

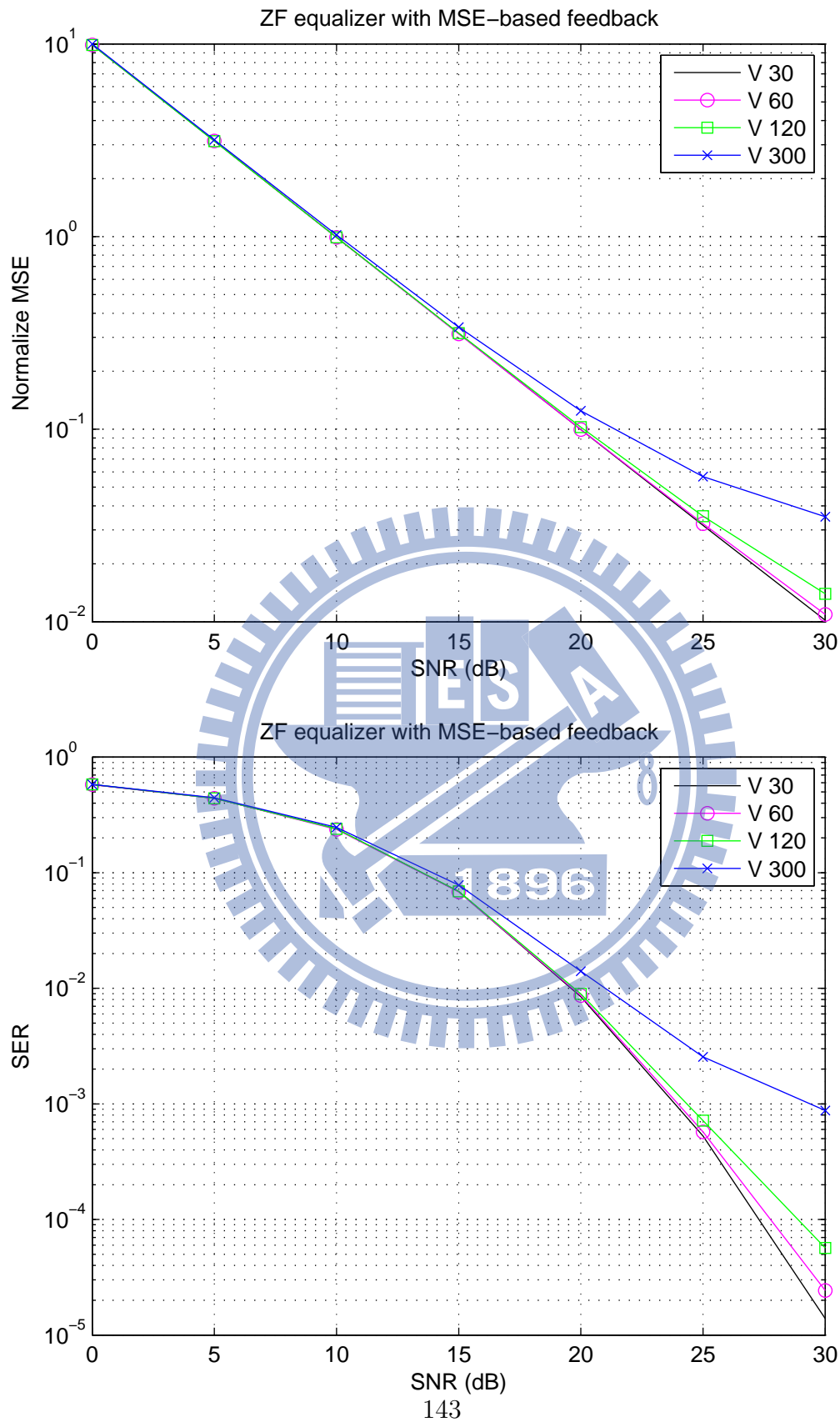


Figure 5.38: MSE and SER for QPSK using ZF equalizer with MMSE-Based exhaustive search feedback in multipath Suburban channel with TX4 RX4 Rank2.

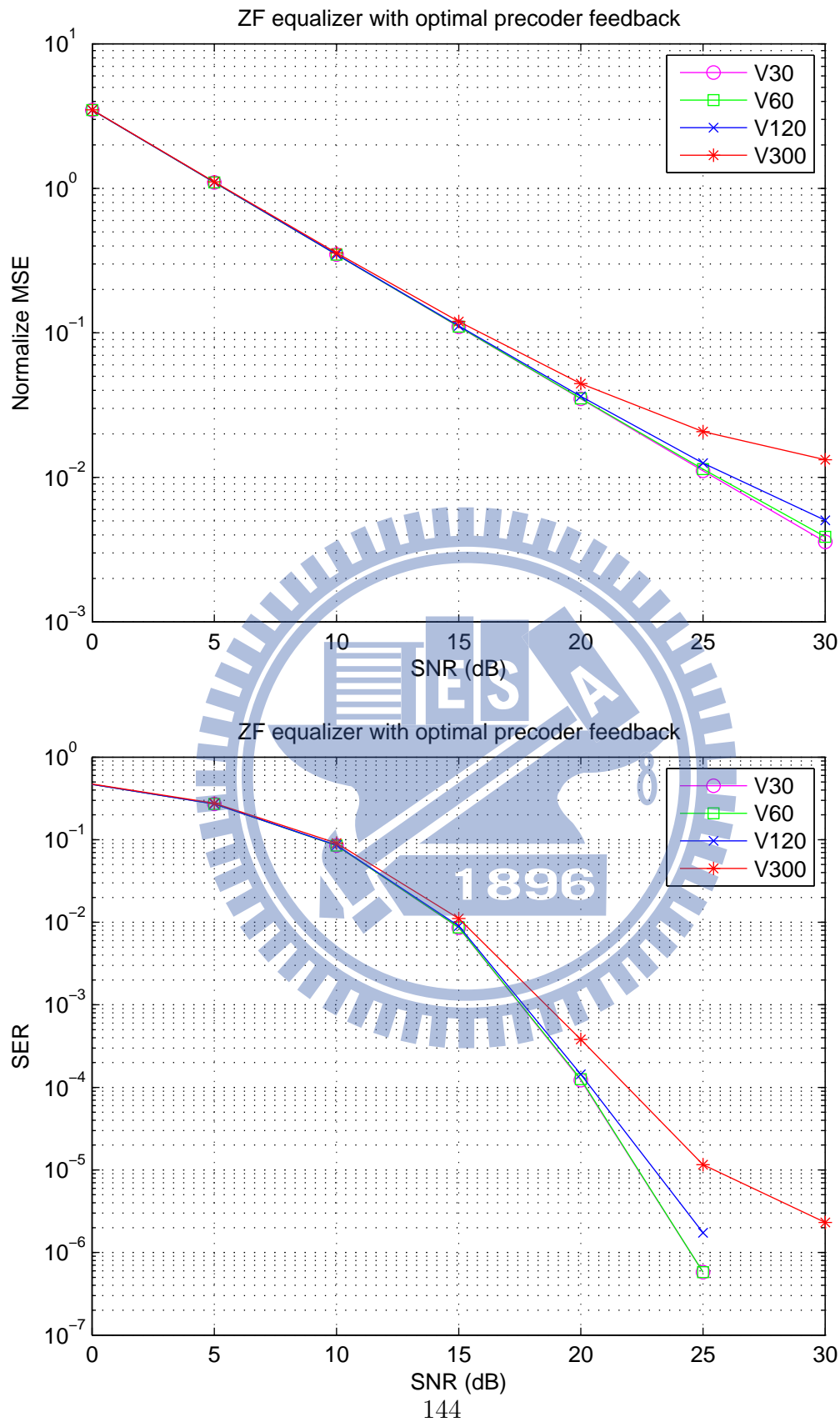


Figure 5.39: MSE and SER for QPSK using ZF equalizer with Optimum precoder feedback in multipath Suburban channel with TX4 RX4 Rank2.

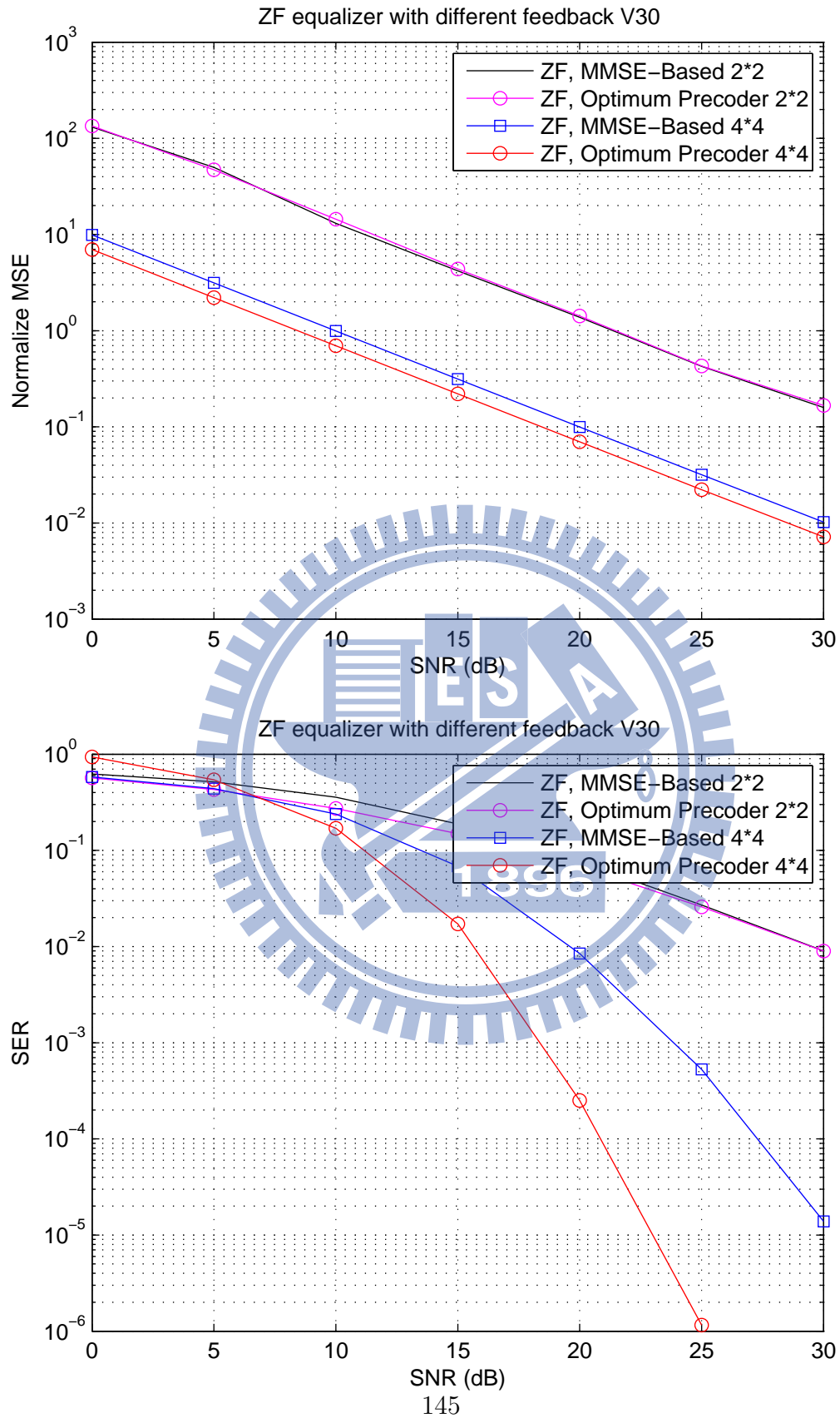


Figure 5.40: MSE and SER for QPSK using ZF equalizer with different feedback methods at 30 km/h in multipath Suburban channel with TX4 RX4 Rank2.

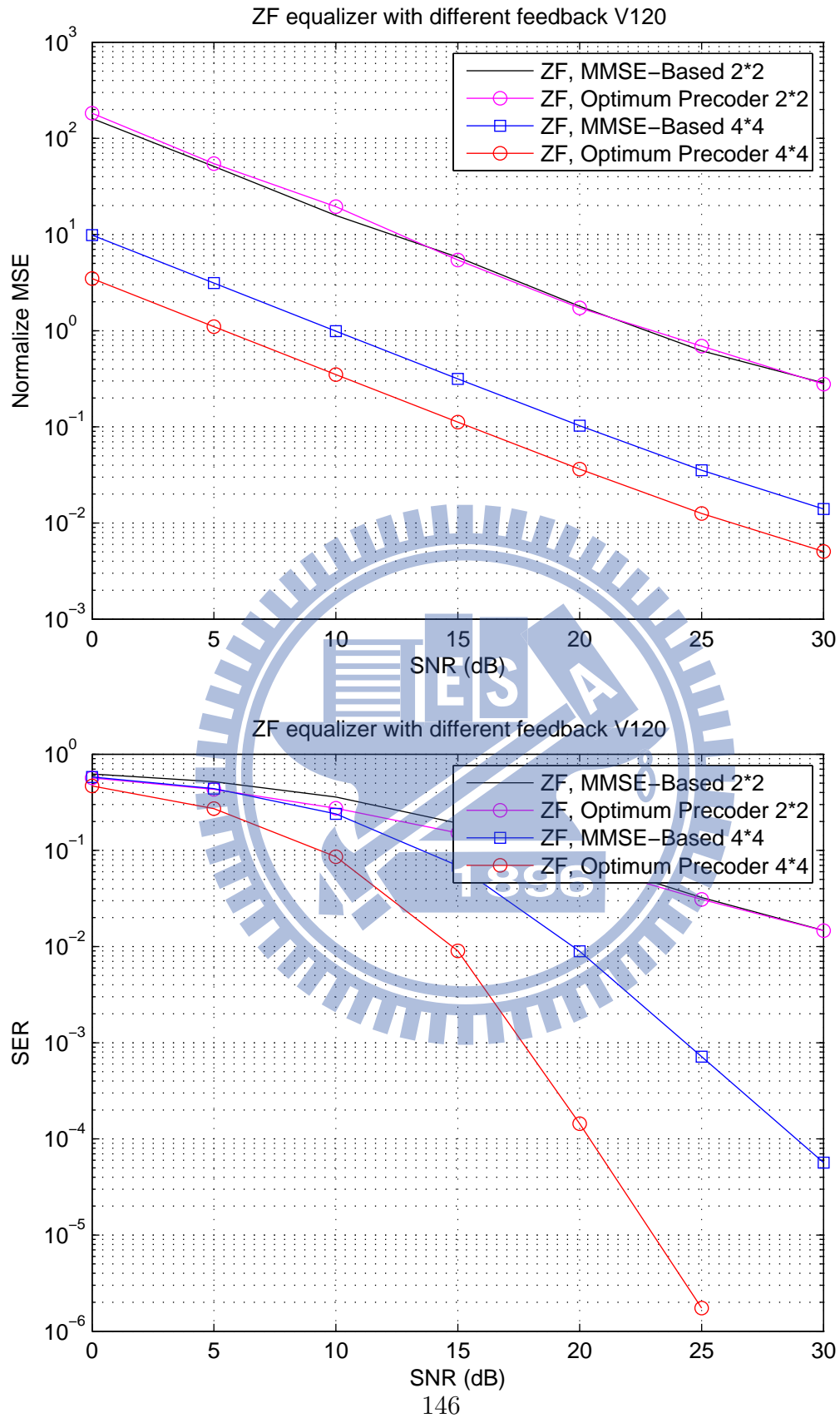


Figure 5.41: MSE and SER for QPSK using ZF equalizer with different feedback methods at 120 km/h in multipath Suburban channel with TX4 RX4 Rank2.

Chapter 6

Conclusion and Future Work

6.1 Conclusion

We first introduced the IEEE 802.16m specifications about basic structure and MIMO system. We considered joint design at both end of the links and introduced two classes of linear equalization: Zero-forcing equalizer and Minimum-mean-square-error equalizer. Then proposed two methods for closed-loop MIMO precoder selection and compared with other two methods in singlepath and multipath. We also considered the complexity of each methods. MMSE equalizer with optimum precoder-based feedback has out performance than other feedback methods. When we used the limited feedback channel, MMSE equalizer with SVD-based feedback has lower complexity and almost the same performance.

6.2 Future Work

There are several possible extension for our research:

- Consider multiuser MIMO system.
- Consider different STC rate.
- Do channel estimation and analyze the impact of the estimation error in MIMO system.

- Consider channel coding and turbo processing for MIMO system.



Chapter 7

Using Matlab to Generate MIMO Channel

In this chapter, we introduce the communication toolbox in matlab.

7.1 System Parameters

- N_t is the transmit antennas
- N_r is the receive antennas
- T_s is the sample time of the input signal, in seconds
- F_d is the maximum Doppler shift, in Hertz
- TAU is the row vector of path delays

We first call matlab command `mimochan` to generate the MIMO channel coefficient.

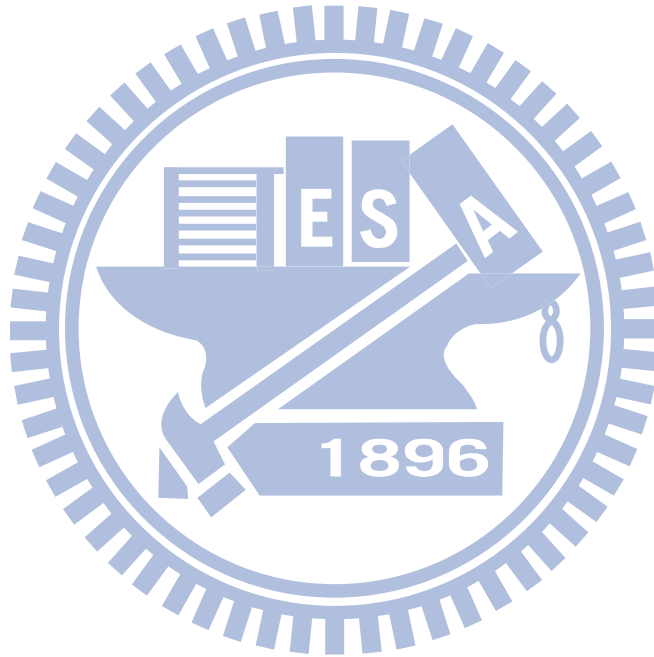
$$chan = mimochan(N_t, N_r, T_s, F_d, TAU) \quad (7.1)$$

Then, we use matlab command `filter` to call MIMO channel

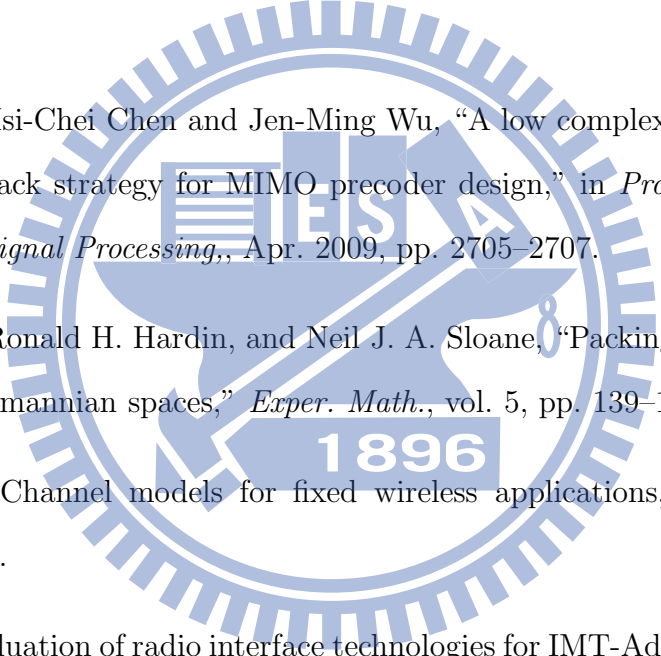
$$y = filter(chan, x) \quad (7.2)$$

where x is the transmit signal and y is the receive signal after passing the channel.

When we use filter, the size of channel affect the running time. If the channel matrix is 8×8 , the running time is very big. So we need to take care that if the channel matrix is big, we need more time to run the simulation.



Bibliography

- 
- [1] A. Barg and D. Y. Nogin, “Bounds on packings of spheres in the Grassmann manifold,” *IEEE Trans. Inf. Theory*, vol. 48, no. 9, pp. 2450–2454, Sep. 2002.
- [2] Glen Ballou, “Filters and equalizers,” in Handbook for *Sound Engineers*, 4th ed. Focal Press, 2008.
- [3] Che-Chen Chou, Hsi-Chei Chen and Jen-Ming Wu, “A low complexity channel decomposition and feedback strategy for MIMO precoder design,” in *Proc. IEEE Int. Conf. Acoustics Speech Signal Processing*, Apr. 2009, pp. 2705–2707.
- [4] John H. Conway, Ronald H. Hardin, and Neil J. A. Sloane, “Packing lines, planes, etc.: packings in Grassmannian spaces,” *Exper. Math.*, vol. 5, pp. 139–159, 1996.
- [5] V. Erceg *et al.*, “Channel models for fixed wireless applications,” IEEE 802.16.3c-01/29r4, July 2001.
- [6] “Guidelines for evaluation of radio interface technologies for IMT-Advanced (Doc ITU-R 5/69),” Draft New Report ITU-R M.[IMT.EVAL], October 2008.
- [7] J. W. Huang, E. K. S. Au, and V. K. N. Lau, “Linear precoder and equalizer design for uplink multiuser MIMO systems with imperfect channel state information,” in *Proc. IEEE Wireless Commun. Network. Conf.*, Mar. 2007, pp. 1296–1301.

- [8] K.-C. Hung and D. W. Lin, "Pilot-based LMMSE channel estimation for OFDM systems with power-delay profile approximation," *IEEE Trans. Veh. Technology*, vol. 59, no. 1, pp. 150–159, Jan. 2010.
- [9] IEEE P802.16m, "Project 802.16m evaluation methodology document (EMD)," IEEE 802.16m-08/004r5, Jan. 2009.
- [10] IEEE 802.16 Task Group m, *Part 16: Air Interface for Fixed and Mobile Broadband Wireless Access Systems — Advanced Air Interface (working document)*. Doc. no. IEEE 802.16m/D4, Feb. 3, 2010.
- [11] S. M. Kay, "Fundamentals of Statistical Signal Processing: Vol. I-Estimation Theory," Englewood Cliffs, NJ: Prentice-Hall, 1993.
- [12] Hongxiang Li and Hui Liu, "An analysis on uplink OFDMA optimality," in *Proc. IEEE Veh. Technol. Conf.*, vol. 3, 2006, pp. 1339–1343.
- [13] Qinghua Li, Xintian Lin, Jianzhong Zhang and Wonil Roh, "Advancement of MIMO technology in WiMAX: from IEEE 802.16d/e/j to 802.16m," *IEEE Communication Magazine*, vol. 47, no. 6, pp. 100–107, June 2009.
- [14] David J. Love and Robert W. Heath. Jr., "Limited feedback precoding for spatial multiplexing systems using linear receivers," *IEEE Trans. Inf. Theory*, vol. 51, no. 8, pp. 2967–2976, Aug. 2005.
- [15] Liangshan Ma and Dongyan Jia, "The competition and cooperation of WiMAX, WLAN and 3G," in *Int. Conf. Applica. Sys. Mobile Tech.*, Nov. 2005, pp. 1–5.
- [16] Gene H. Golub and Charles F. Van Loan, *Matrix Computations*, 2nd ed. Johns Hopkins University Press, 1990.

- [17] D. Palomar, John M. Cioffi, and Miguel Angel Lagunas, "Joint Tx-Rx beamforming design for multicarrier MIMO channels: a unified framework for convex optimization," *IEEE Trans. Signal Processing*, vol. 51, no. 9, Sep. 2003, pp. 2381–2401.
- [18] A. Scaglione, P. Stoica, S. Barbarossa, G. B. Giannakis, and H. Sampath, "Optimal designs for space-time linear precoders and decoders," *IEEE Trans. Signal Process.*, vol. 50, no. 5, pp. 1051–1064, May 2002.
- [19] H. Stark and J. W. Woods, *Probability and Random Processes, 3rd ed.* Upper Saddle River, New Jersey: Prentice-Hall, 2002.
- [20] R. van Nee and R. Prasad, *OFDM for Wireless Multimedia Communications*. Boston: Artech House, 2000.
- [21] Yi-Ling Wang, "Research in and DSP implementation of channel estimation techniques for IEEE 802.16e OFDMA uplink and downlink," M.S. thesis, Dept. Electronics Eng. and Institute of Electronics, National Chiao Tung University, Hsinchu, Taiwan, R.O.C., June 2007.
- [22] L. Wilhelmsson, B. Bernhardsson, and L. Andersson, "Channel estimation by adaptive interpolation," U.S. patent 7,433,433, Oct. 7, 2008.
- [23] W.-R. Wu and T.-H. Hsu, "A low-complexity precoder searching algorithm for MIMO-OFDM systems," in *Proc. IEEE Personal Indoor Mobile Radio Communications Conf.*, Sep. 2009, pp. 2021–2024.